University of Southampton

INVESTIGATIONS OF THE VORTEX PHASE DIAGRAM AND PINNING IN $YBa_2Cu_3O_{7-\delta}$ SINGLE CRYSTALS

BY

KONSTANTINOS DELIGIANNIS

Thesis submitted for examination for the degree of

Doctor of Philosophy

Department of Physics

January 1998

Στους λατρευτους μου Γονεις
και στον αγαπημενο μου Αδελφο

To my beloved Parents
and my dear Brother

UNIVERSITY OF SOUTHAMPTON

ABSTRACT

FACULTY OF SCIENCE

PHYSICS

Doctor of Philosophy

INVESTIGATIONS OF THE VORTEX PHASE DIAGRAM AND PINNING IN $YBa_2Cu_3O_{7-\delta}$ SINGLE CRYSTALS

by Konstantinos Deligiannis

This thesis presents magnetisation studies in the vortex state of high purity $YBa_2Cu_3O_{7-\delta}$ single crystals.

We present magnetic hysteresis results of twinned and detwinned crystals which demonstrate that contrary to previous reports, twin planes can limit the critical current in a broad field and temperature region by facilitating vortex channeling. Twin planes provide easy paths, within which vortices can move decreasing the sample's overall pinning. A detailed angular study of the magnetisation reveals the existence of two critical angles, θ_L and θ_K: for $\theta < \theta_L$ vortices lock-in to the twin planes; for $\theta_L < \theta < \theta_K$ a kinked structure occurs; for $\theta > \theta_K$ the magnetic hysteresis loops reproduce the magnetic response of the untwinned regions, where pinning is produced by random point defects. The two critical angles θ_K and θ_L are shown to depend crucially on the disorder in the untwinned regions.

Comparing magnetic to transport data we demonstrate for the first time that the magnetisation peak line in the phase diagram of $YBa_2Cu_3O_{7-\delta}$ exhibits an impressive similarity with the equivalent line for $Bi_2Sr_2CaCu_2O_8$. Our results reveal the existence of a voltage criteria independent, sharp, magnetisation peak which correlates to the multicritical point. By increasing temperature or oxygen content the magnetisation peak surprisingly shifts to higher fields maintaining its correlation to the critical point. At high temperatures we observe a previously unreported splitting of the magnetisation peak. Our data support the existence of a field-driven transition which separates two different solid regimes: a quasi-ordered lattice (Bragg glass) and a highly disordered phase of entangled vortices.

Finally, we use the presence of lock-in oscillations in the magnetic hysteresis of $YBa_2Cu_3O_{7-\delta}$ single crystals to study pinning by the layered structure in the quasi-2D region. We illustrate how random point disorder can affect the oscillations. A systematic study of the temperature dependence of the magnetisation for parallel applied fields shows that the critical current does not decrease monotonically with temperature. This is a result of the reduced dimensionality of thermal fluctuations of the locked-in between the layers Josephson vortices and their interaction with the extrinsic point defects.

CONTENTS

4. VORTEX CHANNELING

5. THE $YBa_2Cu_3O_{7-\delta}$ PHASE DIAGRAM

6. LOCK-IN OSCILLATIONS

7. SUMMARY

ACKNOWLEDGMENTS

First and foremost, I would like to thank from the bottom of my heart my supervisor, *Peter de Groot*, for his consistent help (in his characteristic, unique way) during these three years and for giving me all the freedom I needed to work. It was an honour to be in the same group with the charismatic *Bryan Rainford*, a great person, teacher and physicist - I thank him for his enormous help. I also thank the remarkable *Peter Lanchester* for always "being there" and his struggle against the ... "cantdo" mentality (you are not alone in this, Peter). *Mohand Oussena* for all his help and the passionate discussions we shared during the first years. *Artem Volkozub* for learning me in the early months what experimental perfectionism means.

I would like also to thank *Iain*, *Darren*, *Adroja*, *Gordon*, *Steve*, *Stephen*, *Stef*, *Andreas*, *Andy*, *Stelios* and *Keith*, for making the lab such a nice place to work in. Our technicians, *Colin*, *Vince*, *Tom* and *Dave*, for keeping the department running. *Robert Gagnon* and *Luc Früchter* for their help, *Sergey Gordeev* for his comments and suggestions on this work.

I am grateful to *Melissa Charalambous*, *Gianni Blatter*, *Eli Zeldov*, *Thierry Giamarchi* and *Lia Krusin-Elbaum*; their profound interest in the work of an unknown student really brought a wind of encouragement and extra motivation at a difficult time.

I can not find the words to thank *Despoina* - without her love and support it would have been so difficult to complete this work.

Last but not least, I am deeply indebted to Profs. *Xenofon Moussas* and *John Georgoulas* for all their valuable advises and substantial support during the last six years.

1. INTRODUCTION

1.1 HIGH TEMPERATURE SUPERCONDUCTIVITY

The high operating temperatures, the small Ginzburg-Landau coherence length ξ, the large magnetic penetration depth λ, and the layered structure characterizing the high temperature superconducting oxides, gave breath to novel aims and perspectives of Superconductivity research. Since the prime feature of most applications considered is the dissipation-free flow of current and the motion of vortices causes dissipation, the role of pinning became more important in the High Temperature Superconductors (HTS) than it ever had been. Indeed, the enhanced strength of thermal fluctuations as given by the Ginzburg number [1] $Gi \propto \gamma^2 T_c^4$, which compares thermal to condensation energy in the coherence volume ξ^3, leads to smoothing of the pinning potential arising from materials defects. In HTS Gi is six orders of magnitude higher than in conventional superconductors. Dissipation is furthermore assisted by the thermal activation of vortices over their pinning barriers.

Though every member of the HTS family has a number of individual characteristics, all of them possess a layered structure based on CuO_2 planes; this is not irrelevant to their sharing of a largely common phenomenology [2], as well. The layered structure is unveiled in a number of important properties and exotic vortex states: for example a transition from a 3D to a 2D vortex lattice has been predicted in certain magnetic field and temperature regions, leading to new vortex pattern structures.

It is, thus, self evident that the technological development which the discovery of High-T_c Superconductivity made possible and attainable in the near future, can be underpinned only by a thorough understanding of vortex dynamics.

1.2 THE $YBa_2Cu_3O_{6+x}$ COMPOUND

1.2.1 STRUCTURE

$YBa_2Cu_3O_{6+x}$ (widely known also with the abbreviations YBCO or 123) was the first of the HTS discovered with a T_c of approximately 90 K, above the liquid nitrogen boiling point of 77 K. Superconductivity in YBCO was discovered almost simultaneously by 3 groups in 1987 [3-5].

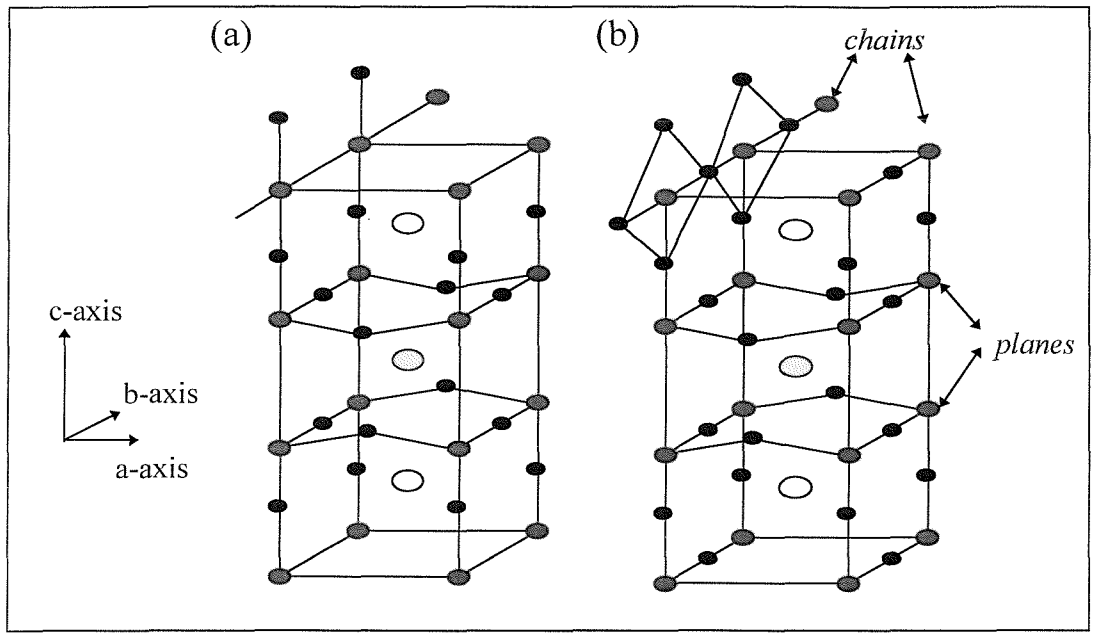

Figure 1.1: *Crystal structure of the YBCO compound.* ● *Stands for oxygen,* ● *for copper,* ○ *for yttrium and* ○ *for barium. (a) Structure of tetragonal and (b) of orthorhombic (superconducting)* $YBa_2Cu_3O_{7-\delta}$.

The oxygen content in $YBa_2Cu_3O_{6+x}$, x, can take any values between 0 and 1 - equivalently and respectively the oxygen deficiency of $YBa_2Cu_3O_{7-\delta}$, δ, varies between 1 and 0. Higher or lower oxidization of YBCO has not been succeeded [6]. As a typical perovskite it has a layered crystal structure. The oxygen exists in ordered form, joining a planar structure with the copper atoms. $YBa_2Cu_3O_{7-\delta}$ is tetragonal for low x - high δ, with a = b, see figure 1.1(a). However, this symmetry is destroyed with oxygen doping,

due to the resulting oxygen ordering and the formation of linear chains, characteristic of $YBa_2Cu_3O_{7-\delta}$ (fig.1.1(b)). The first fragments of chains are created at low x values and grow with increasing oxygen doping; when they are sufficiently organized to all align to the same direction, a transition from the tetragonal to an orthorhombic structure is sustained. Now, the two axes a and b of the original tetragonal cell are no more the same: a = 0.383 nm, b = 0.388 nm, c = 1.171 nm [6,7]. As seen in the schematic presentation of figure 1.2, $YBa_2Cu_3O_{7-\delta}$ is tetragonal for $0.6 \leq \delta \leq 1$ and it is only for δ less than almost 0.6 that a transition to the orthorhombic state takes place. In addition, $YBa_2Cu_3O_{7-\delta}$ contains Y and Ba isolation or separation planes.

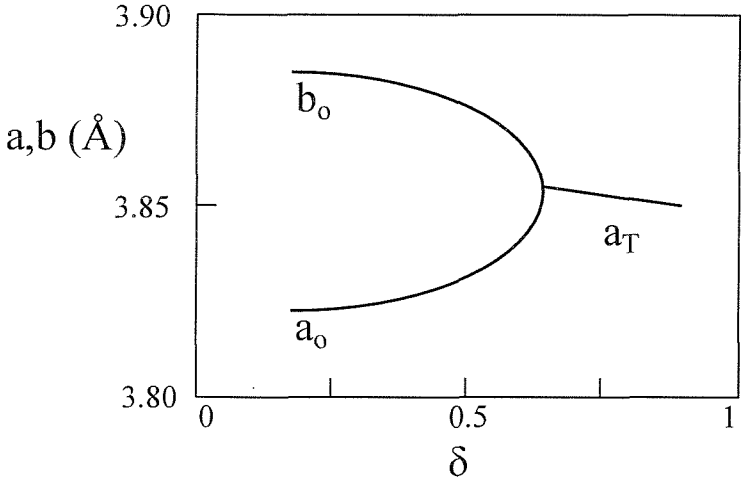

Figure 1.2: *The transition of the lattice parameters* a *and* b *from the orthorhombic* (a_o, b_o) *to the tetragonal phase* (a_T) *with oxygen deficiency,* δ, *in* $YBa_2Cu_3O_{7-\delta}$. *The diagram drawn is based on data by Jorgensen et al. [8].*

The effect of oxygen stoichiometry, which will be discussed in more detail in chapter 3, is dramatic, as the transition from the tetragonal to the orthorhombic phase is joined by a transition from a non superconducting to a superconducting state.

Indeed, oxygen doping in YBCO increases the fraction p of holes per Cu atom in the CuO_2 layer. This increase of the hole concentration p happens specifically in the CuO_2 layers where the "seat" of superconductivity lays. Positive holes are in most HTS the itinerant charge carriers. When δ=1 (p=0) $YBa_2Cu_3O_6$ is an antiferromagnetic insulator (fig. 1.3), but as δ decreases (p increases) the oxide becomes, in sequence, a non-

magnetic insulator and a superconductor for δ less than approximately 0.6 (or a normal conducting metal above T_c). This bewildering complexity of YBCO is common in all HTS oxides and made these materials to seem very improbable superconductors before 1986 [7].

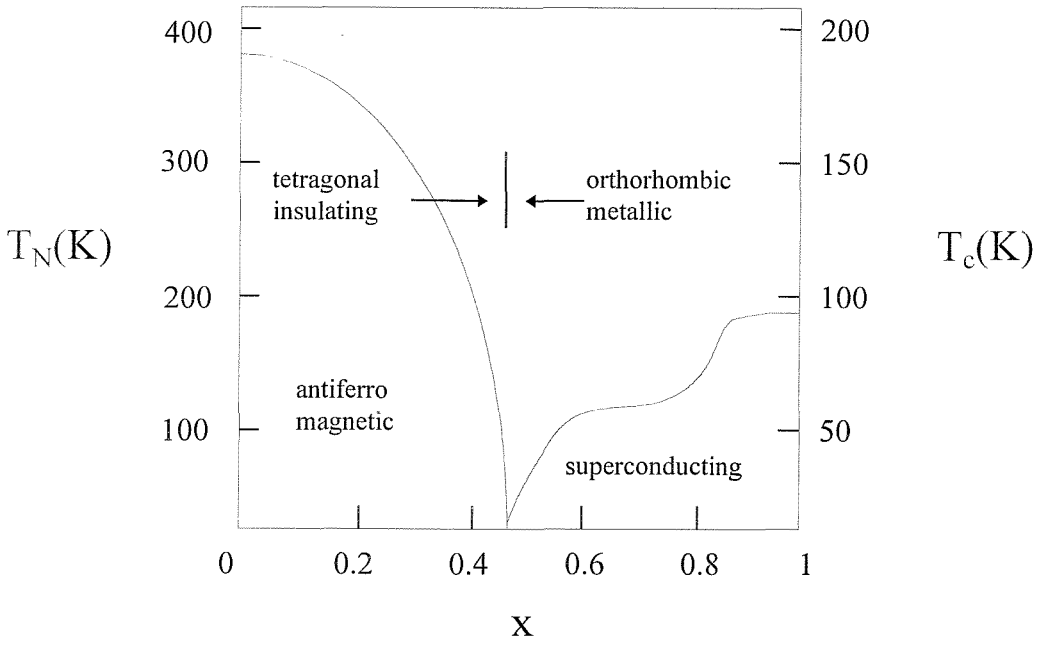

Figure 1.3: *Structural phase diagram of* $YBa_2Cu_3O_{6+x}$ *based on the data of ref.[9].*

1.2.2 PHYSICAL PARAMETERS

As a genuine member of the HTS family, YBCO is an extreme type-II superconductor. This means that it has a very short coherence length ξ and a very large magnetic field penetration depth λ. Due to the arrangement of the atoms in parallel planes there is a strong anisotropy present both in the superconducting and the normal state properties [10]. In the ab plane direction, i.e. parallel to the atomic planes, the superconducting properties are much stronger than in the perpendicular direction (c-axis) [10]. Thus, if λ_{ab} characterises screening by currents flowing in the layers and λ_c

screening by currents across the layers, it is $\lambda_{ab}(0) \approx 150$ nm while $\lambda_c(0) \approx 600$ nm. On the other hand, if ξ_{ab} is the transverse coherence length, within the layers, and ξ_c the coherence length across the layers, it is $\xi_{ab}(0) \approx 1.5$ nm and $\xi_c(0) \approx 0.3$ nm [2,11,12]. In result the Ginzburg-Landau constant κ is much bigger along the layers: $\kappa_c \approx 100$ compared with $\kappa_{ab} \approx 500$ along the c-axis.

The anisotropy parameter γ, defined as the square root of the ratio of the charge carriers effective mass along the c-axis m_c and in the ab plane m_{ab}, $\gamma = (m_c/m_{ab})^{1/2}$ has a value 4-10 as measured by torque magnetometry [13,14] and Bitter decoration technique [15]. Note that the anisotropy can be also defined as a ratio of the penetration depths or of the coherence lengths along the c-axis and in the ab plane, namely $\gamma = (\xi_{ab}/\xi_c) = (\lambda_c/\lambda_{ab})$.

Finally, for an applied field parallel to the ab plane estimates for the upper critical field give an $H_{c2}^{\parallel}(0) \approx 650$ T, while the lower critical field was found to be of the order of $H_{c1}^{\parallel}(0) \approx 180$ Oe; for a perpendicular to the layers applied magnetic field the corresponding values are $H_{c2}^{\perp}(0) \approx 130$ T and $H_{c1}^{\perp}(0) \approx 530$ Oe [12,16,17].

1.3 OUTLINE

This thesis is the outcome of an experimental work which started in October 1994 and lasted for three years. The bulk of the experiments was carried out on a variety of high quality single crystals of YBCO.

Chapter 2 introduces and briefly discusses some basic phenomenological approximations governing vortex dynamics in the HTS family. The reader is familiarized with some of the most useful models and tools which are of frequent use in the interpretation and discussion of experimental results.

Chapter 3 gives a brief account of the main experimental rigs used to produce the results of the next chapters. Simultaneously, the synthesis and the variation of the oxygen content of the studied YBCO single crystals is discussed. Certain very specific and important points on the preparation of the samples used in the experiments, which affect their physical properties, are presented.

In *Chapter 4*, we show by means of magnetic measurements, at a time when twin boundaries were predominantly considered only as strong pinning centres, that easy vortex motion can occur in paths created by the twin planes, with serious consequences in the critical current density. A study of this channeling behavior in a large temperature and magnetic fields regime reveals the competitive nature of planar and point defects.

By combining vibrating sample magnetometry and magnetotransport data, new features of the vortex phase diagram are revealed in *Chapter 5*. A vertical phase transition is traced in the solid region of the vortex state and is studied systematically, whereas oxygen deficiency is shown to have a dramatic effect in the H-T diagram. The obtained results are compared with those recently found in the $Bi_2Sr_2CaCu_2O_8$ compound.

Intrinsic pinning in the layered HTS is examined in *Chapter 6*. The observation of lock-in oscillations in magnetic measurements allows the study of the quasi-2D regime. The detailed mechanism which produces the oscillations is presented and discussed. Lock-in oscillations are shown to be a reliable way of extracting valuable information both for the structure of the vortex lattice and the sample. The critical importance of thermal fluctuations and of point disorder in the observation of the lock-in transition is also demonstrated.

Finally, *Chapter 7* offers a brief summary of the presented work and reiterates the main conclusions.

The work in this thesis was funded throughout its duration by the Bodosaki Foundation in Greece and in periods by the University of Southampton and E.P.S.R.C. (Engineering and Physical Sciences Research Council) in Great Britain. The author gratefully acknowledges the support of the above institutions and organisations.

REFERENCES

[1] G. Blatter, M. V. Feigel'man, V. B. Geshkenbein *et al.*, Rev. of Mod. Phys. **66**, 1125 (1994).

[2] M. Tinkham, *Introduction to Superconductivity*, McGraw-Hill, Singapore (1996).

[3] M. K. Wu, J. R. Ashburn, C. J. Torng *et al.*, Phys. Rev. Lett. **58**, 908 (1987).

[4] S. Hikami, T. Hirai, S. Kagohima, Jpn. J. Appl. Phys. **26**, L314 (1987).

[5] Z. X. Zhao, L. Q. Chen, Q. S. Yang *et al.*, Kexue Tongbao **33**, 661 (1987).

[6] A. W. Sleight, Science **242**, 1519 (1988).

[7] J. C. Gallop, *SQUIDs, the Josephson Effects and Superconducting Electronics*, IOP - Adam Hilger, Bristol (1991).

[8] J. D. Jorgensen, B. W. Veal, A. P. Paulikas *et al.*, Phys. Rev. B **41**, 1863 (1990).

[9] P. Burlet, C. Vettier. M. J. G. M. Jurgens *et al.*, Physica C **153-155**, 1115 (1988).

[10] A. C. Rose-Innes and E. H. Rhoderick, *Introduction to Superconductivity*, Pergamon (1994).

[11] J. G. Ossandon, J. R. Thompson, D. K. Christen *et al.*, Phys. Rev. B **45**, 12534 (1992).

[12] G. Burns, *High-Temperature Superconductivity - An Introduction*, Academic Press (1992).

[13] D. E. Farrell, C. M. Williams, S. A. Wolf *et al.*, Phys. Rev. Lett. **61**, 2805 (1988); D. E. Farrell, J. P. Rice, D. M. Ginsberg *et al.*, Phys. Rev. Lett. **64**, 1573 (1990).

[14] T. R. Chien, W. R. Datars, B. W. Veal *et al*, Physica C **229**, 273 (1994).

[15] G. J. Dolan, F. Holtzberg, C. Feild *et al.*, Phys. Rev. Lett. **62**, 2184 (1989).

[16] U. Welp, W. K. Kwok, G. W. Crabtree *et al.*, Phys. Rev. Lett. **62**, 1908 (1989).

[17] L. Krusin-Elbaum, A. P. Malozemoff, Y. Yeshurun *et al.*, Phys. Rev. B **39**, 2936 (1989).

2. DYNAMICS OF VORTICES

2.1 VORTEX MOTION

As mentioned in chapter 1, the key question in the study of vortices is whether these flux carrying entities move or not. In the imaginary case of a pure, isotropic, type II superconductor, in the mixed state, one expects the formation of the famous triangular Abrikosov lattice [1,2]. If, now, a current density J is passed through the material and B is the local flux density, vortices will experience a Lorentz force equal to:

$$\vec{F}_L = \vec{J} \times \vec{B} \tag{2.1}$$

Under the influence of this Lorentz force, vortices will move in a direction perpendicular to both the current and the applied field (figure 2.1), facing only an impedance of viscous nature [3].

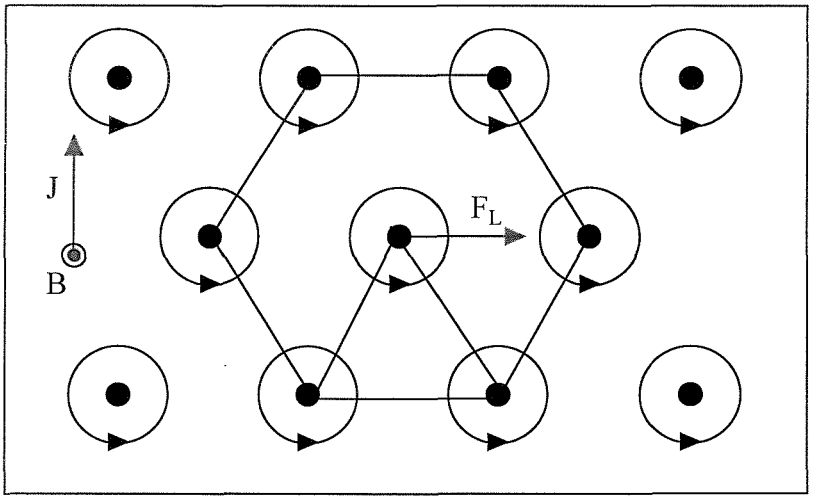

Figure 2.1: *Vortices forming a hexagonal, periodic lattice (Abrikosov lattice). Under the influence of an applied current* J, *a Lorentz force* F_L *moves vortices in a perpendicular to the applied field and current direction.*

This motion of vortices and consequently of their normal cores generates an electric field [4], produces a voltage drop and yields a finite and linear flux flow resistivity,

$$\rho_f = \rho_n \frac{H_a}{H_{c2}} \tag{2.2}$$

where ρ_f is the flux flow resistivity, ρ_n the normal state resistivity, H_a the applied field and H_{c2} the upper critical field.

The above conditions lead to a reversible magnetic response of the superconductor in an external magnetic field (figure 2.2). For an applied field of strength up to H_{c1}, the superconductor exhibits perfect diamagnetism; for higher fields, vortices invade in the interior of the sample and the magnitude of the magnetisation drops until it disappears, together with superconductivity, at H_{c2}. Both transitions at H_{c1} and H_{c2} are predicted to be of second order.

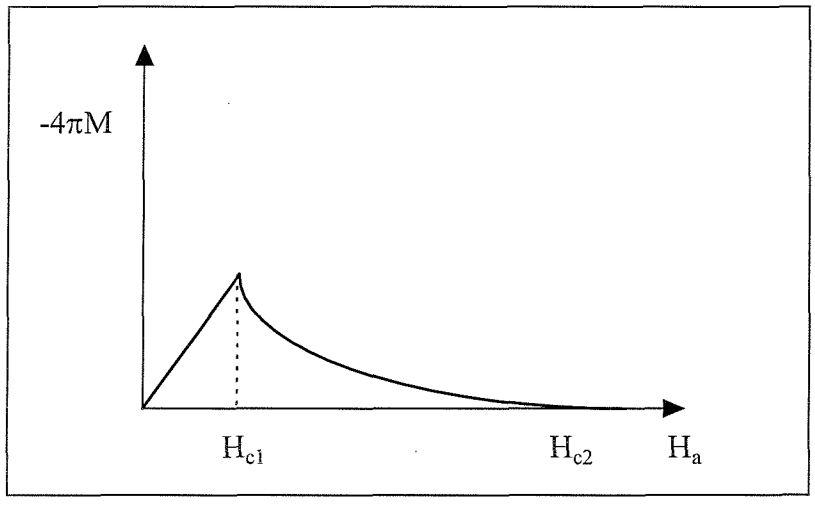

Figure 2.2: *Magnetisation curve for a type II superconductor, in the absence of pinning.*

However "purity" is an unknown term in the science of material synthesis. Real materials often contain a rich variety of point or extended, structural, crystal defects; in the case of superconductors the defects (which can be for example non superconducting impurities, voids etc.) lower the local condensation energy and cause the well-known and very essential immobilisation mechanism called *pinning* of vortices.

Pinning changes and complicates the situation considerably. Now the Lorentz force has to be larger in magnitude than the pinning force exerted on a vortex, for the latter to move: $F_L > F_P$. Early models trying to incorporate this fact, as the Bean model [5,6],

defined a state called the "critical state": vortices arrange themselves in such a way in the sample, that the produced flux profile results to a global equalization of F_L and F_P. In other words, the achieved balance satisfies vortices enough so as to no longer move. The resulting current density is called critical current density, J_c.

In the limit of zero temperature and given the condition $F_L = F_P$ holds, according to the critical state model vortices should stay pinned and flux motion (flux creep) should remain zero. However reality is different: due to quantum tunneling effects, vortices are able to tunnel through the pinning barriers even for Lorentz forces smaller than the opposing pinning ones (quantum creep) [7-10].

Returning to more "realistic" situations (at finite temperatures), thermally assisted effects were accounted for first in the Anderson-Kim model [11,12]. In high temperature superconductors thermal effects are not restricted to the vicinity of T_c, as in conventional superconductors, but are extended in a large temperature regime below the critical temperature. As mentioned in the introduction (chapter 1) and successfully accounted for by the Ginzburg number[1], the small coherence length ξ, the large magnetic penetration depth λ and the large anisotropy of HTS, all greatly enhance thermal fluctuations. The result is the observance of flux creep even at current values lower than the critical one, due to thermal activation over the pinning barriers.

The Anderson-Kim model describes this hopping over the potential barriers considering motion of characteristic flux volumes, the vortex bundles [11-13]. The formation of bundles is energetically favorable, since the range of the repulsive vortex-vortex interactions λ is much larger than the separation of neighboring vortices, α_o [11-13]; vortices, members of the same bundle, act in cooperation and move as a unit[2]. In its simplicity, the model makes some important assumptions. It assumes: a) the bundle volume V and its jumping distance d to be constant and current independent, b) the shape of the pinning potential well to be triangular with a maximum, current independent, value U_0 and c) elastically independent flux bundles .

---

[1] In $YBa_2Cu_3O_{7-\delta}$, Gi ~ 10^{-2}.

[2] More precisely, vortices in one bundle are mutually coupled via the interaction of their magnetic fields and their wavefunctions [11,12].

Assuming that the centre of the bundle sits in a potential well U_0 (figure 2.3(a)), where U_0 is the Gibbs energy difference between the pinned and the unpinned state [14] in the absence of any driving forces, it is possible due to thermal excitation for the bundle to overcome the barrier in a rate:

$$R = \Omega_0 \cdot e^{-\frac{U_0}{\kappa_B T}} \tag{2.3}$$

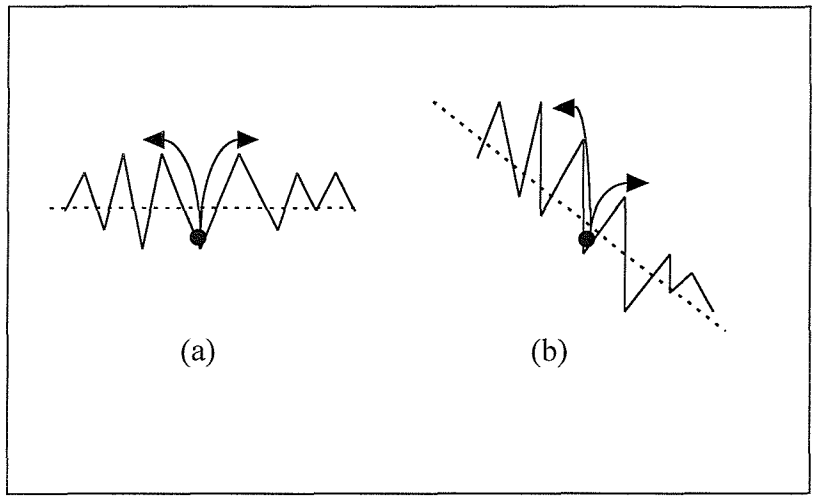

Figure 2.3: *Flux bundles jumping over pinning barriers, after ref.[3]. The continuous line represents the relative total free energy as a function of the position of the centre of the bundle. (a) Without any driving force (b) A driving force due to an applied current or a flux gradient, favors jumps in one, the "downhill", direction.*

where κ_B is the Boltzmann constant and Ω_0 is the average attempt frequency of hopping ($\sim 10^5$-10^{11} Hz) [3], due to the thermal motion of the pins which causes fluctuations in time of the pinning force [15,16]. From eq.(2.3) it is clear that the rate R crucially depends on temperature. However no net motion can be observed, since the rate is the same for both directions of hopping (fig.2.3(a)).

Assuming that each bundle of volume V is intersected by one pinning site, the pinning energy per unit volume should be U_0/V and thus $U_0 = F_P\, Vd = J_0\, BVd$, where d is the distance the bundle jumps once it is unpinned; one can assume that this distance d is approximately equal to the vortex separation $\alpha_0 = (\Phi_0/B)^{1/2}$ [14]. J_0 is the critical

current in the absence of creep. On the other hand, applying a driving force $F_L = JB$, produces an external stress $\Delta W = JBVd = U_0 (J/J_0)$. Now, hopping out of the potential well is clearly favorable in one direction (fig.2.3(b)) and the net hopping rate R becomes, after summing up the two rates for jumping in the opposite directions [11,12]:

$$R_{net} = 2 \cdot \Omega_o \cdot \sinh\left(\frac{\Delta W}{\kappa_B T}\right) \cdot e^{-\frac{U_O}{\kappa_B T}} \tag{2.4}$$

Anderson analyzed the case of large current $J \sim J_c$ and high imposed stress or, equivalently, of very low temperatures, $\Delta W >> \kappa_B T$, the so-called *flux creep* regime [11,13]. He supposed that the trapping barrier U is finite when the applied current density J tends to 0, depending linearly on J:

$$\left.\begin{array}{l} U(J) = U_o \left[1 - \left(\frac{J}{J_o}\right)\right] \\ J \to 0 \end{array}\right\} \Rightarrow U(J) \to U_o \tag{2.5}$$

With the above conditions, the net hopping rate becomes:

$$R = \Omega_o \cdot e^{\frac{\Delta W - U_O}{\kappa_B T}} \tag{2.6}$$

The opposite case, of low current and imposed stress or, equivalently, of high temperatures $\Delta W << \kappa_B T$, was studied much later, only with the appearance of the first high temperature superconductors. Modeling of this regime, often called the *thermally assisted flux flow* (TAFF) regime, came in the late eighties [14,15,17,18].

The TAFF model is essentially an extension of the Anderson-Kim model to the new conditions described above. Again the assumption of a current independent pinning potential at very low currents $J << J_c$ is made, see also eq.(2.5) above. The net rate of hopping is now:

$$R_{net} = 2 \cdot \Omega_o \cdot \frac{\Delta W}{\kappa_B T} \cdot e^{-\frac{U_o}{\kappa_B T}} \tag{2.7}$$

The resulting electric field from the vortex motion is $E = Bv$, where v is the average velocity of the motion $v = R_{net} d = R_{net} \alpha_o$, leading to:

$$E = 2 \cdot \alpha_o \cdot B \cdot \Omega_o \cdot \frac{U_o}{\kappa_B T} \cdot \frac{J}{J_o} \cdot e^{-\frac{U_o}{\kappa_B T}} \tag{2.8}$$

This yields a TAFF resistivity $\rho_{TAFF} = E/J$, equal to:

$$\rho_{TAFF} = 2 \cdot \frac{\alpha_o \cdot B \cdot U_o}{\kappa_B T \cdot J_o} \cdot e^{-\frac{U_o}{\kappa_B T}} \tag{2.9}$$

Substituting for U_0 and then for α_o^2 leads to a TAFF resistivity linear with magnetic induction B; this linear, ohmic resistivity is always nonzero, even if it is exponentially small. Note that the upper limit of ρ_{TAFF} is the flux flow resistivity, ρ_f.

2.2 VORTEX LATTICE ELASTICITY

The elasticity the vortex lattice possesses, is expressed via the elastic moduli: c_{11} describes the rigidity of the vortex lattice against uniform compression and is called the bulk modulus; c_{44} describes the stiffness against tilt of the lattice with respect to the applied field and is called the tilt modulus; finally the shear modulus, c_{66}, expresses the lattice's resistance to shear.

The elastic moduli were first calculated by Brandt [19] using linear elasticity theory, for the case of a continuum, uniaxial, elastic medium. Due to the long range interaction of vortices, extending to distance λ often much larger than α_o, the character of the elastic interactions becomes nonlocal: the elastic energy of a local distortion of the lattice will be contained in a sphere of radius[1] of the order of λ. As a result two of the elastic coefficients, the bulk and the tilt modulus, for the isotropic superconductor case, are dispersive, that is they have a k-dependence. Assuming that $H << H_{c2}$ and the Ginzburg-Landau constant[2] $\kappa >> 1$, the elastic coefficients are [21]:

[1] Actually of radius of several λ, according to Brandt [20].

[2] See section 1.2.2 for values of κ in $YBa_2Cu_3O_{7-\delta}$.

$$c_{11}(k) = \frac{B^2}{\mu_o \cdot \left(1 + k^2 \cdot \lambda^2\right)} \quad , c_{44}(k) = \frac{B^2}{\mu_o} \cdot \left[\frac{1}{1 + k^2 \cdot \lambda^2} + \frac{\ln \tilde{\kappa}}{k_{BZ}^2 \cdot \lambda^2} \right] \qquad (2.10)$$

$$c_{66} = \frac{B \cdot \Phi_o}{16 \cdot \pi \cdot \mu_o \cdot \lambda^2}$$

In the above expressions, λ is the planar penetration depth and $k_{BZ} = 2\sqrt{\pi}/\alpha_o$ is the radius of the Brillouin zone. It turns out that $k_\perp = (k_x , k_y) \leq k_{BZ}$, a condition that protects the continuum limit approximation [22]; in the expression of $c_{44}(k)$, $\tilde{\kappa}$ is a function of the tilt k_z component of the wave vector:

$$\tilde{\kappa} = \sqrt{\frac{1 + \kappa^2 + k_z^2 \cdot \lambda^2}{1 + b \cdot \kappa^2 + k_z^2 \cdot \lambda^2}} \qquad (2.11)$$

with $b = (B/B_{c2})$. Though k_z can be in theory arbitrarily large due to the continuity of vortices along the c-axis, in practice it is limited by the vortex core radius: the shortest tilt waves that pinning can excite have $k_z \leq 1/\xi$ [22]. As seen in eq.(2.10), c_{44} is written as the sum of two terms: $c_{44}(k) = c_{44}^{\,o}(k) + c_{44}^{\,c}(k)$. The first term is of collective origin and stands for the bulk contribution while the second term represents the single or isolated vortex contribution. Note that c_{66} becomes dispersive at very short wavelength scales [23].

The dispersion of c_{11} and c_{44} means that the lattice is much more susceptible in short wavelength compressional and tilt distortions than to uniform ones. Indeed, contrary to the uniform distortions case, where the wavelength $l \rightarrow \infty$ and, thus, $k \rightarrow 0$, now the dispersion of the elastic moduli allows a suppression factor of $(k\ \lambda)^2$ for shorter wavelengths, i.e. for a non-zero wavevector k.

This suppression becomes even larger for k near the Brillouin zone limit, k_{BZ}. Simultaneously, at this limit, $c_{44}(k_{BZ})$ is dominated by the isolated vortex contribution, $c_{44}^{c}(k_{BZ})$ and $c_{11}(k_{BZ})$ is of the order of c_{66} [23] (see figure 2.4).

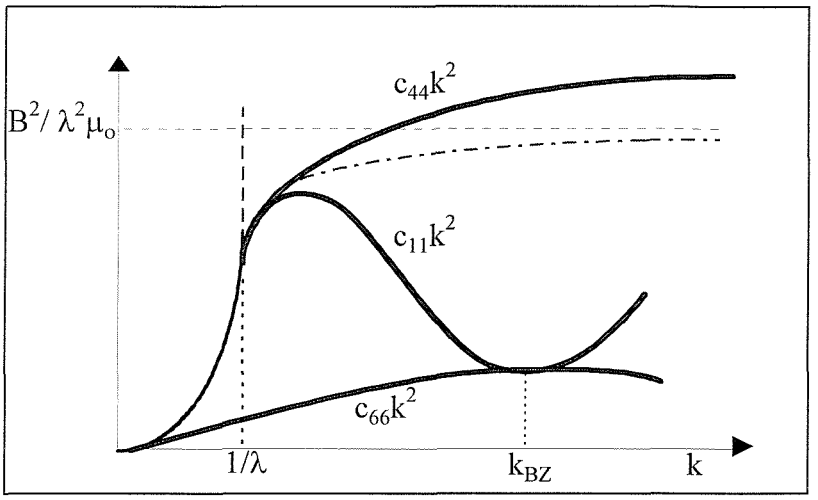

Figure 2.4: *Elastic energies for compressional, tilt and shear distortions of the vortex lattice for unit volume and displacement amplitude estimated in ref.[4]. The parabolic dashed line gives the local contribution for tilt and compressional energies, valid for* $k << \lambda^{-1}$. *The dashed-dotted curve gives the bulk (collective) term of* $c_{44}(k)$, $c_{44}^{o}(k)$. *The difference of the bulk term from the total* $c_{44}(k)$ *is a result of the isolated vortex contribution,* $c_{44}^{c}(k)$. *Both* c_{11} *and* c_{66} *are periodic in k-space. Remarkably, although* c_{66} *is much smaller than* c_{11}, *it recovers at* k_{BZ}.

At very small field values, $B << B_{c1}/\ln\kappa$, the bulk and shear moduli become exponentially small, with $c_{11} = 3c_{66}$ and [23,24]:

$$c_{66} = \left(\frac{\pi \cdot \lambda}{6 \cdot \alpha_o}\right)^{1/2} \cdot \frac{\varepsilon_o}{\lambda^2} \cdot e^{-\frac{\alpha_o}{\lambda}} \qquad (2.12)$$

where ε_o is the line self energy, a very frequently used and basic energy scale. At this low field limit $c_{44}(k)$ is also dominated by the single vortex contribution. At the opposite limit of large fields, $B >> B_{c1}/\ln\kappa$, one has $c_{66} << c_{11} \approx c_{44} \approx B^2/\mu_o$, and the lattice bears the characteristics of an incompressible solid [4] (figure 2.5).

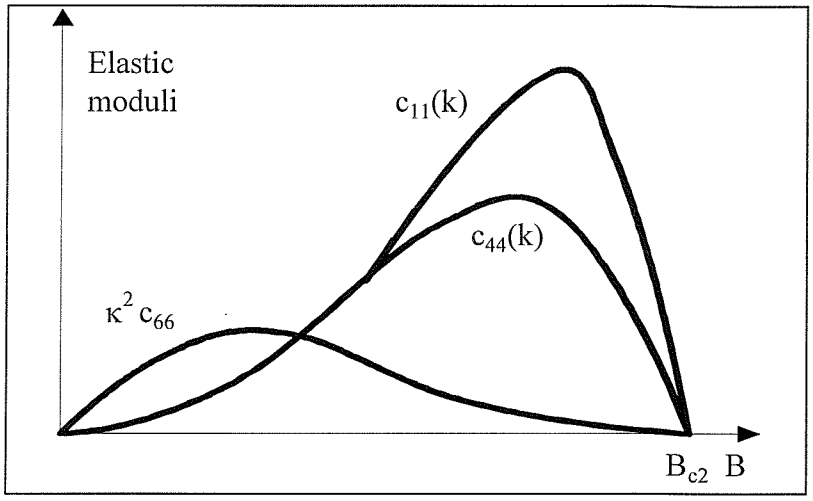

Figure 2.5: *The elastic coefficients as a function of the magnetic flux density,* B *as estimated by Brandt, ref.[20].*

For an anisotropic superconductor, the main difference is the dramatic dependence of c_{44} and c_{66} on the anisotropy.

For an applied field $H_a \parallel$ c-axis[1] and a uniaxially anisotropic superconductor, with penetration depths λ_{ab} along the c-axis and λ_c in the ab plane, one has [21]:

$$c_{11}(k) = \frac{B^2}{\mu_o} \cdot \frac{1 + k^2 \cdot \lambda_c^2}{\left(1 + k^2 \cdot \lambda_{ab}^2\right) \cdot \left(1 + k_\perp^2 \cdot \lambda_c^2 + k_z^2 \cdot \lambda_{ab}^2\right)} \tag{2.13}$$

$$c_{44}(k) = \frac{B^2}{\mu_o} \cdot \left(\frac{1}{1 + k_\perp^2 \cdot \lambda_c^2 + k_z^2 \cdot \lambda_{ab}^2} + \frac{\ln \tilde{\kappa}}{k_{BZ}^2 \cdot \lambda_c^2} \right)$$

The shear modulus, c_{66}, is not altered from expression (2.10), with λ being replaced by the penetration depth λ_{ab}. The same cutoff limits for k hold as for the isotropic case. The results apply as long as $b < 0.25$ and $\kappa > 2$. For fields approaching H_{c2} the penetration depths in the above expressions should be corrected [20] to account for their increase as the Cooper pairs density goes to zero.

Comparing to the isotropic case, c_{44} is smaller by a factor of γ^2, an effect of the much longer range of the interactions, λ_c. It is, therefore, obvious that uniaxially anisotropic

[1] Interestingly, for a general orientation of H with respect to the c-axis, a rotation modulus also appears [25].

high temperature superconductors, as $YBa_2Cu_3O_{7-\delta}$, allow far larger distortions for the same expense of elastic energy.

For fields along the ab plane, it is straightforward to estimate the elastic moduli using the scaling arguments of Blatter *et al.*, see ref.[23,26]. The essential modification is the splitting of the shear and tilt moduli into hard and soft components [25]. For c_{66}, the hard component, $c_{66}^{\perp}$, corresponds to shear direction along the c-axis, while the soft one, $c_{66}^{\parallel}$, parallel to the layers (figure 2.6). Their ratio is:

$$\frac{c_{66}^{\perp}}{c_{66}^{\parallel}} = \gamma^4 \quad \text{with} \quad c_{66}^{\perp} = \gamma \cdot c_{66} \tag{2.14}$$

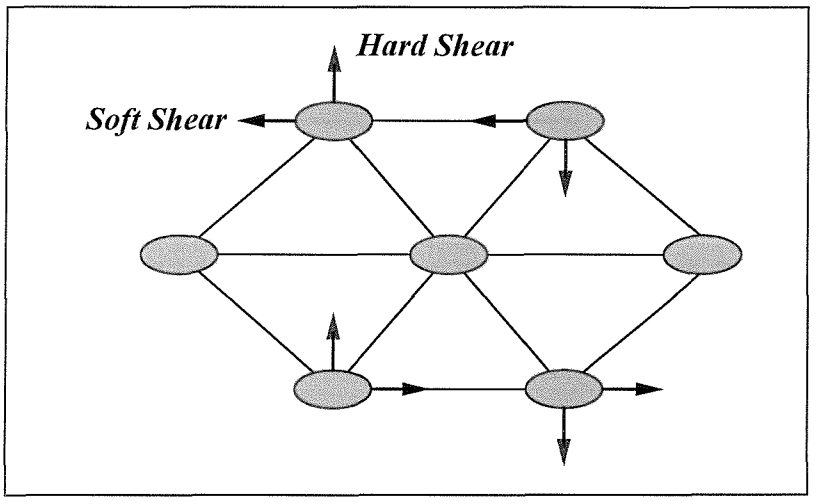

Figure 2.6: *The unit cell of the vortex lattice for an applied field between the layers and the two modes, soft and hard, of a shear wave.*

The tilt modulus, now, due to the splitting of the bulk term, $c_{44}^{\circ}(k)$, in hard and soft components, is affected and has a hard component, $c_{44}^{\perp}$, for out-of-plane tilt and a soft one, $c_{44}^{\parallel}$, for in-plane distortions. The scaling approach leads to the following dependencies [23]:

$$c_{44}^{\perp}(k) = \gamma^2 \cdot c_{44}^{\parallel}(k) \quad \text{with} \quad c_{44}^{\parallel}(k) = c_{44}(k) \tag{2.15}$$

2.3 COLLECTIVE PINNING

The *collective pinning* theory developed by Larkin and Ovchinnikov [27,28] came to interpret experimental situations which were in serious contradiction with the strong and weak pinning concepts, as these were distinguished until then by the metastability or Labusch criterion [29]. According to the metastability criterion, if a vortex displacement u(0) causes greater variation of the elementary pinning force f_p exerted on it than that of the elastic force f_{el} due to vortex-vortex interactions, then pinning dominates (strong pinning regime, figure 2.7) [16]:

$$\frac{d|f_p|}{du(0)} > \frac{d^2E_{el}}{du(0)^2} \tag{2.16}$$

where E_{el} is the elastic energy of the lattice associated to the displacement field u(0).

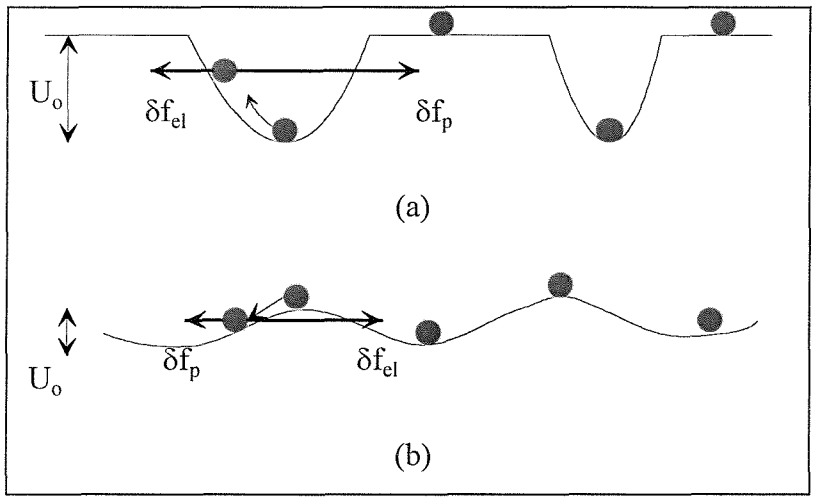

Figure 2.7: *Visualisation of the metastability criterion. (a) Strong pinning; a small displacement of a vortex leads to a larger variation of the pinning force* δf_p *than that of the interaction force with other vortices,* δf_{el}. *(b) weak pinning; the opposite.*

The metastability criterion, called Labusch criterion when the displacement fields of neighboring pinning centres do not overlap [16], was regarded as the definition of the absolute threshold below which macroscopic pinning cannot exist. However, the weak

pinning "landscape" realised in high temperature superconductors, soon gave results which could not be understood in the aforementioned frame.

Collective pinning came to accommodate the pinning paradox, emerging due to the interplay of a random pinning potential and the vortex lattice elasticity, much enhanced in the anisotropic HTS. Indeed, a perfectly periodic and rigid lattice, or line, cannot be pinned by a random collection of pinning centres [3,23]: taking the case of a volume of the flux line lattice V, containing N pinning centres, the Lorentz force for any applied current density J grows linearly with V, as JV. On the other hand, the summation of the random pinning forces on V grows only sublinearly as $\sqrt{N}$, or as $\sqrt{V}$, since N = nV, where n is the pinning centres density. It is straightforward to see that the critical current density J_c at which the Lorentz force is equal to the total pinning force, drops as $V^{-1/2}$, vanishing at large V.

In other words, the summation of the random pinning forces f_p in the volume V has as a result the summation, due to their randomness, of opposing pinning forces and, thus, the total pinning force is smaller than $\sum_V f_p$, what a direct summation would give - an effect known as "frustration" [16].

Solving this discrepancy, the collective pinning theory [27,28] suggests the description of the vortex lattice distortions in terms of correlated volumes, V_c. The main idea of the collective pinning theory is that there are two competing energies for any lattice distortions: the elastic energy and the pinning energy. Vortices will prefer to pass from certain pinning sites, lowering their free energy; such a departure from the perfect periodic arrangement, though, has to be paid for at the expense of the elastic energy. The sum of these two energies will be a minimum for the equilibrium configuration, allowing correlated volumes of the lattice, V_c, to be pinned independently from each other. V_c corresponds to the smallest scale above which a direct summation of the random pinning forces is justified, or else V_c is the desired cutoff limit for the sublinear growth of the pinning force, resulting from the statistical summation.

According to the above, there are two main conditions which the new theory brings forward:

1. At scales smaller than V_c the vortex lattice can be considered as perfectly rigid (figure 2.8). More precisely, the maximum pinning-caused mean-square vortex displacements $g(\vec{r}) = < |u(\vec{r})-u(0)|^2 >$ are smaller than the pinning force range r_p squared, $g(\vec{r}) \leq r_p^2 \approx \xi^2$.

2. The existence of a large density of weak, random, point pinning centres, $nV_c >> 1$, where n is the pinning sites density.

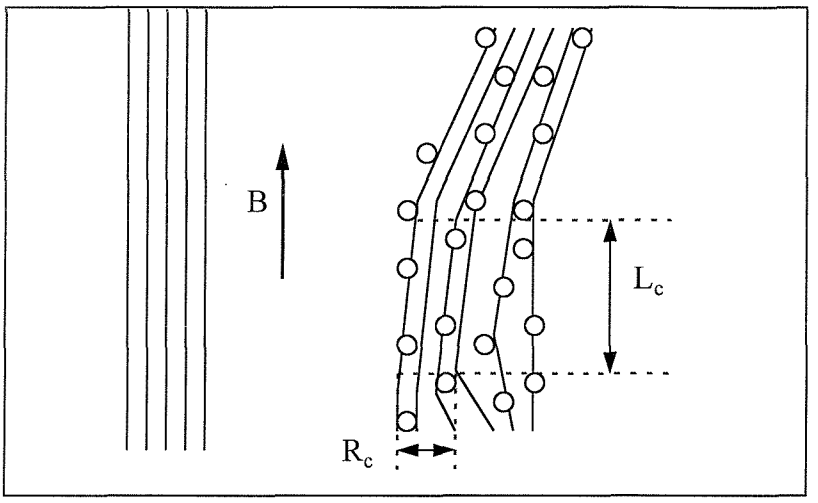

Figure 2.8: *The correlation volume concept. In the absence of pinning, vortices (thin lines) align perfectly with the field, forming a periodic lattice (a). In the presence of a large density of weak, random pins (open circles) they deviate from the field and break the positional order of the lattice, to profit from the pinning energy (b). Periodicity, in this case, according to collective pinning theory, is approximately preserved within a correlation volume,* $V_c = R_c^2 L_c$. *Within* V_c *the distortions are negligible (short range order).*

The dimensions of the correlated volume, V_c, along and perpendicular to the field direction, for an applied field normal to the layers, are L_c and R_c, respectively: $V_c = L_c R_c^2$. Due to the presence of pinning centres, the net free energy change per unit volume of the vortex lattice can be found by subtracting the pinning energy gained from the accommodation to these centres from the elastic energy, at zero current density. Pinning forces statistically sum, inside V_c, to $(nV_c)^{1/2} f_p$ [27,28]; taking into account the range of the pinning forces $r_p \approx \xi$, the amplitude of the pinning energy is $\xi(nV_c)^{1/2} f_p$, that

is $\xi n^{1/2} f_p / V_c^{1/2}$ per unit volume. The elastic energy, now, is estimated as a sum of the shear and tilt energy - we consider only the shear and tilt elastic moduli [4]. For the shear energy, the relevant length scale is the transverse correlation length R_c, while for the tilt energy it is the longitudinal correlation length L_c. The elastic energy is usually given as:

$$E_{el} = \frac{1}{2} \cdot \left[c_{66} \cdot \sigma_{66}^{\ 2} + c_{44} \cdot \sigma_{44}^{\ 2} \right] \tag{2.17}$$

where σ_{66} and σ_{44} are the shear and tilt fractional distortions (strains), respectively. Since maximum deformations[1] are of the order of ξ, the final outcome for the net free energy change per unit volume is:

$$\delta F = \frac{1}{2} \cdot c_{66} \cdot \left(\frac{\xi}{R_c} \right)^2 + \frac{1}{2} \cdot c_{44} \cdot \left(\frac{\xi}{L_c} \right)^2 - f_p \cdot \xi \cdot \left(\frac{n}{V_c} \right)^{1/2} \tag{2.18}$$

Minimising this expression in respect to L_c and R_c yields an ellipsoid or cigar-shaped V_c of radius $R_c = (2c_{44})^{1/2} c_{66}^{\ 3/2} \xi^2 / W$ and length $L_c = 2c_{44} c_{66} \xi^2 / W$, with $W = n\langle f_p \rangle^2$ being the total average pinning force per unit volume squared, a characteristic parameter of the pinning strength. Thus[2], $V_c = 4 c_{44}^{\ 2} c_{66}^{\ 4} \xi^6 / W^3$.

A softer, more elastic, lattice would offer better adjustment to the pinning sites and, consequently, provide smaller correlation volumes. Similar effects would result from stronger pinning. For pinning energies large enough for R_c to become comparable to α_o, the collective pinning of bundles gives its place to the collective pinning of individual vortices (single vortex collective pinning). Further increase of pinning can lead to a shrinking of L_c to length scales comparable to r_p or ξ and validate a direct summation of the pinning centers, having as unique criterion the spacing of the pins compared to α_o [4].

The zero temperature critical current J_o can be easily defined by the maximum Lorentz force density that can be sustained:

---

[1] In the estimation of the critical current, maximum deformations are the relevant ones.

[2] A more accurate calculation of V_c at 3D requires to approximate it as a spherical volume: $V_c = (4/3)\, \pi\, L_c\, R_c^2$.

$$J_o \cdot B = \left(\frac{W}{V_c}\right)^{1/2} \Rightarrow J_o = \frac{n^2 \cdot f_p^4}{2 \cdot c_{44} \cdot c_{66}^2 \cdot \xi^3 \cdot B} \tag{2.19}$$

At this point, some remarks should be made on the elasticity theory used. First, the elastic moduli expressions omit any corrections arising due to nonlocality, unless $R_c < \lambda$. Second, collective pinning theory as this described uses linear elasticity theory which breaks down with the c_{66} vanishing at the melting line, see chapter 5.

2.4 COLLECTIVE CREEP

All the above discussion is valid as long as thermal activation is zero, i.e. for $T = 0$. As soon as we depart from this condition, $T > 0$, collective pinning theory gives way to the theory of *collective creep*. In its attempt to explain the giant flux creep observed in high temperature superconductors in the frame of collective pinning by weak disorder, collective creep considers a new current dependence of the correlation volume and the activation energy. In this way, a large departure from the more or less "classic" models of creep, like the Anderson-Kim model and its derivative TAFF model, is made.

The transition between metastable states is due to thermal activation and the free energy barriers that are opposing these transitions, U(J), are estimated down to very small current densities, $J << J_c$ [30,31]. Furthermore, collective creep theory considers the correlation between the jumping flux unit and the surrounding ones. The new current dependent correlation lengths, R_J and L_J, define the smallest possible volume V_J which can jump while the neighboring lattice is kept fixed. The balance of the elastic energy E_{el} and the energy produced by the Lorentz force, $E_L = JBV_Jd_J$, determines this jumping volume V_J and consequently defines the stable configuration. The jumping distance d_j is an also current dependent quantity. Unlike the case of collective pinning, the compression modulus c_{11} plays an active role in the physics of collective creep, since it is the main mechanism of interaction between the jumping flux bundles, or correlated volumes.

An estimation of V_J in this way by Feigel'man *et al.* [30] yields a correlated volume that increases with J decreasing, becoming infinite at $J \rightarrow 0$. The divergence of V_J obeys a power law, $V_J \propto J^{-\mu}$, with $\mu > 0$.

The estimated current dependence of U(J) is the most important result of the collective creep approach [30-32]. While the Anderson-Kim condition of $U(J) = U_o + f(J)$ led to the recovery of a finite barrier even at zero applied currents, now, due to the current dependence of V_J, U(J) grows with the decrease of J following a power law: $U(J) \propto V_J \propto J^{-\mu}$. This results in a free energy barrier which is infinite at zero current - in other words in a resistivity ρ which is truly zero in the limit $J \rightarrow 0$.

The exponent μ varies depending on the size of V_J or, equivalently, the applied current density. According to Feigel'man *et al.* [30], for a bundle consisting of a segment L_J of a vortex line, $\mu = 1/7$. For small J, V_J acquires a transverse size $R_J < \lambda$, and for this small bundle regime $\mu = 3/2$. For even lower current densities, $R_J > \lambda$ and $\mu = 7/9$. Also in this large bundle limit, as in the case of collective pinning, the elastic moduli loose their nonlocality corrections. Blatter *et al.* [23] give a still wealthier analysis of the variations of the exponent μ.

Following the above, collective creep gives a non-linear current-voltage (I-V) characteristic, of the form:

$$E(J) \propto \exp\left[-\frac{U_o}{kT}\cdot\left(\frac{J_c}{J}\right)\right]^{\mu} \qquad (2.20)$$

There is an important limitation to the reliability of collective creep. Collective creep, like collective pinning, considers only elastic procedures and at high temperatures or very low currents there is always the danger that U(J) grows enough to surpass the threshold for plastic deformations, U_{pl}. Then the activation energy should remain finite even in the limit $J \rightarrow 0$, since it is plastic procedures that control the creep and U_{pl} is essentially current independent [30].

2.5 VORTEX GLASS

Similarly to collective creep, the Vortex Glass model predicts the destruction of long range order in the vortex lattice, in the presence of disorder and infinite activation barriers for zero densities of applied currents [33,34], of the form $U \propto J^{-\mu}$, recovering, thus, truly superconductive properties in the limit of zero current density. As a result, like in the collective creep case, non-linear I-V characteristics are obtained:

$$E(J) \propto \exp\left[-\left(\frac{J_T}{J}\right)\right]^{\mu}, 0 \leq \mu \leq 1 \qquad (2.21)$$

where $J_T \approx \varepsilon_l^2 / \kappa_B T$ sets the current scale [35], ε_l being the line tension of the single vortex.

One of the main changes the Vortex Glass theory brings forward is its starting point: it provides a very general approach to the problem of quenched disorder. Thus, although, as in the collective creep model, it reaches the conclusion that disorder completely destroys the long range periodicity of the Abrikosov lattice and positional order survives only at small scales [33,34], now there is no need to start by assuming elastic properties for the vortex lattice and their preservation in the presence of weak disorder [23].

The model introduces a certain temperature T_g: as the temperature approaches T_g from below, a characteristic correlation length ξ_G, the size of the jumping volume in the vortex lattice, diverges as $\xi_G \propto |T - T_g|^{\nu}$, ν being a critical exponent. Furthermore, T_g separates linear (ohmic) resistance, for $T > T_g$, from non-linear (exponentially small), for $T < T_g$, at the limit of vanishing current densities; the transition from one regime to the other is continuous. For the boundary $T = T_g$ a power-law I-V characteristic is predicted by Fisher *et al.* [33,34].

Finally, the Vortex Glass theory predicts universal scaling laws: physical quantities should scale with an appropriate power of $(T-T_g)$. Indeed, scaling of the I-V curves has been one of the most frequently used tools in the quest of a Vortex Glass phase, e.g. in the work of Koch *et al.* in thin films of $YBa_2Cu_3O_{7-\delta}$ [36,37] or Gammel *et al.* in single crystals [38].

REFERENCES

[1] A. A. Abrikosov, Zh. Eksp. Teor. Fiz. **32**, 1442 (1957); Sov. Phys. JETP **5**, 1174 (1957).

[2] W. H. Kleiner, L. M. Roth, S. H. Auther, Phys. Rev. **133**, A1226 (1964).

[3] M. Tinkham, *Introduction to Superconductivity*, McGraw-Hill, Singapore (1996).

[4] E. H. Brandt, Rep. Prog. Phys. **58**, 1465 (1995).

[5] C. P. Bean, Phys. Rev. Lett. **8**, 250 (1962).

[6] C. P. Bean, Rev. Mod. Phys. **36**, 31 (1964).

[7] J. G. Lensink, C. F. J. Flipse, J. Roobeek *et al.*, Physica C **162-164**, 663 (1989).

[8] R. Griessen, Phys. Rev. Lett. **64**, 1674 (1991).

[9] L. Glazman and N. Ya Fogel', Sov. J. Low Temp. Phys. **10**, 51 (1984).

[10] L. Radzihovsky, Phys. Rev. Lett. **74**, 4919 (1995).

[11] P. W. Anderson, Phys. Rev. Lett. **9**, 309 (1962).

[12] P. W. Anderson and Y. B. Kim, Rev. Mod. Phys. **36**, 39 (1964).

[13] M. R. Beasley, R. Labusch, W. W. Webb, Phys. Rev. **181**, 682 (1969).

[14] D. Dew-Hughes, Cryogenics **28**, 674 (1988).

[15] P. H. Kes, J. Aarts, J. van den Berg *et al.*, Sup. Sci. Tech. **1**, 242 (1989).

[16] P. Manuel, J. Phys. III **4**, 209 (1994).

[17] C. W. Hagen, R. P. Griessen, E. Salomons, Physica C **157**, 199 (1989).

[18] R. Griessen, J. G. Lensink, T. A. M. Schröder *et al.*, Cryogenics **30**, 563 (1990).

[19] E. H. Brandt, J. Low Temp. Phys. **26**, 709 (1977); J. Low Temp. Phys. **26**, 735 (1977); J. Low Temp. Phys. **28**, 263 (1977); J. Low Temp. Phys. **28**, 291 (1977).

[20] E. H. Brandt, Physica C **195**, 1 (1992).

[21] D. Feinberg, J. Phys. III **4**, 169 (1994).

[22[E. H. Brandt, Physica C **180**, 426 (1991).

[23] G. Blatter, M. V. Feigel'man, V. B. Geshkenbein *et al.*, Rev. Mod. Phys. **66**, 1125 (1994).

[24] G. Blatter, V. Geshkenbein, A. Larkin *et al.*, Phys. Rev. B **54**, 72 (1996).

[25] V. G. Kogan and L. J. Campbell, Phys. Rev. Lett. **62**, 1552 (1989).

[26] G. Blatter, V. B. Geshkenbein, A. I. Larkin, Phys. Rev. Lett. **68**, 875 (1992).

[27] A. I. Larkin, Zh. Eksp. Teor. Fiz. **58**, 1466 (1970).

[28] A. I. Larkin and Yu. V. Ovchinnikov, J. Low Temp. Phys. **34**, 409 (1979).

[29] R. Labusch, Cryst. Latt. Defects **1**, 1 (1969).

[30] M. V. Feigel'man, V. B. Geshkenbein, A. I. Larkin *et al.*, Phys. Rev. Lett. **63**, 2303 (1989).

[31] M. V. Feigel'man and V. M. Vinokur, Phys. Rev. B **41**, 8986 (1990).

[32] V. Geshkenbein, A. Larkin, M. Feigel'man *et al.*, Physica C **162-164**, 239 (1989).

[33] M. P. A. Fisher, Phys. Rev. Lett. **62**, 1415 (1989).

[34] D. S. Fisher, M. P. A. Fisher, D. A. Huse, Phys. Rev. B **43**, 130 (1991).

[35] D. A. Huse, M. P. A. Fisher, D. S. Fisher, Nature **358**, 553 (1992).

[36] R. H. Koch, V. Foglietti, W. J. Gallagher *et al.*, Phys. Rev. Lett. **63**, 1511 (1989).

[37] R. H. Koch, V. Foglietti, M. P. A. Fisher, Phys. Rev. Lett. **64**, 2586 (1990).

[38] P. L. Gammel, L. F. Schneemeyer, D. J. Bishop, Phys. Rev. Lett. **66**, 953 (1991).

3. INSTRUMENTATION AND MATERIALS

The core of the presented work has been performed using three experimental setups. The bulk of the experiments was carried out in a Vibrating Sample Magnetometer (VSM). An important part of the magnetic measurements was executed in a rf Superconducting Quantum Interference Device (SQUID) magnetometer. Finally a home-made torque magnetometer was also used. All the experiments were carried out on single crystals of $YBa_2Cu_3O_{7-\delta}$, grown in McGill University, Canada.

3.1 VIBRATING SAMPLE MAGNETOMETER

The commercial (Oxford Instruments 3001) VSM, achieves dc fields up to 12 T and temperatures from 1.7 K - 300 K. The main components of the system, depicted in the schematic representation of figure 3.1, are:

a) *VSM main cabinet.* It consists of a transducer mounted below a platform which can be raised or lowered vertically, by means of a stepper motor, along two ballscrew shafts.

b) *The superconducting magnet*, consisting of a number of concentric solenoid sections together with compensating coils including shimming coils (to achieve specified levels of homogeneity). Each section is wound from multifilamentary superconducting wire from NbTi filaments. These are surrounded by a stabilising copper matrix. Copper is an electric insulator compared to a superconductor; however, it has much larger electronic mean free paths, that is, thermal conductivity. In this way it provides excellent thermal conduction and problems of thermal instability due to flux creep are avoided [1]. The magnet is fitted with inner coil sections of Nb_3Sn. The homogeneity is 0.1% over a sphere of 10mm diameter (DSV). The magnet's power supply, an Oxford Instruments PS120, gives operating currents with an upper limit of approximately 105 A, at a variable voltage of ±10 V. The magnetic field can be cycled from plus to minus 12 T. The field's sweep rate can be set between 10 and 200 Oe/sec.

The remnant field of the magnet is approximately 5mT. As the setup does not have a superconducting (persistent mode) switch, in order to maintain a constant applied field, the power supply has to remain "on".

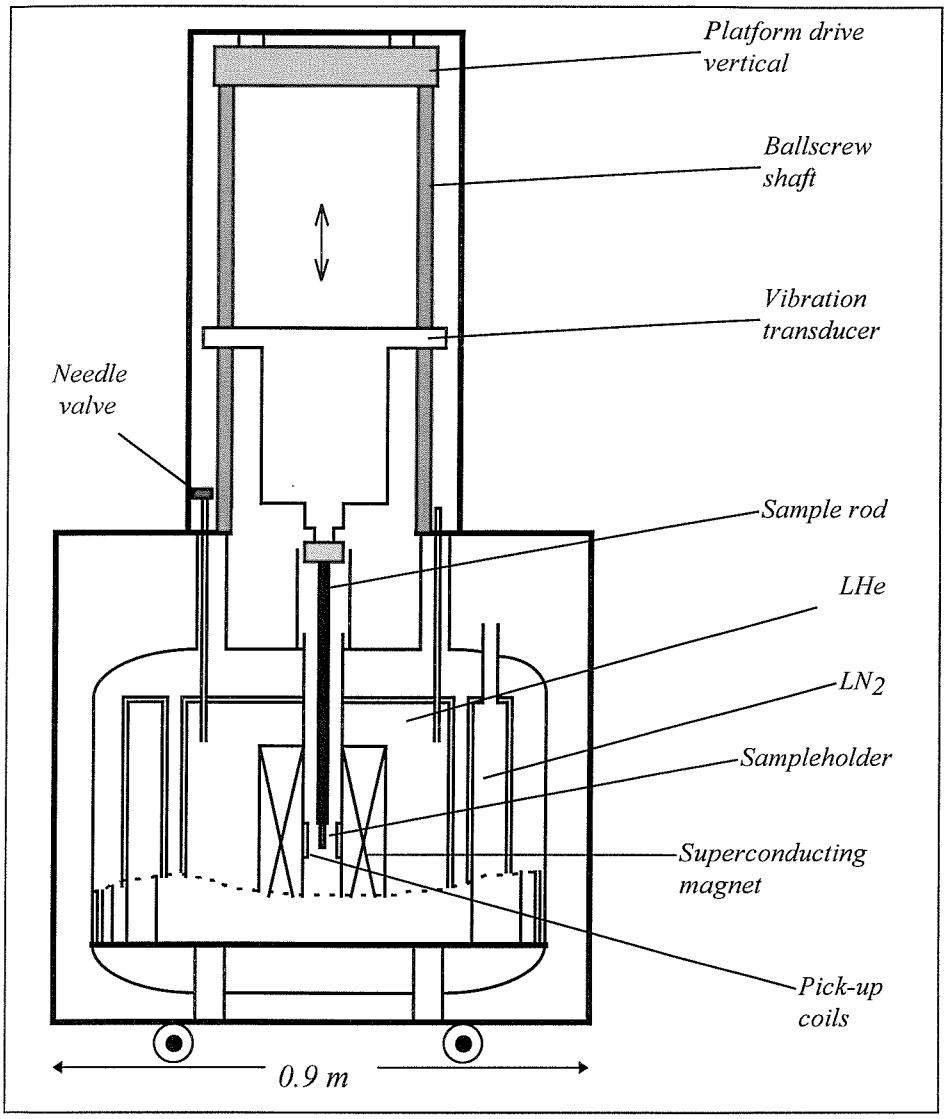

Figure 3.1: *Side diagram of the 12 T Oxford Instruments VSM-3001.*

c) The *sense coil arrangement* mounted in the magnet system employs two coils, separated by a distance of 5mm. The coils are wound in the opposite way, forming a first order gradiometer and are positioned coaxially with the magnet.

d) As seen in fig.3.1, the magnet is surrounded by a helium reservoir of a nearly 30 lt useful volume, which maintains the magnet temperature at 4.2 K. For reasons of

improved insulation, there is a nitrogen dewar around it and further out multilayer super-insulation which minimises the evaporation rate. Finally, the whole assembly is surrounded by a stainless steel vacuum vessel. Due to the standards of the provided shielding, a full He reservoir is sufficient for experiments in high fields for a duration of five full days.

e) The *variable temperature insert* (VTI), is loaded from the top of the cryostat. He gas is drawn from the LHe dewar through a needle valve, which controls the gas flow, and enters the sample space of the VTI, where a gold-iron/chromel thermocouple for temperature measurement and a heater situated close to the sample are fitted. An Oxford ITC-4 temperature controller regulates the power to the heater. To achieve the target temperature, the controller sets the heater's output so as to balance the cooling effect of the helium gas flow. In this way the sample's temperature is adjusted in the VTI heat exchanger. For the range 4.2 K-100 K it is the flow rate that defines the temperature, adjusted by using the needle valve. Temperatures between 1.7 K - 4.2 K are achieved by reducing the vapour pressure of LHe after it passes from the needle valve.

Samples are fitted with vacuum grease on sampleholders made of tufnol (see e.g. fig.3.2). For the measured single crystals, the sample mass can be anything between 100 μg and 3 g. Wrapping the sample with P.T.F.E. thread seal tape, ensures that it does not move or drop in the VTI space, during the measurement procedure.

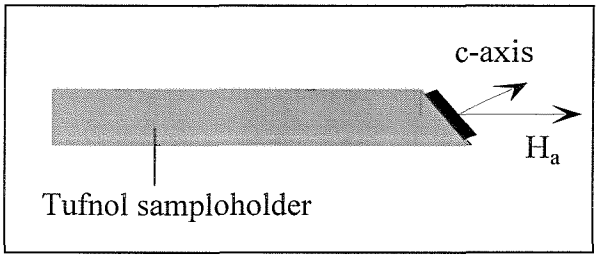

Figure 3.2: *The VSM sampleholder configuration for introducing the sample with its c-axis in a 7° angle with the applied magnetic field (measurement presented in chapter 4).*

The sampleholder is screwed onto a carbon fibre rod (tube section of approximately 6 mm in diameter) which is both extremely rigid and light. Thus, lateral vibration of the

sample is avoided. The rod is attached to the vibration transducer (fig.3.1), which is locked to the frequency of the mains supply.

The heart of the system's automation, the VSM electronic sub-rack, is connected to a PC via serial interfaces; this enables the control of the setup, with the transmission and reception of VSM control characters. Using AEROSONIC written software, a complete set of measurements can be defined through a combination of low level VSM control codes and high level pre-defined routines. The magnetic moment can be measured and recorded as a function of temperature, field, sweep rate or time.

During the measurement, the sample, after it has been positioned (within 0.1 mm) at the centre of the pick-up coils with the use of a calibration routine, vibrates vertically through a distance of 0.7 mm in the space between the two sense coils. The vibrator transducer produces a highly stable sinusoidal motion with a frequency of 66.66 Hz. Two weights on spring sections around the transducer ensure that there is the necessary damping to minimise transmitted vibrations to the magnet and the sense coil assembly. Due to the sample' s vibration, the first order gradiometric configuration gives effectively the output of a second order's one.

The vibraton of the sample in the magnetic field induces an emf in the coils. The output voltage of the pick-up coils, which is directly proportional to the sample's magnetic moment, is amplified and compared to the well known saturation magnetisation value of a nickel sample, which is used for calibration. The final output is the sample's magnetic moment, in emu. The VSM has a resolution of 10^{-5} emu.

3.2 SQUID MAGNETOMETER

The Cryogenics Limited 6T rf SQUID susceptometer, allows studies in dc magnetic fields of ranges up to 6 T. Structurally, see figure 3.3, it is similar to the VSM:

The superconducting magnet is installed in a LHe bath dewar with a N_2 dewar around it, for insulation from the ambient temperature. In the outer shells of the cryostat there is a vacuum shield followed by super-insulation. Finally, the cryostat is surrounded by a μ-metal shield which reduces the ambient field within the cryostat

down to a few μT. With an average boil-off of 3-4 litres per day, a full He reservoir is sufficient for six full days of high fields measurements.

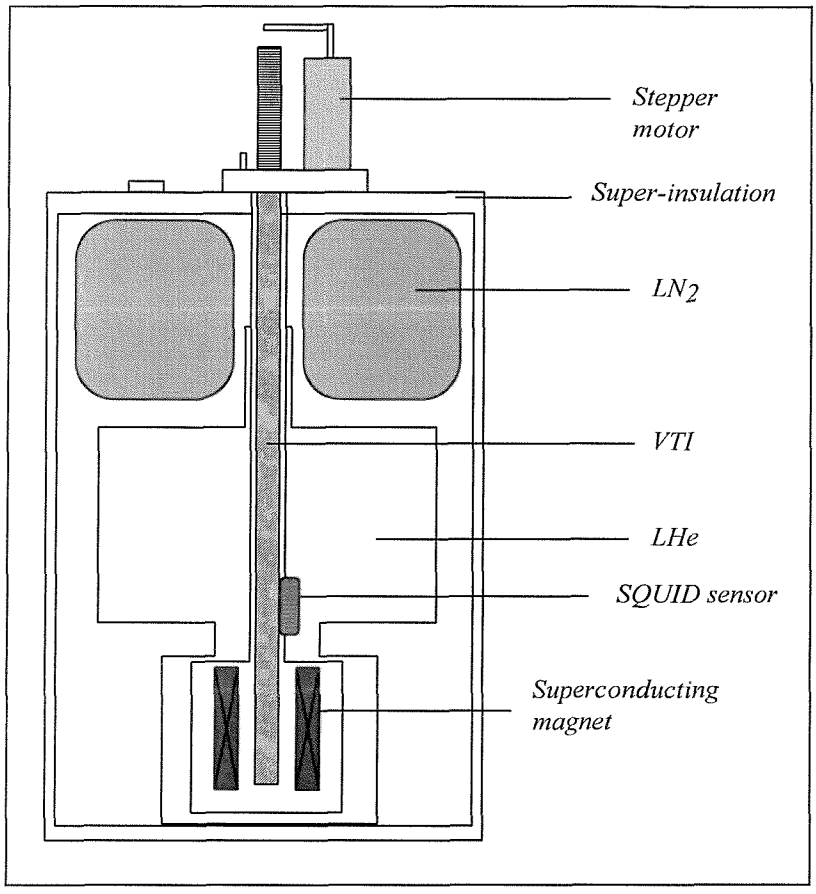

Figure 3.3: *Main features of the 6 T rf SQUID magnetometer configuration.*

The sense coil arrangement consists of a set of three pick-up coils, located centrally in the bore of the magnet, with a distance of few mm between them: two identical coils wound in the same direction and a third one, in between them, having twice the number of turns of the first two, wound in the opposite direction. Thus, a second order gradiometer is formed, which gives an output only when the second derivative of the magnetic field is changing, ensuring much better protection from unwanted signals (e.g. magnet's drift). Only the asymmetry of the configuration can limit its ability; the field of the magnet is rejected to typically 0.1%. The pick-up coils are, in the case of the SQUID susceptometer, fabricated from superconducting wire. The sense coils are coupled to the input coil of the SQUID, forming the flux transformer.

The magnet's power supply is capable of delivering 80 A at 5 V. An installed superconducting switch, across the terminals of the magnet, allows the circulation of large currents in the magnet, without the need of continuous support from the power supply. Apart from the heater attached to the superconducting switch, a second heater is used to drive the sense coils normal whenever the set field is change, to avoid any flux change through them. A zero oscillations option oscillates the magnet about zero field in ever decreasing steps, impressively reducing the remnant field in the magnet down to 5 Oe (figure 3.4).

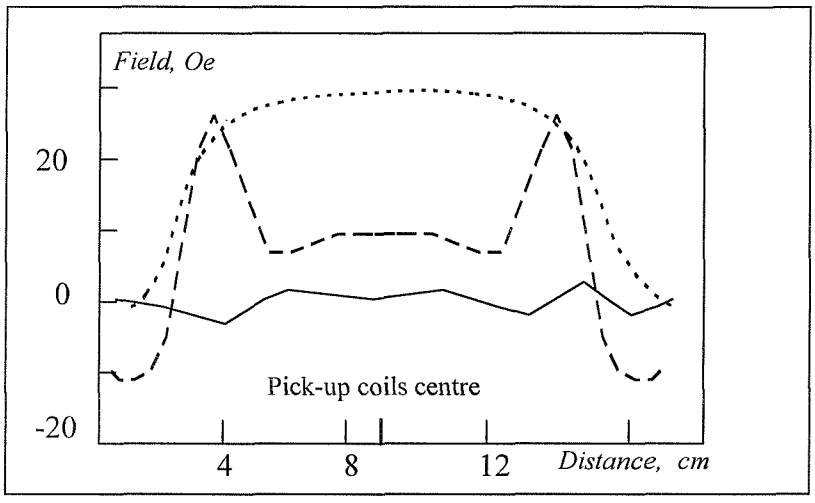

Figure 3.4: *The field profile in the 6 T SQUID susceptometer (Magnetic field in Oe as a function of the distance from the VTI bottom, in cm). The dashed and solid lines give the field profile at 0 Oe, respectively without and with the performance of zero oscillations. As seen, zero oscillations increase the field homogeneity and reduce the remnant field, within a 5 Oe margin. The dotted line gives the field profile (scaled by a factor of 30) for a set field of 830 Oe: now the applied field is nearly homogeneous over a distance of approximately 4 cm.*

A Lakeshore DRC-91CA temperature controller is used. It monitors two different rhodium-iron thermometers, located within the VTI, one close to the sample (sensor B) and another several cm away (sensor A), on the heat exchange space. The sample space is cooled with a continuous flow of helium gas driven from the LHe reservoir. This time the needle valve operates automatically, while the temperature controller adjusts the

heater's output. Contrary to the VSM, a system of valves controlling the gas flow in the VTI allows the sample's removal keeping the VTI's temperature stable at any value, within the accessible range.

The sample (single crystals in the present case) is confined in a cylindrical tube of quartz, 18.5 cm long and of 3 mm diameter, which gives negligible magnetic signal and is mounted on an oxygen-free copper wire. The tube is fitted with P.T.F.E. tape in the end of a brass (Cu-Zn) rod. The sample is positioned 5 cm from the bottom of the quartz tube and 12.5 cm from the brass rod, to avoid a finite length signal.

The thin film rf SQUID sensor measures relative changes in magnetic flux and for this reason it is necessary to move the sample through the pick-up coils. A stepper motor (fig.3.3) controls and defines the movement of the rod; thus, the sample can be smoothly moved any distance between 1-12 cm. The sample's motion sets up a screening current in the flux transformer circuit to oppose the resultant alteration in the flux threading the pick-up coils. The SQUID detects this current, which is strictly proportional to the sample's induced magnetic moment. The output from the SQUID electronics then gives a voltage, directly proportional to the signal detected at the SQUID sensor.

The choice of the appropriate scan length depends on the nature of the measurement and can be very crucial, especially when a very homogeneous magnetic field is desirable. As depicted in fig.3.4, at the relatively low applied field value of 830 Oe, the field is, within 1%, homogeneous over a scan length of less than 4cm (with the central position of the sample being the centre of the pick-up coils). However, for each data point a number of scans are averaged and the background signal is automatically subtracted by the control software. It is worth, also, to note that the very useful 1 cm scan length option is not easily met in other, home-made or commercial, SQUID magnetometers.

The setup is fully automated (PC controlled) and able to perform measurements of the sample's magnetic moment as a function of temperature, within the range of 1.7 K - 325 K, applied field and time. The control software is also capable of fully

compensating for any residual drift signal coming from the magnet circuit during a measurement routine.

At the expense of measuring time, the SQUID magnetometer has a much larger resolution than the VSM, detecting magnetic moments down to 10^{-8} emu, that is, 1000 times smaller than the VSM.

3.3 TORQUE MAGNETOMETER

As a result of the collaboration with Dr. L. Früchter in the Université Paris-Sud, in Orsay, a certain set of measurements has been performed by using a home-made torque magnetometer.

Figure 3.5 shows a schematic representation of the rig. A superconducting coil provides fields up to 4 T. The magnet's power supply is an Oxford Instruments MK3 with a maximum current output of 120 A at 4 V.

The rotation of the magnetic field, necessary for a torque measurement, is executed with the help of a stepper motor. The field rotates in the horizontal plane, in minimum steps of 0.037°. In addition to this, two smaller transverse coils, which can give 0.3 T at 10 A, are adjusted in the setup. In conjunction with the principal coil they can produce an even more precise orientation of the applied field.

The whole configuration is installed in a LHe reservoir, with a liquid nitrogen bath surrounding it. These two spaces are separated by a vacuum shield, while another one isolates the LN_2 bath from the outer space.

The temperature in the sample area is varied by a usual helium gas flow mechanism and a heater installed close to the sample (figure 3.6). Monitoring and control of the temperature is achieved via two complementary thermometers. A Carbon-Glass thermometer is used for the region from 4 to 40 K, with a resistance varying from 700 to 20 Ω, respectively. In the high temperature region of 40 to 300 K, a Platinum resistance thermometer is used, with the corresponding range of resistances varying between 20 and 120 Ω.. The temperature is regulated with a precision of 0.05 K. Before the

insertion of the measurement probe in the VTI, it is thoroughly pumped down to 10^{-4} mbar.

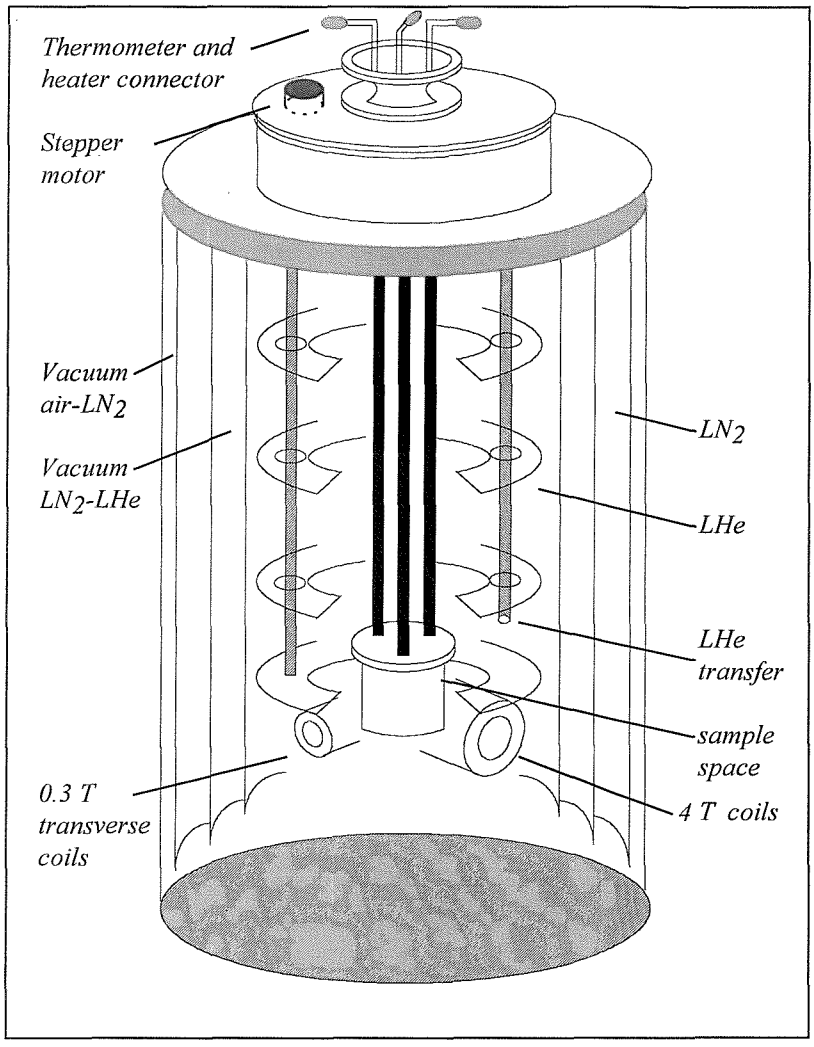

Figure 3.5: *The main characteristics of the 4 T torque magnetometer.*

The method followed in the present work is based on the deflection measurement of an elastic system. It is the most frequently used method, easily realised and performed. It has a very good sensitivity, down to 10^{-4} erg. In its most common application a flat metallic capacitor is used, which is the present case, as well. One of the two plates is mobile and supports the sample. The sample is attached to the plate with grease and a protective copper cover is fixed above the sample-capacitor system.

In an applied magnetic field, the superconducting ($YBa_2Cu_3O_{7-\delta}$) sample's anisotropy

γ results in a torque[1] on it [2] and the attached plate of the capacitor deflects from its initial parallel position. Under the condition of small deflection angles, a linear relation holds between the torque on the sample and the variations of the capacitance due to the presence of this torque, finally leading to the estimation of the sample's anisotropy.

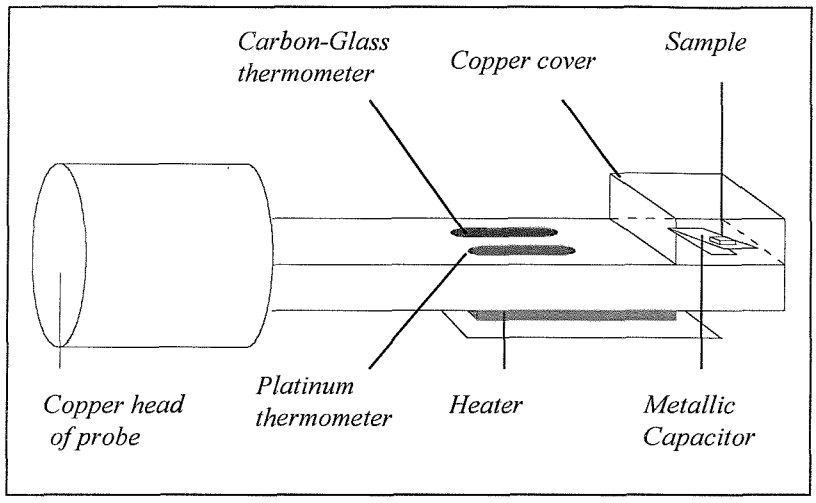

Figure 3.6: *The configuration of the sample bearing head of the measuring probe.*

The measurement of the capacitance is carried out with the use of a capacitance bridge General Radio 1615A, which in turn is equilibrated with use of a lock-in amplifier. The setup is PC controlled and fully automated. The software provides the user the facility to compose one or series of measurement sequences, the only limit being the LHe autonomy of the cryostat.

3.4 MATERIALS

Experiments were performed on single crystals of $YBa_2Cu_3O_{7-\delta}$ grown in the University of McGill, in Canada, by R. Gagnon and L. Taillefer. The synthesis of the crystals was based on a self-decanting flux method [3] using yttria-stabilised zirconia crucibles [4-6]. The method is known to give crystals of high purity.

[1] See chapter 6.

The initial mixture is composed of powders of Y_2O_3 (99.9999%), $BaCO_3$ (99.999%) and CuO (99.9999%) with a Y : Ba : Cu molar ratio of 1 : 18 : 45 [5]. Then the mixture is reacted above 900° C in yttria-stabilised zirconia crucibles. It has been shown [6-8], that this kind of crucible contaminates the fabricated $YBa_2Cu_3O_{7-\delta}$ crystals to a very small degree, since it is very difficult for the Zr^{4+} ions to be incorporated into the 123 crystals. Indeed, Zr^{4+} ions have a much larger charge compared to the Cu ions in $YBa_2Cu_3O_{7-\delta}$ and cannot substitute for them [7]. In addition, their ionic radius of 0.84 Å is much smaller than the 1.02 Å of Y^{3+} so they are unable to replace Y^{3+}, as well [7]. Thus, the few impurities are mostly Al, Fe and Zn atoms [7].

After cooling, the crystals have to acquire an increased oxygen content, since the tetragonal $YBa_2Cu_3O_{7-\delta}$ ($0.6 \leq \delta \leq 1$) is not superconductive. Therefore, they are oxygenated for 10 days at low temperatures, at 500° C, below the temperature of the tetragonal-to-orthorhombic structural phase transition [3,9], in flowing O_2, and quenched to room temperature.

The procedure yields highly oxygenated $YBa_2Cu_3O_{7-\delta}$ single crystals with an oxygen content of $7-\delta \cong 6.91$, according to the existing diffusivity studies [10] and a high critical temperature, $T_c = 93.6$ K. The magnetic width of the superconducting transition of the crystals is sharp: $\Delta T_c < 0.3$ K. It is defined as the temperature range over which the zero field cooled magnetisation, in a field of 0.1 mT, varies from 10% to 90%. The crystals have a typical size of the order of 0.7 x 0.7 x 0.05 mm^3; crystal thickness throughout this work is estimated using the mass and the theoretical density of 6.8 g/cm^3. The specific details of the crystals will be given in the description of the various experiments they were used in, in the sections to follow.

As a result of the internal stresses which are experienced during the low temperature annealing described above, at the transition between the tetragonal and the orthorhombic state[1] [3,11], extended, planar defects called *twin planes* are formed, see figure 3.7. Twin planes or twin boundaries, as they are called, accommodate these internal stresses and separate regions where the Cu-O chains[2] run alternately along the a and b axes of the original tetragonal cell [12]. They have a typical width of 50 Å; their separation

[1] See chapter 1.

[2] The creation of the Cu-O chains is the cause of the appearance of internal stresses.

varies, and in our samples is in the range of 0.5-5 μm. In polarised light microscopy they show up as straight, bright red lines along the [110] or [1 $\bar{1}$ 0] direction (fig.3.7).

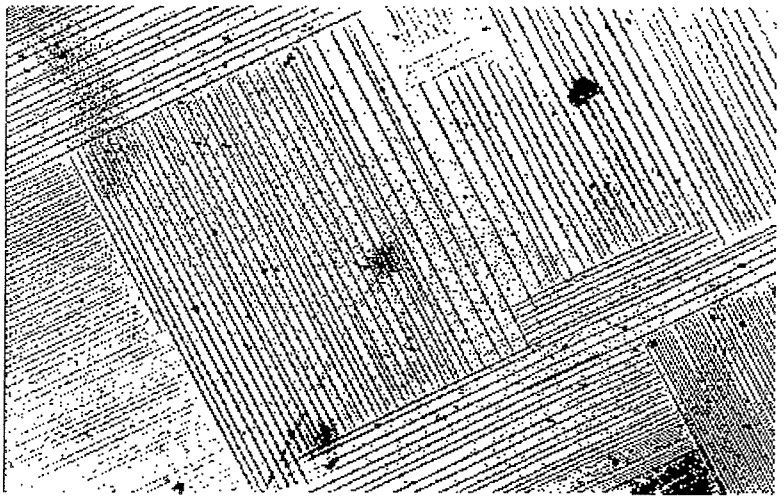

Figure 3.7: *Photograph of a part of a microtwinned* $YBa_2Cu_3O_{7-\delta}$ *crystal in a polarising light microscope; the different domains of twin planes and the randomness of the distance between successive twins is clearly illustrated.*

The crystals are detwinned by applying about 50 Mpa of uniaxial stress at 550° C in air for 30 minutes and then reoxygenating for one day at 500° C in flowing oxygen [13]. The procedure is highly successive and gives detwinned crystals for which polarising light microscopy reveals a surface fraction of misaligned phase of much less than 1% [14] (figure 3.8).

Generally, along with the twin boundaries other common defects in $YBa_2Cu_3O_{7-\delta}$ single crystals are copper and oxygen vacancies [15,16], interstitials [17] and non-superconducting impurities of Mg, Zn, Al, Fe, Mn, Ti, Au, La, Sr or Zr, depending on the synthesis method. Also possible are screw dislocations and voids. Point or extended (linear) pinning centers can be artificially introduced in $YBa_2Cu_3O_{7-\delta}$ crystals by electron or heavy ion irradiation, e.g. ref.[18,19] and references therein. The technique is very promising for the future applications of high temperature superconductors, since it can enhance very efficiently the sustained critical currents.

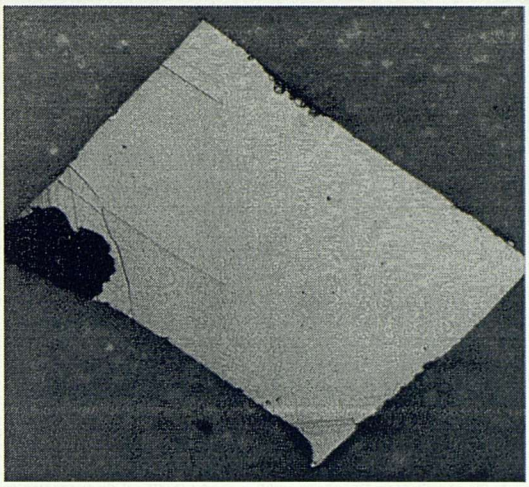

Figure 3.8: *Photograph of a detwinned* $YBa_2Cu_3O_{7-\delta}$ *crystal under polarised light conditions.*

3.5 Oxygen Content Variation

As it was mentioned in section 1.2.1, oxygen doping in $YBa_2Cu_3O_{7-\delta}$ increases the fraction p of holes per Cu atom in the CuO_2 layer [20]. Positive holes are the itinerant charge carriers in HTS and by doping oxygen is added in the Cu-O chains [21]. Previous studies [22,23] have revealed that the chains play the role of charge reservoirs for the CuO_2 layers, controlling T_c. The T_c dependence on p has been shown experimentally by Tallon *et al.* [20] to obey a generic phase behaviour in all the high temperature superconductors, expressed by the parabolic dependence:

$$\frac{T_c}{T_{c,\,max}} = 1 - 82.6 \cdot (p - 0.16)^2 \qquad (3.1)$$

where $T_{c\,,\,max}$ is the optimum T_c accessible when $p = 0.16$.

Tallon and coworkers also established the relationship of p and δ in $YBa_2Cu_3O_{7-\delta}$. They demonstrated [20] that for $\delta < 0.55$:

$$p = 0.187 - 0.21\delta \qquad (3.2)$$

Using these two relationships, Tallon *et al.* [20] reproduced satisfactorily the experimental results and the crucial T_c dependence on δ. Indeed, as previous studies of

the effect of oxygen concentration on T_c in the case of $YBa_2Cu_3O_{7-\delta}$ have revealed [20,23,24] there exist two plateaus in $T_c(\delta)$, as figure 3.9 shows.

The first plateau (the "60 K plateau") stretches in the underdoped region between $0.6 < \delta < 0.4$ with a T_c almost constant at around 60 K. Then, with the enhancement of p, T_c increases with the oxygen content until the point of optimum doping around $\delta \sim 6.90$ where it is maximised. What follows is the overdoped region, where T_c remains almost constant, with only a very slight decrease from its maximum value. This "90 K plateau" is the peak in the parabolic curve of $T_c(p)$ [20].

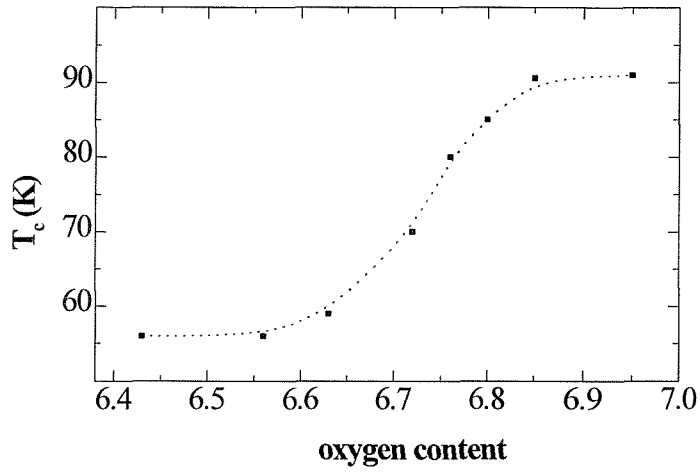

Figure 3.9: *Dependence of* T_c *on oxygen content in* $YBa_2Cu_3O_{7-\delta}$, *after Cava et al., ref. [23].*

Coming to our case, to produce different oxygen concentrations, crystals were subject to different annealing treatments under oxygen pressure of 1 Atm. To achieve a homogeneous oxygen content, the annealing time was approximately 10 days. Subsequently the samples were quenched in room temperature.

As it has been established, e.g. ref.[25-28], the final oxygen concentration of the samples depends systematically on the annealing temperature; more precisely, the oxygen content decreases for increased annealing temperature. Thus, determination of the new oxygen stoichiometry x (or deficiency δ) can be based on previously published diffusivity studies which provide a calibration between the annealing temperature and

the oxygen content in $YBa_2Cu_3O_{7-\delta}$ [10]. This is the method we have followed throughout the present work. Though it is difficult for $\delta < 0.1$ to provide accurate values of δ [23,24,29] the distinctively different annealing temperatures allow us to be consistently precise. The oxygen content of the received crystals with $7-\delta \cong 6.91$ corresponds to a $T_c = 96.3$ K. For this initial oxygen content of 6.91, annealing temperatures of 450°, 485° and 520° C lead respectively to oxygen contents of 6.96, 6.93, 6.90. The optimum oxygen doping is observed at $7-\delta = 6.93$ with $T_c = 93.8$ K.

It worths noticing that there are also other ways to estimate the oxygen concentration of an $YBa_2Cu_3O_{7-\delta}$ crystal, e.g. with measurement of the c-axis lattice parameter and use of the relation $7-\delta = 74.49 - 5.78$ c(Å) [30].

REFERENCES

[1] M. Tinkham, *Introduction to Superconductivity*, McGraw-Hill, Singapore (1996).

[2] V. G. Kogan, Phys. Rev. B **38**, 7049 (1988).

[3] W. Assmus, W. Schmidbauer, Sup. Sci. Tech. **6**, 555 (1993).

[4] R. Gagnon, M. Oussena, M. Aubin, J. Cryst. Growth **114**, 186 (1991).

[5] R. Gagnon, M. Oussena, M. Aubin, J. Cryst. Growth **121**, 559 (1992).

[6] R. Gagnon, C. Lupien, L. Taillefer, Phys. Rev. B **50**, 3458 (1994).

[7] R. Liang, P. Dosanjh, D. A. Bonn *et al.*, Physica C **195**, 51 (1992).

[8] T. A. Vanderah, C. K. Lowema, D. B. Bliss *et al.*, J. Cryst. Growth **118**, 385 (1992).

[9] C. N. R. Rao, R. Nagarajan, R. Vijayaraghavan, Sup. Sci. Tech. **6**, 1 (1993).

[10] J. R. LaGraff and D. A. Payne, Physica C **212**, 478 (1993).

[11] J. Chrosch, E. K. H. Salje, Physica C **225**, 111 (1996).

[12] A. W. Sleight, Science **242**, 1519 (1988).

[13] R. Gagnon, S. Pu, B. Ellman *et al.*, Phys. Rev. Lett. **78**, 1976 (1996).

[14] R. Gagnon, private communication.

[15] J. Giapintzakis, W. C. Lee, J. P. Rice *et al.*, Phys. Rev. B **45**, 10677 (1992).

[16] A. Legris, F. Rullier-Albenque, E. Radeva *et al.*, J. Phys. I **3**, 1605 (1993).

[17] E. H. Brandt, Rep. Prog. Phys. **58**, 1465 (1995).

[18] L. Krusin-Elbaum, A. D. Marwick, R. Wheeler *et al.*, Phys. Rev. Lett. **76**, 2563 (1996).

[19] R. C. Budhani, M. Suenaga, S. H. Liou, Phys. Rev. Lett. **69**, 3816 (1992).

[20] J. L. Tallon, C. Bernhard, H. Shaked *et al.*, Phys. Rev. B **51**, 12911 (1995).

[21] J. D. Jorgensen, M. A. Beno, D. G. Hinks *et al.*, Phys. Rev. B **36**, 3608 (1987).

[22] J. D. Jorgensen, B. W. Veal, A. P. Paulikas *et al.*, Phys. Rev. B **41**, 1863 (1990).

[23] R. J. Cava, A. W. Hewat, E. A. Hewat *et al.*, Physica C **165**, 419 (1990).

[24] E. Kaldis, E. Liarokapis, K. A. Müller, *Workshop on High-T_c Superconductivity 1996: Ten Years after the Discovery*, NATO ASI Series, Kluwer Ac. Publishers, (London 1997), p.411.

[25] N. Kobayashi, K. Hirano, T. Nishizaki *et al.*, Physica C **251**, 255 (1995).

[26] O. B. Hyun, M. Yoshida, T. Kitamura *et al.*, Physica C **258**, 365 (1996).

[27] A. A. Zhukov, H. Küpfer, G. Perkins *et al.*, Phys. Rev. B **51**, 12704 (1995).

[28] V. Breit, P. Schweiss, R. Hauff *et al.*, Phys. Rev. B **52**, R15727 (1995).

[29] J. L. Vargas and D. C. Larbalestier, Appl. Phys. Lett. **60**, 1741 (1992).

[30] M. E. Parks, A. Navrotsky, K. Mocala *et al.*, J. Solid State Chem. **79**, 53 (1989).

4. VORTEX CHANNELING

4.1 THEORY OF EXTENDED DEFECTS

4.1.1 VORTEX STRUCTURE IN THE PRESENCE OF TWIN PLANES

Soon after the discovery of $YBa_2Cu_3O_{7-\delta}$ it was realised that the extended, planar defects naturally created in this compound, namely the twin boundaries, can have a dramatic effect on vortex pinning. As a result, an important part of the subsequent theoretical investigations was focused on verifying the role of twin planes. The complications arising from the presence of the twin planes became evident right from the beginning. The first theoretical studies were inconclusive on whether the superconducting order parameter is suppressed in the twin planes, as Deutcher and Müller suggested [1] (see also Kes *et al.*, ref.[2]) or not, as Khlusticov and Buzdin [3] and Abrikosov estimated [4].

However, the tendency of regarding the twin planes as strong pinning centres soon prevailed, especially after the careful analytical work of Blatter *et al.* [5,6] where the enhanced pinning properties of twin boundaries for magnetic fields aligned or applied at small angles with the planar defects are discussed. Furthermore, it was conceived [5,7,8] that the strain fields associated with the twin boundaries make them an ideal place for accumulation of atomic defects and impurities, weakening superconductivity in the twin planes and attracting vortices.

The equilibrium configuration of a single vortex in the presence of twin planes can be derived in a straightforward way, considering a simplified model [5,6]. The pinning potential of the twin planes is represented by a periodic array or lattice of extended 2D pinning structures. Although in reality the distance d_{TP} between the twin planes varies (randomly spaced defect boundaries, see fig.3.7), d_{TP} can be satisfactorily approximated as a constant. A pivotal point is, of course, the assumption that the order parameter is

suppressed within the twin planes, reinforced as we will later see, by the experimental observation of vortex attraction to the twin boundaries. Finally, in a first approximation, all the effects of point disorder can be neglected [5].

Assuming, thus, a suppression of the order parameter in the twins, the vortex with its normal core will be attracted to them and adjust in such a way, as to accommodate to the planar defects and gain from the pinning energy. Blatter *et al.* [5,6] studied the situation when the applied field lies within the ab plane. For an external field H_a making an angle θ with the twin boundaries, three different vortex structures can arise, depending on the value of θ (figure 4.1): straight vortices collinear with the magnetic field, vortices forming a kinked structure or, finally, straight vortices locked-in to the planar defects.

More precisely, when the field is applied at large angles to the twins, above a threshold value θ_K called the *trapping* angle, vortices are straight and aligned to the direction of the external field, see figure 4.1(a). In other words, θ_K is the critical angle above which it is unfavorable for a flux line, in terms of elastic energy, to adjust to the planar defects. Considering the single vortex case, this critical angle is given as a function of the line tension ε_l and the pinning potential of the twin boundaries ε_{TP}:

$$\theta_K = \sqrt{\frac{2 \cdot \varepsilon_{TP}}{\varepsilon_l}} \tag{4.1}$$

Note the expected dependence of θ_K on ε_{TP}: the value of the trapping angle decreases as the pinning potential ε_{TP} of the twin boundary weakens.

When the direction of the external field, relatively to the twins, drops below θ_K, vortices are deformed (fig.4.1(b)); a kinked structure arises, with the vortex being aligned to a twin plane for a certain distance L (the kink length) and, thus, pointing along the magnetic field only on average in one period of the periodic pinning array (fig.4.1(b)).

By balancing the tilt energy (line tension ε_l for the single vortex case) with the twin boundaries pinning potential ε_{TP}, Blatter *et al.* [6] estimated the length of the vortex trapped segment in the defect, always for in-plane rotation of the applied field. The number n of kinks per vortex is shown to increase linearly with θ:

$$n = \frac{s \cdot |\theta|}{d_{TP}} \tag{4.2}$$

where s is the sample's dimension along the field.

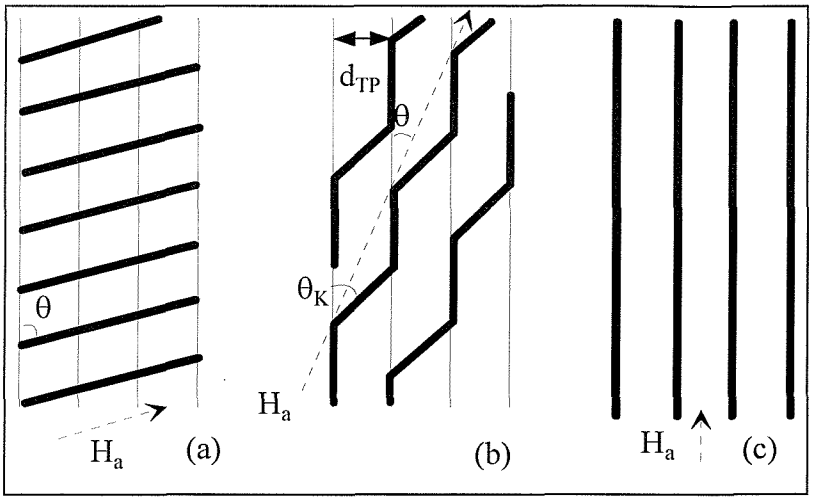

Figure 4.1: *Vortex structure (thick lines) for different angles* θ *of the applied magnetic field* H_a *relative to the twin planes (thin lines). (a) A collinear phase for* $\theta > \theta_K$, *(b) a kinked vortex phase for* $\theta_L < \theta < \theta_K$ *and (c) a locked-in vortex phase for* $\theta < \theta_L$. *Within the kinked structure, the linking vortex segments make an angle* θ_K *with the twin planes [5,6].*

Finally, the presence of the planar defects leads to a lock-in transition when the magnetic field is applied at angles, relatively to the twin planes, smaller than a critical angle θ_L ($\theta_L < \theta_K$) [6]. Now the vortex is accommodated throughout its whole length in the twin plane: it is *locked-in* to the twin boundary (fig.4.1(c)). The lock-in angle θ_L is equal to:

$$\theta_L = \frac{4 \cdot \pi \cdot \varepsilon_l}{\Phi_o \cdot H_a} \cdot \theta_K \tag{4.3}$$

Abandoning the single, isolated vortex approximation and considering the vortex-vortex interactions, as in the case of high magnetic fields, the trapping angle θ_K is reduced due to the increased elastic energy and is given by the relation [6]:

$$\theta_K \approx \sqrt{\frac{2\cdot\varepsilon_{TP}}{\varepsilon_l}}\cdot\left[\ln\left(\frac{\kappa}{\varepsilon}\right)\cdot\left(\frac{\alpha_o}{d_{TP}\cdot\sqrt{\varepsilon}}\right)^3\right]^{1/2} \qquad (4.4)$$

In eq.(4.4) α_o is the vortex lattice constant, κ the GL constant and the parameter $\varepsilon = 1/\gamma$ expresses the anisotropy. As in the single vortex case, the calculation is based on the balance of tilt energy and pinning energy, assuming that a fraction of the vortices is trapped by the twin planes [6]. It is worth noting that in the tilt energy used for the estimation of the trapping angle in the collective case, the wave vector corresponding to fluctuations perpendicular to the twin planes k, has a cutoff limit given by the spacing of the twin planes d_{TP}, at $k = (\pi/d_{TP})$.

Lowering the value of the external field, the above result eq.(4.4) goes over to the single vortex result, eq.(4.2).

4.1.2 BOSE GLASS MODEL

Simultaneously with the Vortex Glass model, developed for systems with random disorder, a pinning model for correlated disorder, e.g. twin planes, grain boundaries, forests of screw dislocations or columnar defects, was proposed [9,10]. The essential difference in the case of correlated disorder is that the extended defects produce pinning forces which add up coherently and not in a random way, as happens with point disorder. Thus, a strong rise of pinning energies can occur, which is particularly crucial for the high temperature superconductors.

Considering an external field H_a parallel to the extended defects, the situation is mainly characterised by the attraction of vortices by the defects, for similar reasons to those analysed above, in the case of the twin boundaries. Similarly to the Vortex Glass model, there is a well defined transition temperature, T_{BG}. Above T_{BG}, the thermal energy is sufficient to cause wandering of the flux lines among the defects on an unconfined diffusive path [11] resulting in a linear (ohmic) resistance as a response to an externally imposed Lorentz force.

Below T_{BG} the strong pinning conditions, valid for the type of disorder under discussion, restrict and localise vortices within, at most, the limit of a few neighboring

defects [11]. The phase is called Bose or Boson Glass phase, since the statistical mechanics of vortex localisation in a 3D extended defect can be mapped onto the quantum mechanics developed for the problem of the localisation of a boson particle in a potential minimum at 2D. The linear resistance is now zero at low currents, $J << J_c$ and non-linear I-V curves are expected, of the form:

$$E \propto \exp\left[-\left(\frac{J_2}{J}\right)\right]^{\mu} \tag{4.5}$$

J_2 sets the current scale and is a function of the distance between the defects and the distribution function of the vortex pinning energies [12]. Assuming a short range repulsive vortex-vortex interaction, the predicted value for the exponent μ is 1/3 for low currents [13] and 1 for higher ones.

Contrary to the existence of only one characteristic length, ξ_G, in the Vortex Glass model, in the Bose Glass model two important localisation lengths can be defined, namely the $l_{\parallel}$ and $l_{\perp}$, expressing the distances within which the localised vortex fluctuates, parallel and perpendicular to the z axis (H_a direction), respectively (see figure 4.2). Both these two characteristic lengths diverge as the temperature approaches T_{BG}:

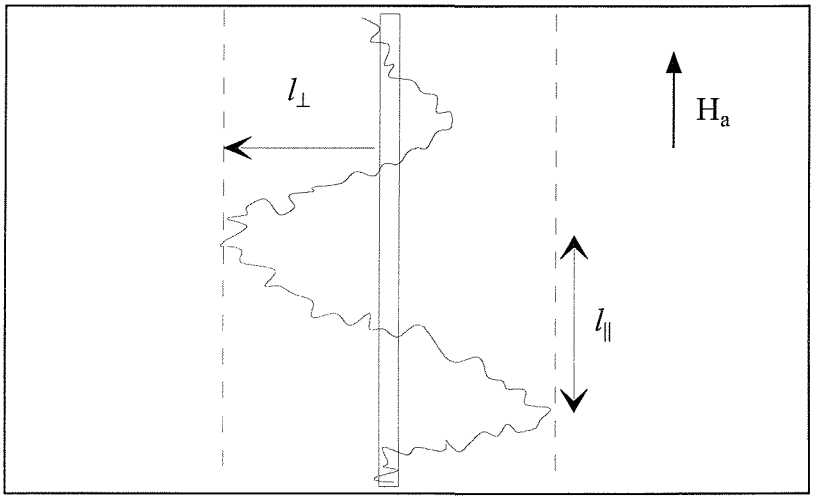

Figure 4.2: *Vortex localised in a tube of radius $l_{\perp}$; $l_{\parallel}$ is the distance along z that it takes the vortex to "diffuse" across the diameter of the localisation tube.*

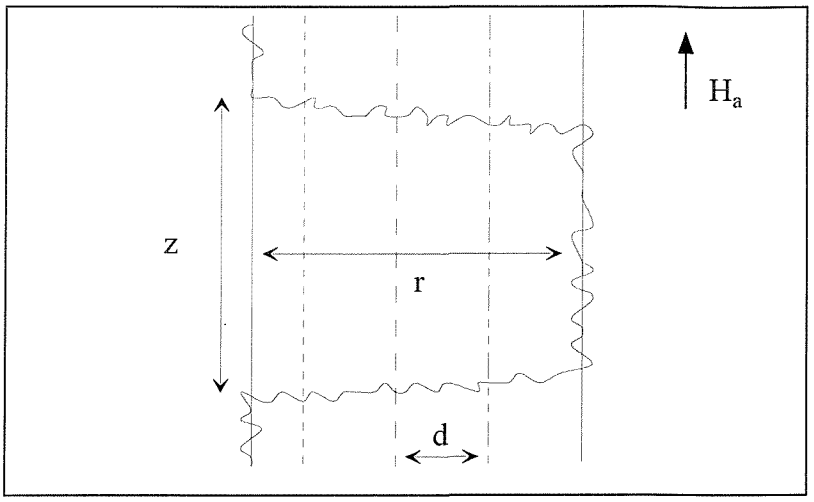

Figure 4.3: *Superkink configuration, with the flux line tongue of transverse length* r *and extension along the magnetic field* z*, seeking a convenient low energy pin to spread [13].*

$$\begin{cases} l_{\perp} \propto \left(T_{BG} - T\right)^{-\nu_{\perp}} & ,\nu_{\perp} \geq 1 \\ l_{\parallel} \propto \left(T_{BG} - T\right)^{-\nu_{\parallel}} & ,\nu_{\parallel} = 2\nu_{\perp} \end{cases} \tag{4.6}$$

The main transport mechanism of vortices in the Bose Glass phase, at low currents, is tunneling between defect sites. For reasons of optimum tunneling probability, usually the vortex tunnels to a distant defect with similar pinning energy. This variable-range-hopping (VRH) transport mechanism, as it is called, is achieved via the formation of double kinks or, at even lower current densities, of superkinks, as depicted in figure 4.3.

An essential characteristic of the Bose Glass phase is the infinite value of the tilt modulus, c_{44}, resulting from the vortex confinement. Furthermore, a Mott insulator phase has been predicted [13], buried deep inside the Bose Glass phase, at low temperatures. This occurs at vortex densities that match the density of the defects; note that the Mott insulator phase has been explicitly worked out for the case of columnar defects. At these matching conditions both the tilt modulus, c_{44}, and the compressional modulus, c_{11}, acquire infinite values. The Bose Glass model gives similar universal scaling laws to the Vortex Glass and physical quantities scale now with an appropriate

power of $(T-T_{BG})$ [11]; the main difference is the slightly different scaling exponents expected for each of these two glass models [6].

As in the Vortex Glass model at T_g, at T_{BG} one expects power-law I-V characteristics. The phase transition from the Bose Glass to the phase above T_{BG}, which is believed to be an entangled liquid of delocalised vortices, is predicted to be sharp and of second order [12]. Due to the directional character of the correlated pinning a strong angular dependence of the position of the irreversibility line in the phase diagram has been also predicted [13]. This dependence is not expected in the isotropic Vortex Glass case, being therefore the most pronounced and distinguishing difference between these otherwise similar models.

4.2 Experimental Studies of Twin Planes

Preceding and following the theoretical developments, the experimental studies of twinned $YBa_2Cu_3O_{7-\delta}$ samples, from the earlier stages till recently, were focused on investigating the strong pinning properties of the twin boundaries.

First Vinnikov *et al.* [14] and Dolan *et al.* [15] using the Bitter decoration technique managed to demonstrate, at low magnetic fields, the attraction of vortices in the defect boundaries; the vortex density appeared to be larger within the twin planes than in the bulk. This was also evidence for the suppression of the order parameter within the twins.

Transport data of Worthington *et al.* [16] in bulk and twinned $YBa_2Cu_3O_{7-\delta}$ showed a characteristic shoulder in the resistivity above the melting point of the solid. They also showed an abrupt increase of the viscosity at the temperature this shoulder starts - on lowering T. Marchetti and Nelson [17] explained the data in a frame of vortex entanglement and strong pinning by twin planes. Due to entanglement the viscosity of the vortex liquid is increased. Twin planes, acting as pinning centres and taking advantage of the flux liquid's enhanced viscosity, manage to anchor a large portion of the vortex liquid.

SQUID magnetometry measurements in a wide temperature and field regime by Welp *et al.* [18], both in untwinned and in twinned crystals containing a dense pattern of

opposite twin planes domains, demonstrated an increased critical current in the case of the twinned samples. This increase occured for both orientations of the applied field: H_a parallel to the c-axis and H_a within the ab plane. At about the same time, Kaiser *et al.* [19], again by means of magnetic measurements, also concluded that twin planes enhance pinning and subsequently critical current densities in $YBa_2Cu_3O_{7-\delta}$. The strong pinning picture was also supported by torque measurements by Gyorgy *et al.* [20], with the applied field's direction being rotated relatively to the extended defects.

A study of the angular dependence of the resistive transition curves in simply twinned[1] single crystals of $YBa_2Cu_3O_{7-\delta}$ was performed by Kwok *et al.* [21]. This confirmed, at the time, the strong pinning character of twin planes, for orientations of the magnetic field parallel, and a transport current applied at 45° with the planar defects. This careful experimental work showed that resistivity is minimum for applied fields orientated within 1° of the twins, giving a critical angle between the field and the twin planes of the order of 1° - 3°, the angle above which the kinked structure ceases to exist, see figure 4.4.

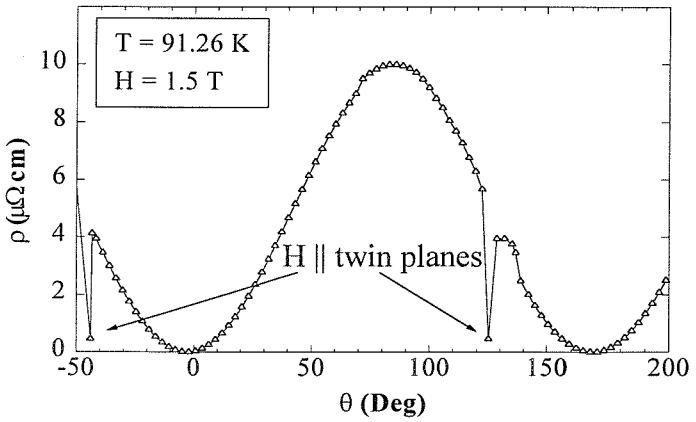

Figure 4.4: *Angular dependence of the resistivity, after Kwok et al. [21].* θ *is the angle between the applied field and the measuring current which flows in the* ab *plane [21].*

[1] We will call throughout this work *simply twinned* the crystals that contain twin planes oriented in only one direction.

Similar results were presented in a follow-up work by the Argonne group [22]. Flesher and coworkers used a number of simply twinned crystals. The applied field was rotated from the c-axis to the ab plane whereas the transport current was applied in the ab plane. They succeeded in having a variety of different Lorentz force directions: 0°, 45° and 90° relative to the twin boundaries. For all the different geometries studied, twin boundaries enhanced vortex pinning both in the locked-in regime (vortices parallel to the defects) and in the kinked structure regime, for the trapped length of the flux lines. The angular variation of the resistivity verified the results of Kwok *et al.* [21].

Evidence for the existence of a kinked structure came also from the work of Grigorieva *et al.* [23,24], who used the Bitter decoration technique. Twin planes appeared to be effective in attracting vortices for a large angle interval between the applied field and the planar defects, supporting the kinked structure picture.

A novel approach to the problem of twin planes was made by Duran *et al.* [25] who used a real time magneto-optical imaging technique to study their effect. Their measurements were on lightly twinned $YBa_2Cu_3O_{7-\delta}$ single crystals and in a restricted range of applied fields (up to 500 Oe) and temperatures (around 50 K). However their results showed that contrary to previous reports twin planes could also facilitate and guide vortex motion. In particular, twin planes provided paths for easier flux penetration into the sample, in the case of motion along these extended defects; however, as before, for transverse vortex motion the defects acted as strong pinning centres.

Nevertheless, Dorosinskii *et al.* [26,27] and Vlasko-Vlasov *et al.* [28] used the same real time imaging technique but with an improved resolution to reach to the opposite conclusions. They studied twinned $YBa_2Cu_3O_{7-\delta}$ crystals with various distances between the twins, in low magnetic fields, roughly up to 260 Oe. They concluded that twin boundaries are strong pinning centres which never facilitate vortex motion. Flux is prohibited to cross the boundaries; when during penetration flux encounters a planar defect, the first vortices to "arrive" at the boundary are pinned there blocking, by their mutual repulsion, the path of the following vortices. Thus, the latter ones promptly change the direction of their motion and start moving along the boundary. In this way, an increased flux density builds up on the side of the twin plane facing the flux motion, the so-called "shadow effect". Motion along the twin boundary, contrary to Duran *et al.*

[25], is not easier and is not guided, since it is realised in the presence of only one twin boundary and not a pair [28]. Vortex motion does not occur, either, within the boundary: Vlasko-Vlasov *et al.* [28] propose that within the planar defect itself vortices are pinned against both parallel and transverse motion and do not move.

The contradicting interpretations of the magneto-optical imaging results proved the necessity for clear experimental evidence on the existence of easy vortex motion along twin planes. Furthermore, the technique's intrinsic weakness of being restricted in very low magnetic fields was another complicating factor. Inevitably, even if any definite conclusions could be drawn from such measurements, it would be difficult to apply them in the case of external fields higher by orders of magnitude. Our magnetic measurements aimed exactly there, to clearly detect a possible existence of easier vortex motion due to the presence of twin planes and study this effect in an extended field and temperature regime.

4.3 Results and Discussion

The experiments in the University of Southampton were carried out in a variety of twinned and detwinned $YBa_2Cu_3O_{7-\delta}$ single crystals, using both the 12 T VSM and the 6 T rf SQUID magnetometer [29-31]. Samples were first zero field cooled at the desired temperature and then subjected to a magnetic field H_a.

The dimensions, mass and the nature of the crystals (twinned and detwinned) are shown below, in table 4.1, with α_x, α_y and α_z being, respectively, the length, width and thickness. All crystals have[1] an oxygen content of 6.91 and T_c of 93.6 K, unless otherwise specified. The microtwinned crystals investigated are either multi-domained containing a pattern of domains with twin boundaries of different orientation or they are simply twinned, containing twin planes oriented in a unique orientation, see figure 4.5. The twin planes separation varies in the micrometer scale, between 0.5 and 5 μm.

[1] Chapter 3, section 3.5, for more details.

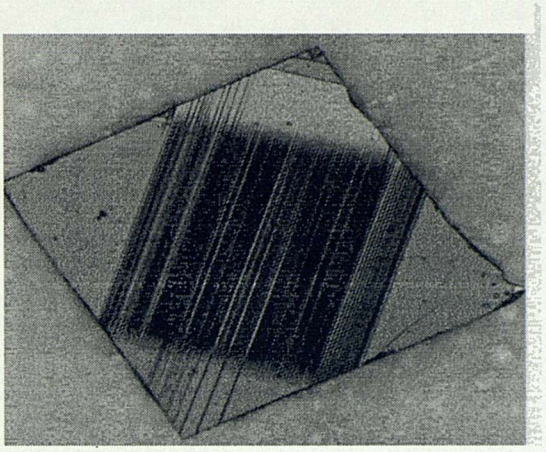

Figure 4.5: *Photograph of simply twinned crystal L under polarised-light.*

Crystals	α_x (mm)	α_y (mm)	α_z (μm)	m (μg)	Twinning
A	1.15	0.80	57	363	twinned
A1	0.71	0.47	53	120	simply twinned
A2	0.75	0.50	61	155	twinned
A3	0.70	0.35	48	80	twinned
B	0.88	0.80	13	64	twinned
C	0.90	0.70	112	483	twinned
D	0.72	0.70	52	179	detwinned
E	0.78	0.79	20	81	simply twinned
F	1.04	0.80	52	293	detwinned
L	0.67	0.63	24	70	simply twinned

Table 4.1: *Details of the investigated* $YBa_2Cu_3O_{7-\delta}$ *single crystals. Simply twinned crystals contain only one orientation of twin planes (see text).*

Figure 4.6 [29,30] shows a set of comparative VSM magnetic hysteresis measurements, hysteresis loops, at 60 K, for twinned crystals A, B, C (figure 4.6(a)), and detwinned D (fig.4.6(b)). The measurements have been carried out with a magnetic field sweep rate of 5 mT/sec; the field H_a was applied parallel to the c-axis, avoiding the complication of the layered structure. In order to make a direct comparison between the signals the different crystals produce, the magnetisation of each one is divided by its characteristic size R, where R is:

$$R = \frac{3 \cdot \alpha_y}{4}\left(1 - \frac{\alpha_y}{3 \cdot \alpha_x}\right) \quad , \alpha_x > \alpha_y \tag{4.7}$$

The Bean model predicts that for crystals with similar pinning properties, all M/R curves are identical [32]. Indeed, comparing data of microtwinned crystals A, B, C with data of detwinned D, these first measurements demonstrate that we can experimentally define two field values (shown in fig.4.6(a)), H_1 and H_2. The existence of twin planes has little effect on the hysteresis width ΔM (and, thus, on the critical current J_c) at high fields: a satisfying agreement exists, for $H_a > H_2$, as fig.4.6 shows. However, they seem to substantially increase ΔM and therefore effective pinning at low fields, for $H_a < H_1$, in a region which also includes the so called magnetisation's "neck".

Our interest is focused on the intermediate fields regime, indicated on fig.4.6(a) between H_1 and H_2, where the width of the hysteresis varies and for crystals A and B an unexpected flattening occurs instead of the well expected "fishtail" peak. As seen in table 4.1, crystals A, B, C contain both types of twins, [110] and [1$\bar{1}$0]. However, polarising light microscopy showed that crystal C has many (more than 10) domains with twins of opposite orientation, while crystals A and B have only a few such domains (less than 4). As seen in fig.4.6 and repeatedly verified, a well defined magnetisation peak is only observed in the case of multi-domained microtwinned crystals and for detwinned ones; in the case of microtwinned crystals with few domains, though, a *depression* in the hysteresis width and of the critical current is observed, always for intermediate fields, $H_1 < H_a < H_2$.

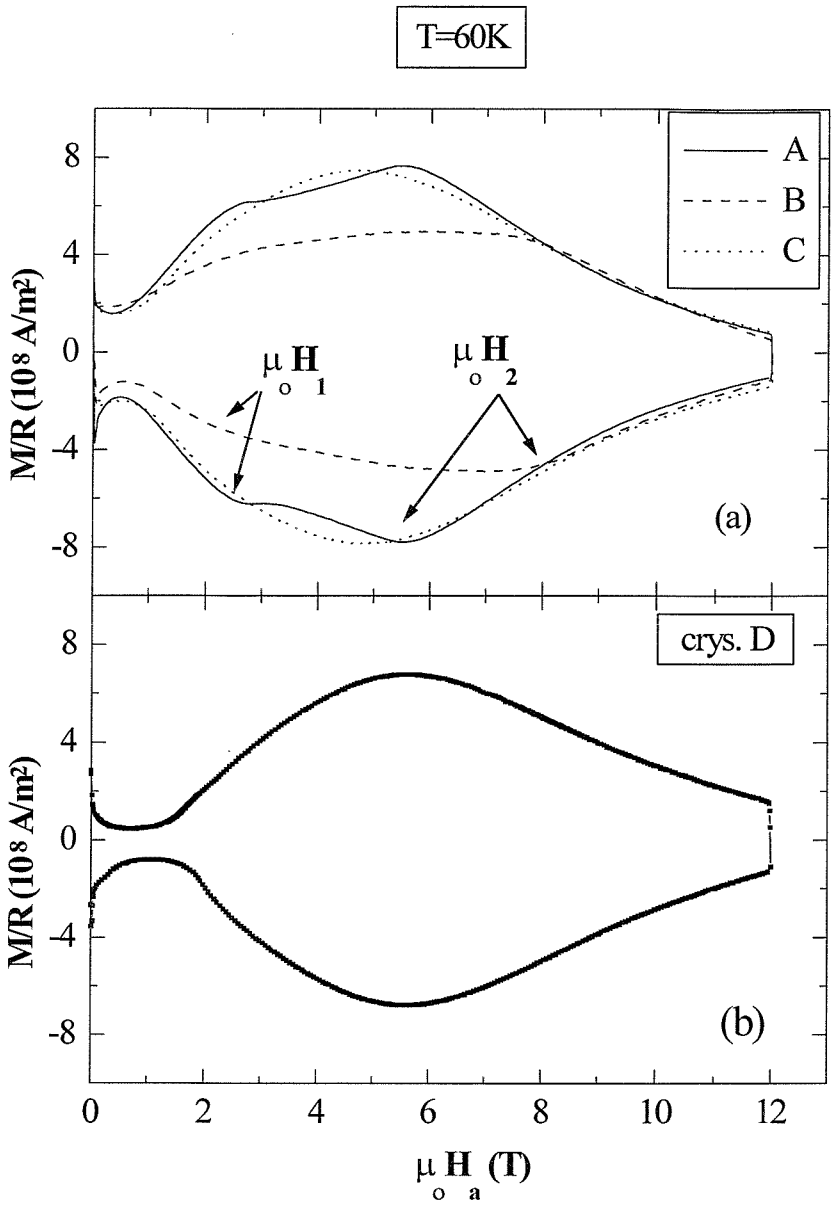

Figure 4.6: *Magnetic hysteresis for twinned crystals A, B, C, and for detwinned D.* H_1 *and* H_2 *are the empirical boundaries of the intermediate field region, where a depression of the magnetisation occurs. Occasionally, they appear either as small peaks (e.g. case of sample A) or as a change in the slope of the magnetisation curve (sample B).*

A more careful study of samples A and C under the polarising light microscope, shows that many twin planes of one type cross the whole crystal (as depicted for crystal A in fig.4.7). Thus, our measurements seem to support the channeling picture given earlier by Duran *et al.* [25], but in a much broader field regime. The depression of the hysteresis width can be explained as a result of the easier motion of the flux through the behaving as channels twin planes, leading to the reduction of the sample's overall pinning. This preferential motion means that vortices feel in the twin planes a *reduced* pinning force per unit length f_{TP}, compared to the equivalent pinning force f_u they experience in the untwinned regions. Indeed, as fig.4.6(a) shows, the depression of the hysteresis is observed around the magnetisation fishtail peak, where one expects f_u to be larger. Nevertheless, in multi-domained twinned crystals this channeling mechanism is expected to be far less plausible. The boundaries between the different domains constitute strong, columnar-like, extended defects which hinder flux motion and immobilise vortices.

To verify further that vortex channeling along the twin boundaries causes the magnetisation depression, we cut crystal A into three pieces, A1, A2 and A3, with crystal A1 containing a unique twinned domain, while in crystals A2 and A3 there are small regions with twin planes of the opposite direction. The sketch in fig.4.7 indicates the distribution and orientation of twins in all samples. At low and high fields, the magnetisation loop of all the pieces, once scaled by R, has exactly the same width as that of the "mother" crystal A. However, in agreement to the discussion above, in the intermediate field region where the flattening is observed, a remarkable further decrease of ΔM takes place. Moreover, in all the parts, A2, A3 and especially A1, the plateau is much more prominent and extended. As a result, unexpectedly, parts of a single crystal exhibit a *lower* critical current density than the whole. The limited number or the absence of any intersections of different twinned domains gives a chance for faster and easier channeling to vortices, decreasing even further the sample's overall pinning. The same experiment on crystal C, gave similar results.

This vortex channeling situation is in a sense similar to the more recent experimental findings of Pastoriza and Kes [33] who artificially - by irradiation - created weak pinning channels and observed flow of vortices through them; also to the numerical

results of Brass *et al.* [34] and Jensen *et al.* [35], where a preferential motion of vortices along easy paths was demonstrated. Here these easy paths are (naturally) provided by the twin planes. Later measurements by other groups led to the verification of our results and conclusions, for instance similar magnetic measurements of ref.[36]. In addition, more recent, high resolution magneto-optical studies in applied fields up to 1 T support the conclusion that vortices penetrate *inside* the planar defect, and are not guided along it [37].

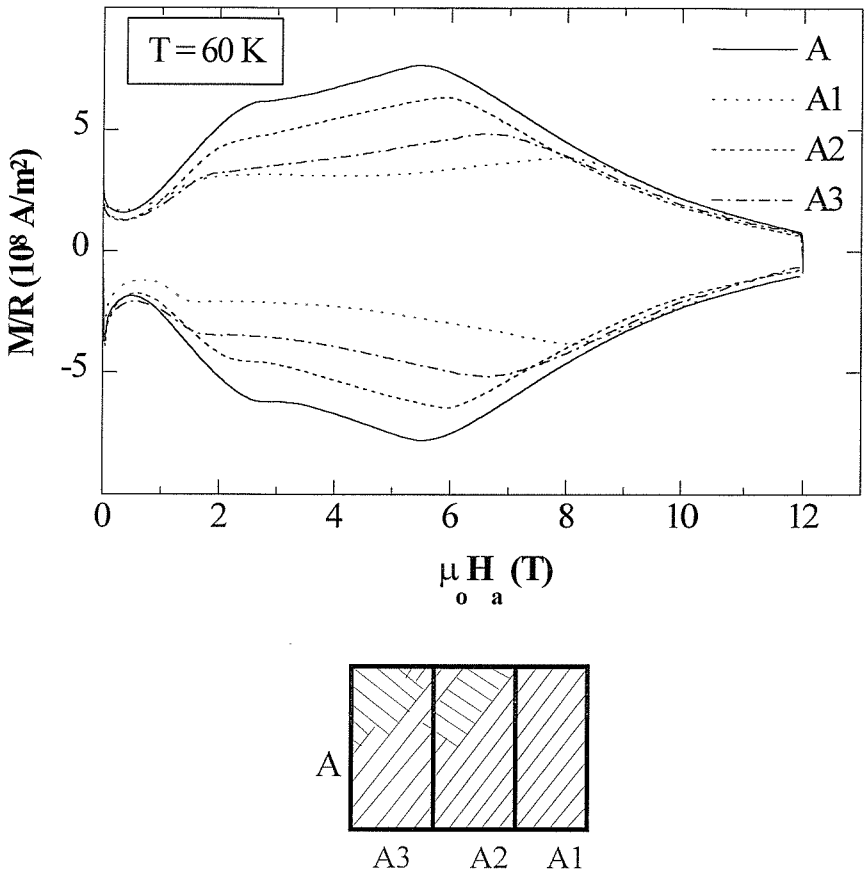

Figure 4.7: *Comparison of the scaled to size magnetic hysteresis for twinned crystal A and its pieces A1, A2, A3.*

Since channeling takes place in directions along the twin planes it should rely crucially on vortices being locked-in to the twin planes. It follows that removing the effect of the twin boundaries, by for example tilting the applied field H_a, channeling as a mechanism should weaken; on the contrary, pinning should increase. Therefore to

further investigate the validity of the above drawn conclusions, we carried out a thorough angular study of the magnetisation in the presence of twin planes [31], in fields up to 6 T and temperatures up to 70 K.

For this purpose we used the 6 T rf SQUID magnetometer. To mount the sample into the quartz tube, we created a step of oxygen-free copper wire under the microscope, giving to the step the desired inclination for our measurements (figure 4.8(a)). The sample was mounted on this step. In this way we applied the field at angles θ relatively to the crystal c-axis between 0° and 20°, the uncertainty in the angle being less than 0.5°. The applied field H_a is rotated in the plane defined by the c-axis and the normal to the twin planes, as depicted in figure 4.8(b).

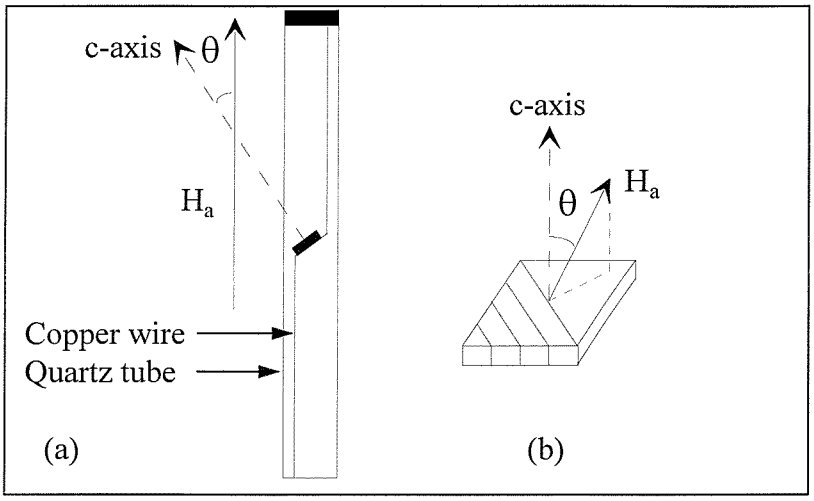

Figure 4.8: *Representation of (a) a sample mounted in the quartz tube for the SQUID measurements and (b) of the way the magnetic field* H_a *was tilted for the measurements (out of the twin planes).*

Crystals D and E were used (table 4.1). In the simply twinned crystal E the twin planes make an angle of 45° to the samples edges. In order to avoid problems of field inhomogeneity the measurements were performed using an excursion length of the sample equal to the minimum available, namely 1 cm.

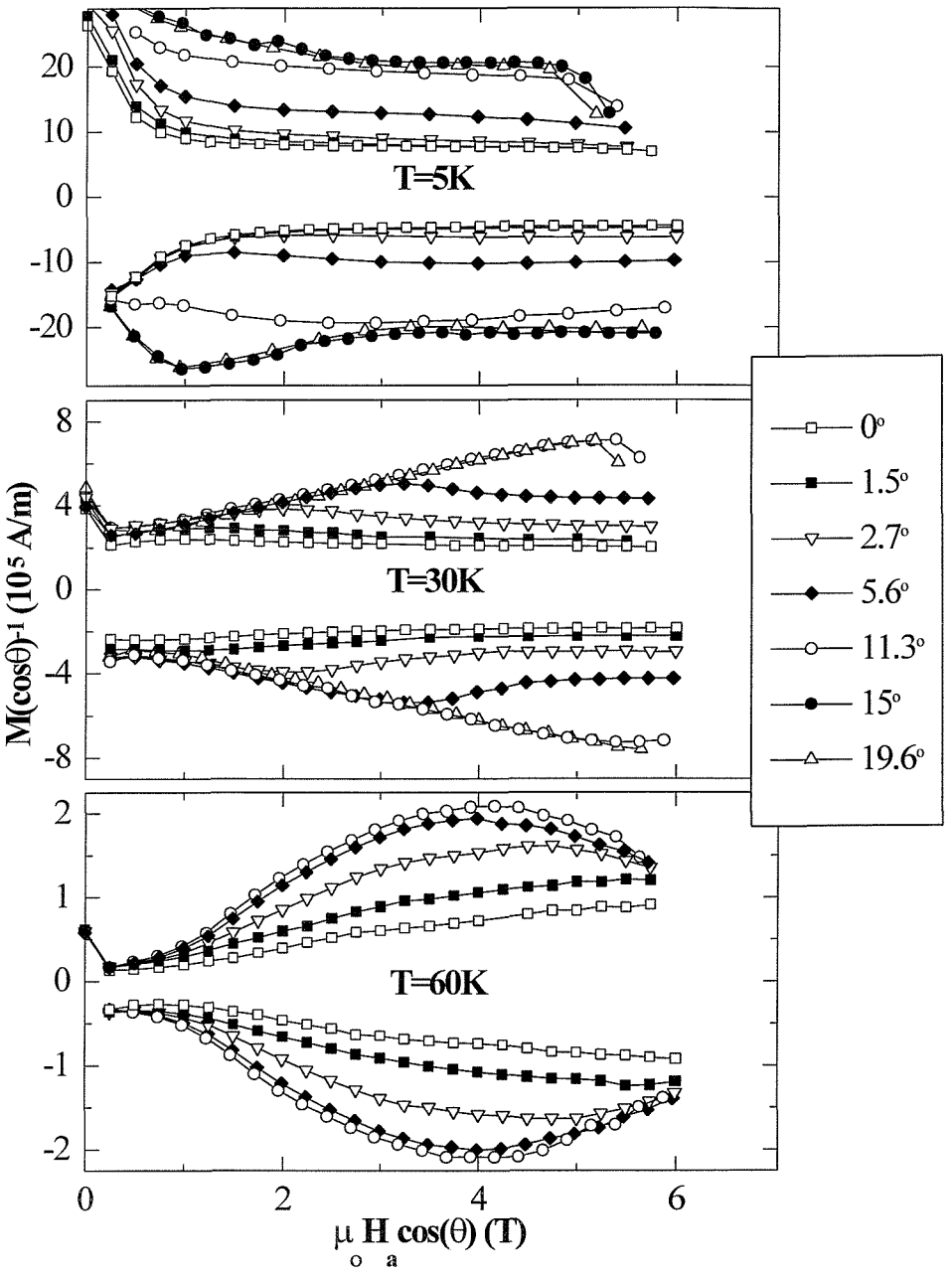

Figure 4.9: *Isothermal magnetisation* M(H) *at the indicated temperatures and angles for microtwinned crystal E.*

Figure 4.9 [31] represents a detailed angular analysis of the magnetisation, for crystal E. When H_a is tilted away from the c-axis the measured magnetisation M arises mainly

from the projection of the component along the c-axis of the magnetisation, $M_\perp$ [38]. It is given by:

$$M(H_a) = M_\perp(H_a\cos\theta)\cdot\cos\theta \qquad (4.8)$$

Thus, figure 4.9 shows $M_\perp = M / \cos\theta$ as a function of the component of H_a along the c-axis, $H_\perp = H_a \cos\theta$, at the indicated angles and temperatures.

Indeed, consistently with the idea of channeling, at a given temperature and in the field region where the hysteresis flattening occurs, the width ΔM increases as H_a is tilted away from the planar defects. As we will explain, this is expected from the theoretical predictions [6] for the existence of a kinked structure. It is important to emphasize that in our case the locked-in situation and the kinked structure are revealed through channeling of the trapped vortex segments in the twin planes, thereby leading to a depression of the magnetisation.

From fig.4.9 two characteristic angles of the applied field with respect to the planar defects can be defined: an angle θ_L above which ΔM starts to increase and an angle θ_K above which ΔM stops increasing with the tilt angle. At small tilt angles between H_a and the c-axis, $\theta < \theta_L$, lock-in of vortices to twin planes is expected [6]; twin planes trap the whole length of a vortex and exert on it a pinning force $f_{TP}(\theta \leq \theta_L) = f_{TP}(0)$. Theoretically [6], a region of kinked vortices follows; in our measurements this is demonstrated via the increasing of the magnetisation with θ, for $\theta_L < \theta < \theta_K$. The channel produced by the twin planes will obviously be less effective when vortices are only partly trapped. The kinks [39] organise themselves into chains so that the twin boundaries are still fully occupied, but this time by vortex segments. Vortex segments, which feel an increased pinning force in the twin planes since they are anchored by the parts of the vortices which lie in the untwinned regions, with the stronger pinning force f_u. Finally, at still larger tilt angles, $\theta > \theta_K$, vortices intersect twin planes at points, the magnetisation saturates and thereafter the untwinned regions are expected to dominate the crystal's magnetic response. Let us emphasize the fact that this was the first work, at the time, to produce experimental evidence for the (theoretically predicted) existence of *two* critical angles, the lock-in angle θ_L and the trapping angle θ_K. Until then only one of these two

angles was experimentally reported, which sometimes carried the meaning of θ_L and sometimes the meaning of θ_K (e.g. ref.[22]).

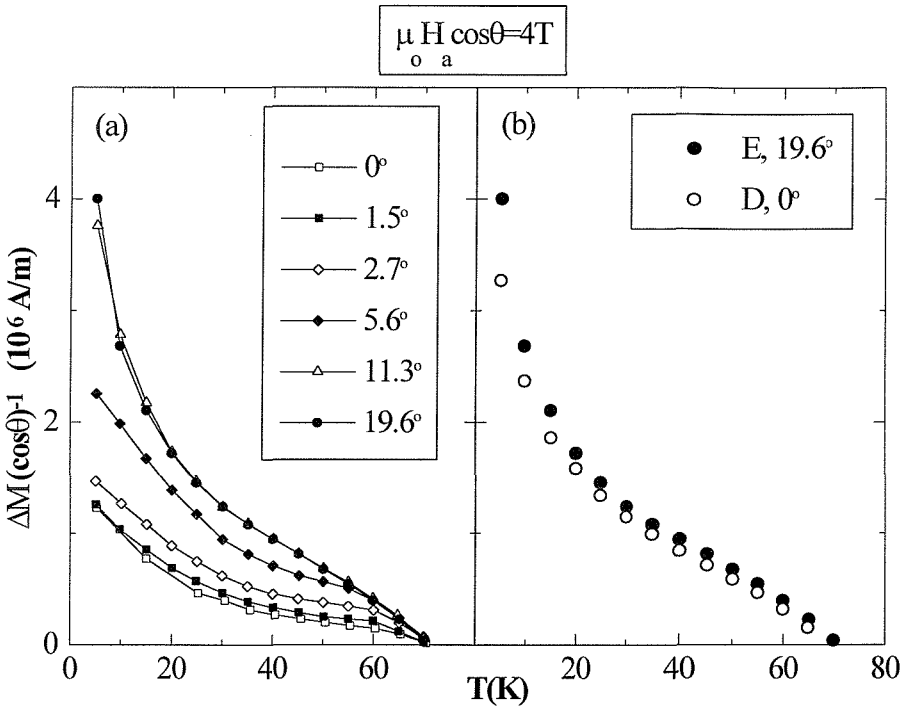

Figure 4.10: *(a) Temperature dependence of the hysteresis width at the indicated angles and at a constant applied field of 4 T along the* c-axis. *(B) A comparison between twinned crystal E for* $\theta > \theta_K(T)$ *and the detwinned crystal D for* $\theta = 0°$.

Figure 4.10(a) presents the temperature dependence of the hysteresis width ΔM at the indicated angles and at the applied field of 4 T. As the angle θ increases, the temperature dependence of $\Delta M(T)$ evolves gradually into the curve for $\theta = 19.6°$. It is clear that by removing the effect of the planar defects the critical current gradually builds up. It is worth noticing that the value of θ_K above which the magnetisation saturates, increases with decreasing temperature, i.e. with increasing the pinning force in the untwinned regions $f_u \propto \Delta M(\theta_K)$. Our results show[1] that at 5 K, θ_K is approximately 12° whereas at

[1] See also figure 4.11(a).

30 K it becomes equal to 7.9° and at 60 K it is a mere 3.7°. Going back to fig.4.9, we have observed a similar magnetic field dependence of θ_K, its value increasing with f_u increasing: the angle θ_K increases as the difference between the outer hysteresis loop ($\theta > \theta_K$) and the inner hysteresis loop ($\theta = 0$) increases, i.e. with the increase of $\Delta M(\theta = \theta_K) - \Delta M(\theta = 0)$. This behavior is clearly seen at T = 30 K.

For $\theta < \theta_K$, not only the hysteresis width is reduced due to channeling, but also its temperature dependence is deteriorating, as θ tends to 0°. The weakest temperature dependence of ΔM is observed at $\theta = 0°$. This supports earlier theoretical investigations of the twin boundaries [6]. The twin planes are planar defects and therefore the pinning potential along them is less sensitive to thermal fluctuations: twin planes are expected to *reduce* the dimensionality of thermal fluctuations, restricting fluctuating vortices in 2D. As a result the critical current's decrease with temperature is expected to obey a power law [5,6]. On the contrary, for random point disorder, due to the 3D character of thermal fluctuations, this decrease is theoretically expected [6] and experimentally observed [40] to be exponential with T.

The observed decrease of channeling with the reduction of f_u with temperature, is in agreement with a later report on computer simulations by Groth *et al.* [41], who verified the critical role of the relative strength of f_{TP} and f_u on the vortex motion along the twin planes. The results of Groth and coworkers suggest that due to the reduced dimensionality of thermal fluctuations in the twin planes, a temperature increase will have a much more dramatic effect on f_u and therefore, above a certain "threshold" temperature, channeling will cease. As seen in fig.4.10(a), our measurements show vortex channeling up to a temperature of around 70 K; thus, according to what was mentioned, above this temperature regime we expect f_u to become small enough for the twins to no longer provide an easy and preferable vortex path. The same conclusions on the relative temperature sensitivity of f_{TP} and f_u were also drawn in a number of other theoretical [42] and experimental works [20,43].

Also illustrated in fig 4.10(b) is a comparison of the temperature dependence of the width of the hysteresis for microtwinned crystal E, at $\theta = 19.6°$, and detwinned crystal D, at $\theta = 0°$, for the same applied field of 4 T. Normalization of the data of detwinned D to the size of twinned E allows a direct comparison to be made. As seen in fig.4.10(b),

although there is some extra amount of disorder in the case of the microtwinned crystal, once $\theta > \theta_K$ the magnetic behavior of the twinned sample is dominated by the untwinned regions, and we get a close quantitative and qualitative match with the behavior of the detwinned sample.

Even more revealing is figure 4.11(a) [31], shown below. It shows the angular dependence of the magnetic hysteresis width $\Delta M(\theta)$ at low (5 K), intermediate (30 K) and high (60 K) temperatures, at a constant applied field of 4 T along the c-axis. For each temperature the respective critical angles, θ_L and θ_K, are shown; data are normalised by the maximum hysteresis width, ΔM_{max}, obtained for $\theta > \theta_K$.

Figure 4.11(a) supports what was stated above: the trapping angle θ_K increases as the pinning force in the untwinned regions f_u increases, when temperature is lowered. This temperature dependence is an important experimental finding. Previous theoretical investigations of the interaction of vortices with twin planes [13,39,44] showed that as the order parameter is suppressed within the extended defect, there exists an energy barrier ε_{TP} which impedes transverse motion. Because of this barrier [13,6] vortices are locked-in for angles of the applied field relatively to the twins smaller than the lock-in angle; for larger angles, yet lower than the trapping angle, it is ε_{TP} that causes the kinked structure. On the other hand, the trapping angle θ_K has been theoretically estimated [6] to vary as $(\varepsilon_{TP})^{0.5}$ (see relations (4.1) and (4.4)) and to depend weakly on temperature, in the temperature regime that we study; this temperature dependence becomes stronger only when approaching T_c [6]. What our results strongly suggest, however, is a fairly strong temperature dependence of the trapping angle.

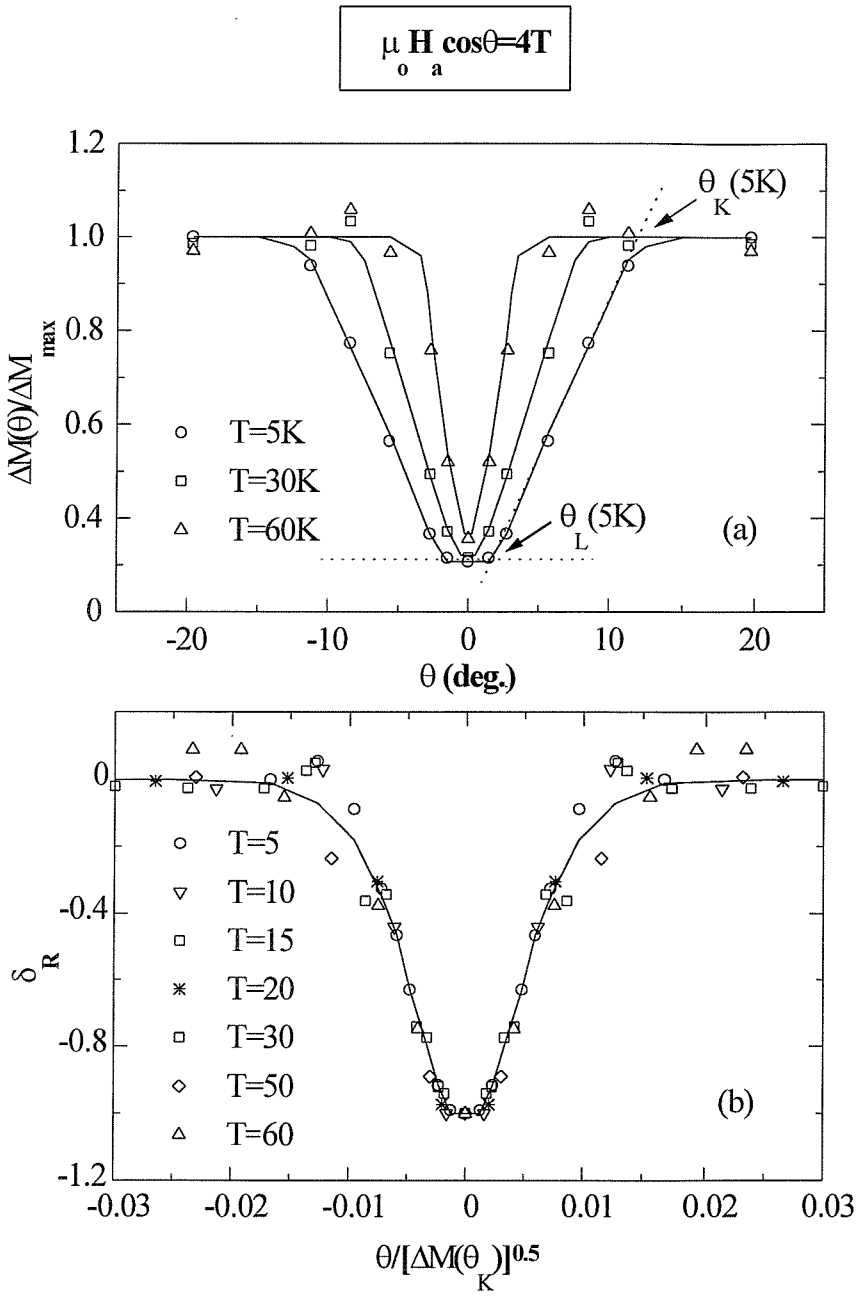

Figure 4.11: *(a) Angular dependence of the normalised* ΔM *to its maximum value, at the indicated temperatures and at the fixed applied field of* $\mu_0 H_a \cos\theta = 4$ *T. Note the existence of two characteristic angles* θ_L *and* θ_K*. (b) Scaling of the curves illustrated in (a), with* δ_R *being the relative decrease of* ΔM *(see text). The lines are a guide to the eye.*

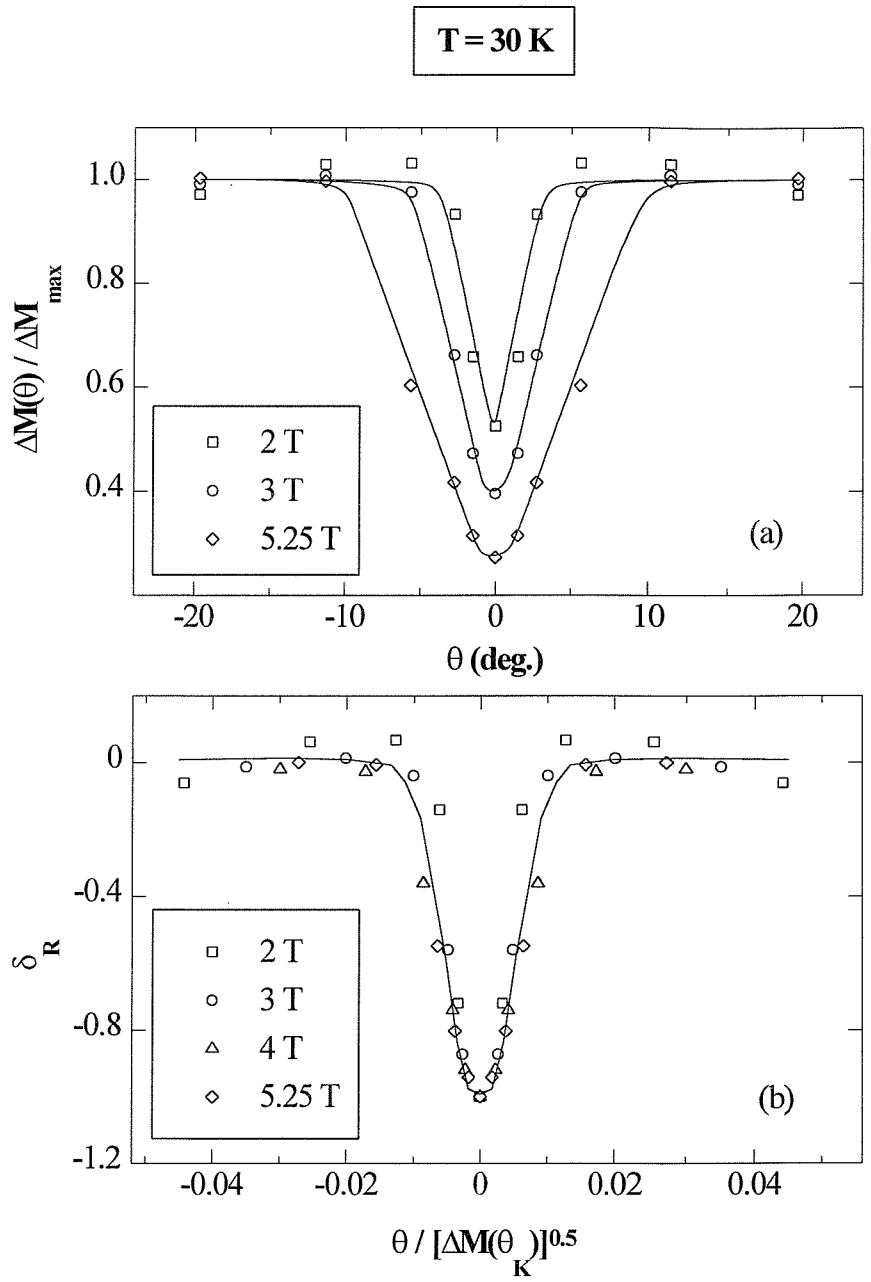

Figure 4.12: *Similar analysis for a constant temperature of 30K at the indicated applied fields. (a) The angular dependence of the normalised to its maximum value* ΔM *and (b) scaling of the represented in (a) curves with* $[\Delta M(\theta_K)]^{0.5}$. *The lines are a guide to the eye.*

As clearly seen in fig.4.11(a), the hysteresis width $\Delta M(\theta)$ varies linearly with θ for $\theta_L < \theta < \theta_K$. In order to understand this, we must recall that at this stage, the kinked structure stage, fractional vortices feel an increased pinning force due to their parts lying in the untwinned regions. The average force per unit length exerted on the vortices will increase with the number of kinks, produced by the increase of θ as predicted by equation (4.2). This is a direct result of the decrease of the size of the trapped segments in the twin planes [6]. We can express this force in terms of the relative variation of the length of the trapped segments δL / L, where L is the initial trapped length for the limit $\theta = \theta_L \cong 0$ and $\delta L = L - L(\theta)$:

$$f_{TP}(\theta) - f_{TP}(\theta_L) \approx [f_{TP}(\theta_K) - f_{TP}(\theta_L)] \cdot \frac{\delta L}{L} \tag{4.9}$$

In relation (4.9) $f_{TP}(\theta_K) = f_u$, the pinning force in the untwinned regions, is assumed to be angle independent, since in the magnetic field range of interest and for small angles only the component along the c-axis is relevant for the magnetic response of the untwinned regions [38]. For the angular variations considered here and from simple geometrical reasoning (fig.4.1(b)), δL / L can be approximated as:

$$\frac{\delta L}{L} \approx \frac{\tan\theta}{\tan\theta_K} \approx \frac{\theta}{\theta_K} \tag{4.10}$$

In addition, the relative decrease of the width of the magnetisation can be writen as:

$$\delta_R = \frac{\Delta M(\theta) - \Delta M(\theta_K)}{\Delta M(\theta_K) - \Delta M(\theta_L)} \tag{4.11}$$

Thus, combining relations (4.9) - (4.11) and taking into account that $f_u \propto \Delta M(\theta_K)$, $f_{TP}(\theta_L) \propto \Delta M(\theta_L)$ and $f_{TP}(\theta) \propto \Delta M(\theta)$, one finds that:

$$\delta_R \sim \frac{f_{TP}(\theta) - f_{TP}(\theta_L)}{f_u - f_{TP}(\theta_L)} - 1 \approx \frac{\theta}{\theta_K} - 1 \tag{4.12}$$

in agreement with the experimentally observed linear behavior of δ_R depicted in fig.4.11(a).

Figure 4.11(b), on the other hand, shows a striking scaling of the curves represented in fig.4.11(a). The relative decrease δ_R, as defined by eq.(4.11), is plotted as a function of θ / $[\Delta M(\theta_K)]^{0.5}$ at the indicated temperatures. As shown, also, in figure 4.12, a similar

analysis at T = 30 K for various applied fields leads to the same results. All the curves at all the temperatures for magnetic fields above 2 T converge into one.

From the above it is evident that θ_L and θ_K have the same temperature and field dependence. Furthermore, the successful scaling with $\Delta M(\theta_K) \propto f_u$ proves that the two critical angles depend only on the disorder in the untwinned regions. This behavior further supports that only the current density flowing in the untwinned regions, J, is relevant for the effectiveness of the trapping potential of the twin planes. It seems that the increase or decrease of the strength of the point disorder in the untwinned regions and consequently of f_u, is followed by changes in the effective potential barrier produced by the twin planes.

Vortex dynamics in the presence of extended defects has been the focus of a number of important, recent, theoretical works [10,12,13,39,44-49]. As discussed before, point disorder is theoretically expected to promote flux line wandering, while correlated disorder[1] to "inhibit wandering and promote localisation" [13], establishing the Bose Glass phase. In particular, in the case these two kinds of disorder coexist, weak random point disorder has been shown to destabilise the Bose Glass phase, inducing roughening of vortices. The angular study we performed is the indicated tool to distinguish which is the dominant pinning structure [13]. Nelson and Vinokur [13] but also Brandt [44] showed that in the presence of a Lorentz force perpendicular to a twin plane, segments of a vortex can be unpinned, forming half loops. These half loops extend for a distance $L_{\parallel}$ and $L_{\perp}$ in the directions parallel and perpendicular to the twin boundary, see fig.4.13.

Our experimental data verifies these theoretical predictions. Indeed, if w is the width of the potential barrier ε_{TP} of the twin plane, when we consider that a vortex is confined to a width $L_{\perp}$ instead of w, we can renormalise ε_{TP} [50]. Thus the effective potential barrier responsible for the vortex lock-in, is now:

$$\varepsilon_{TP}' = \varepsilon_{TP} \cdot \left(\frac{w}{L_{\perp}} \right) \tag{4.13}$$

[1] For directions of the applied field parallel to the extended defects.

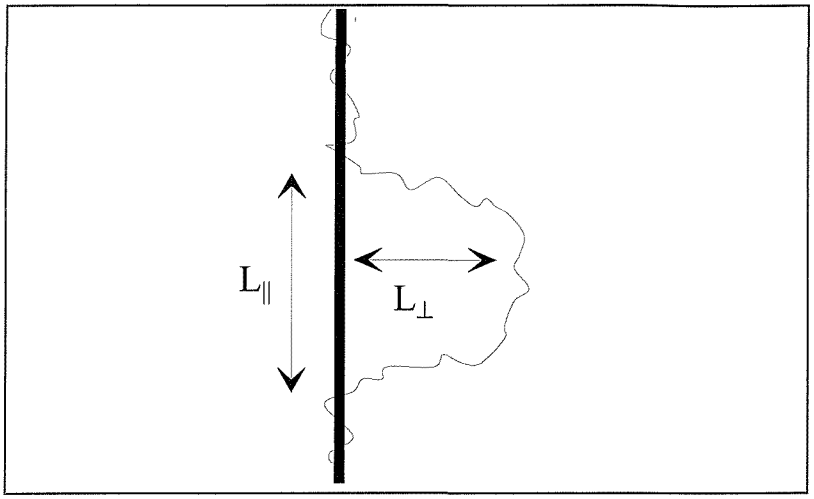

Figure 4.13: *Schematic representation of the half loop excitation of a vortex line out of a twin plane.*

Recalling the theoretical dependence of θ_K on ε_{TP} as found by Blatter *et al.* [6], $\theta_K \propto (\varepsilon_{TP})^{0.5}$, but using the effective potential barrier we have:

$$\theta_K \propto \left(\varepsilon_{TP} \cdot \frac{w}{L_\perp} \right)^{0.5} \tag{4.14}$$

Furthermore, Nelson and Vinokur [13] demonstrated that the perpendicular confinement length is inversely proportional to the current density J which produces the Lorentz force exerted on the trapped vortex (in our case J is the current density in the untwinned regions, $J \propto \Delta M(\theta_K)$), $L_\perp \propto 1/J$. Relation (4.14) then automatically gives,

$$\theta_K \propto J^{0.5} \Rightarrow \theta_K \propto \left[\Delta M(\theta_K)\right]^{0.5} \tag{4.15}$$

explaining the expirementally observed scaling. Consequently, our data verified for the first time, the theoretical predictions for the behavior of a vortex localised in an extended defect, in the presence of random point disorder.

Finally, the importance of the pinning strength in the untwinned regions f_u for vortex channeling means that there should be two consequences. First, at low fields, at the magnetisation's neck, one should not expect channeling to be favorable, due to the much smaller value of f_u (of the hysteresis width). We have seen before that indeed this seem to be the case (fig.4.6(a)), but it is difficult to easily distinguish any effects there,

since the hysteresis "neck" extends up to only about 1 T. Thus, we carried out measurements on the simply twinned crystal L (table 4.1), with an oxygen content of 6.96 (T_c = 93.4 K). For this crystal the low field part of the hysteresis extends up to around 3 T, for a temperature of 50 K. The twin planes are at 45° to the sample's edges. We compared three different orientations of the applied field[1]: parallel to the c-axis, tilted at 7° within the twin planes (denoted as 'in') and tilted at 7° in the plane defined by c-axis and the normal to the twin planes (denoted 'out'). As our previous results showed, a measuring angle of 7° is higher than the trapping angle at 50 K; thus, we can make a safe comparison of the aligned to the extended defects vortices case with the response of the bulk. Figure 4.14 presents the magnetic hysteresis of L at 50 K, for the three orientations. The contrast of the lower field behavior to that of the field region around the peak effect is clear. Tilting the applied field *in* the twin planes leaves unaffected the hysteresis width throughout the whole field range from 0 to 12 T, since the trapped in the twin planes vortices do not experience any change of the pinning force exerted on them. However, by tilting the applied field *out* of the twin planes, there is a double change. At fields above 3.6 T and around the peak effect vortex channeling is stalled, returning the pronounced magnetisation peak. However, at low fields, below around 3.6 T, ΔM and consequently the critical current are decreased, demonstrating that as expected twin planes act as strong pinning centres in this low f_u regime.

The second consequence the critical role of f_u on channeling should have, is that we should be able to observe pronounced changes on the vortex channeling mechanism in the same sample, by altering the oxygen concentration. Indeed, it has been shown (for example ref.[51,52]) that for high quality, pure samples the dominant pinning centres are oxygen vacancies; thus, an increased oxygen content reduces the existing microscopic point defects and, consequently, pinning in the untwinned regions, f_u. As a result, one should expect that in the field and temperature regime channeling is observed in a certain sample, this to be quenched with an adequate reduction of f_u by doping.

[1] See figure 3.2 for a schematic represantation of the sampleholder.

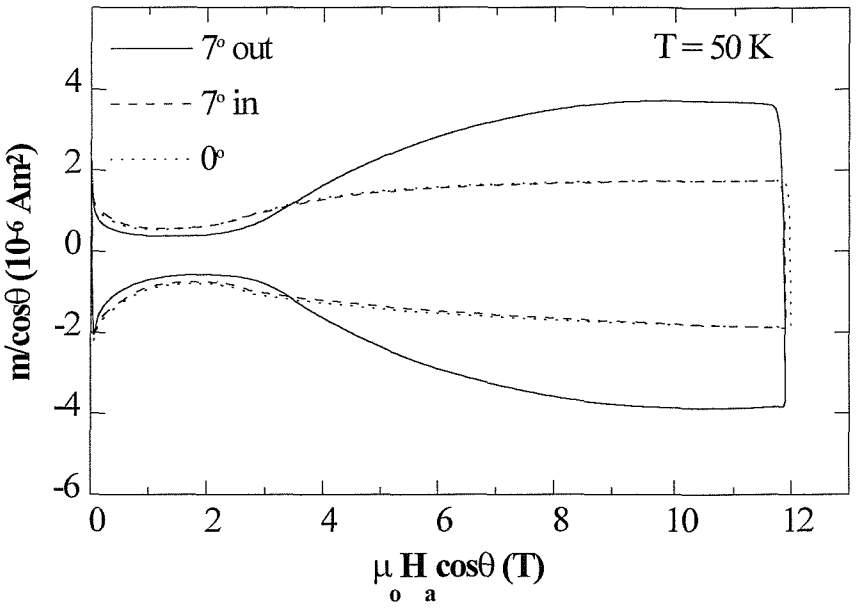

Figure 4.14: *Magnetic hysteresis of simply twinned crystal L for three different orientations of* H_a *in respect to the twin planes: at 0° aligned with them, tilted at 7° within the planar defects and tilted at 7° in the normal to the twins plane.*

To verify this, we have changed by annealing the oxygen content of twinned crystal A3 which exhibits vortex channeling. Figure 4.15(a) shows the isothermal magnetic hysteresis of sample A3 at 60 K for an oxygen content of $7-\delta = 6.90$ where channeling clearly occurs. Increasing the oxygen content to 6.96, as fig.4.15(a) vividly demonstrates, vortex channeling disappears. For comparison, scaled to size data of the detwinned crystal F at the same oxygen contents are presented. According to what was stated before, for a given oxygen content of a sample (and thus for A3 with the new oxygen content of 6.96) we can strengthen the pinning force f_u of the untwinned regions by lowering the temperature (as discussed before, due to the screening of thermal fluctuations by twin planes f_{TP} is much less sensitive to temperature variations than f_u). As a result, an adequate decrease of temperature should introduce again the flattening of the magnetic hysteresis (vortex channeling) in our results. Indeed, by lowering now the temperature from 60 K down to 40 K for sample A3 at the oxygen content of 6.96, the

characteristic for vortex channeling shape of the magnetic hysteresis depression appears again, as figure 4.15(b) shows.

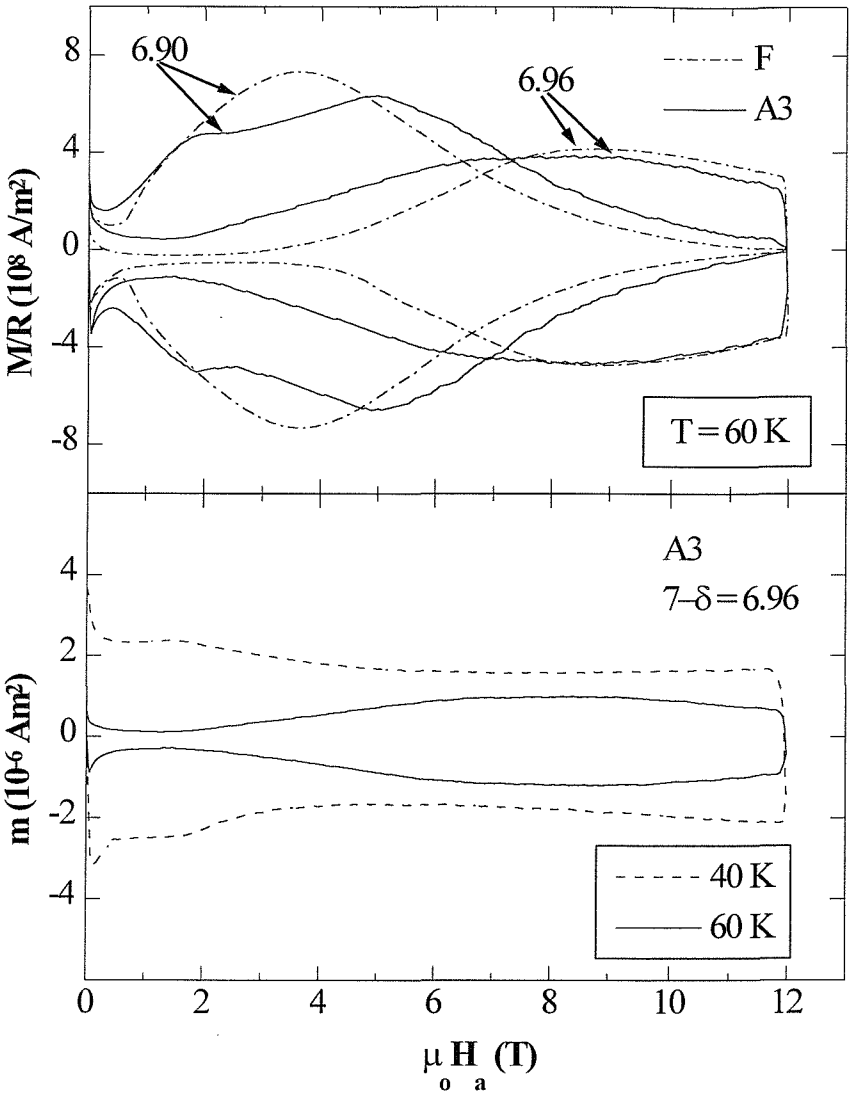

Figure 4.15: *Hysteresis loops (a) at 60 K for oxygen contents of 7-δ = 6.90 and 6.96 for A3 and F (see text) (b) at 60 K and 40 K for A3 with an oxygen content 7-δ = 6.96.*

Unavoidably, our measurements led to the clarification of the seemingly contradicting previous works. Thus, the strong pinning behavior of twin planes as this was demonstrated in transport measurements [21,22] can be easily explained in

accordance to the discussion above, in terms of the competition of the pinning force in the untwinned regions and in the twin planes. It is important to note the restriction of the magnetotransport measurements at high temperatures, around 85 - 90 K. At the elevated temperatures the transport technique is employed, f_u is expected to be much weaker than f_{TP} and therefore channeling is not feasible. On the other hand, previous works based on magnetisation measurements did not consider the strong pinning role of the intersections of different twin planes domains [18] or focused in the temperature and field regimes where channeling is not anticipated [19]. Furthermore, under the light of the undeniable existence of vortex channeling and in an effort to bridge the initial discrepancy of their results [25-28], the Argonne-Chernogolovka and the Bell groups in more recent magneto-optical reports [53-55] attributed this discrepancy to the angle of the twin planes with the natural flux gradient. For flux entering the sample, i.e. applied fields near H_{c1}, twin boundaries can prohibit or facilitate vortex motion depending on their angle to the edge of the sample and thus to the flux gradient; late numerical results by Groth *et al.* [41] backed their conclusion.

4.4 CONCLUSIONS

By studying the magnetisation of $YBa_2Cu_3O_{7-\delta}$ single crystals in a broad regime of temperature, magnetic field and angle, we have shown that twin planes can indeed act as channels for easier vortex motion and consequently limit pinning and critical currents. This depression of the magnetic hysteresis width due to vortex channeling is favorable only when the pinning force in the untwinned regions is stronger than the pinning force in the twin planes, up to a temperature of the order of 70 K and at fields centered around the magnetisation peak. At low applied fields, away from the peak region, twin planes enhance both pinning and critical current density. Of major importance is also the existence of intersections of different domains of twin boundaries in the sample, which can provide strong columnar-like pinning centres, inhibiting channeling and hence preventing the decrease of the critical current.

Our results present clear experimental evidence for the existence of two critical angles. Below a lock-in angle θ_L vortices are locked-in to the twin planes while above a

trapping angle θ_K ($\theta_L < \theta_K$) point defects dominate pinning. In the case of fractional vortices ($\theta_L < \theta < \theta_K$) ΔM grows linearly with θ. Our results demonstrate that as the pinning force in the untwinned regions increases, either by temperature or by field, θ_K increases.

We demonstrate that the two characteristic angles θ_L and θ_K scale with the hysteresis width obtained for $\theta > \theta_K$. This scaling suggests that contrary to theoretical expectations, the two critical angles depend critically on the disorder in the untwinned regions. The scaling of the data can be explained in terms of vortices being localised in a width larger than the potential well produced by the twin planes and fixed by the current flowing in the untwinned regions.

REFERENCES

[1] G. Deutscher and K. A. Müller, Phys. Rev. Lett. **59**, 1745 (1987).

[2] P. H. Kes, Physica C **153-155**, 1121 (1988).

[3] I. N. Khlustikov and A. I. Buzdin, Adv. Phys. **36**, 271 (1987).

[4] A. A. Abrikosov, A. I. Buzdin, M. L. Kulic *et al.*, Sup. Sci. Tech. **1**, 260 (1989).

[5] G. Blatter, J. Rhyner, V. M. Vinokur, Phys. Rev. B **43**, 7826 (1991).

[6] G. Blatter, M. V. Feigel'man, V. B. Geshkenbein *et al.*, Rev. Mod. Phys. **66**, 1125 (1994).

[7] M. Sarikaya, R. Kikuchi, I. A. Aksay, Physica C **152**, 161 (1988).

[8] G. P. E. M. van Bakel, D. A. Hof, J. P. M. van Engelen *et al.*, Phys. Rev. B **41**, 9502 (1990).

[9] M. P. A. Fisher, P. B. Weichman, G. Grinstein *et al.*, Phys. Rev. B **40**, 546 (1989).

[10] D. R. Nelson and V. M. Vinokur, Phys. Rev. Lett. **68**, 2398 (1992).

[11] M. Tinkham, *Introduction to Superconductivity*, Mc Graw-Hill, Singapore (1996).

[12] U. C. Täuber and D. R. Nelson, Phys. Rev. B **52**, 16106 (1995).

[13] D. R. Nelson and V. M. Vinokur, Phys. Rev. B **48**, 13060 (1993).

[14] L. Ya. Vinnikov, L. A. Gurevich, G. A. Emelchenko *et al.*, Solid St. Comm. **67**, 421 (1988).

[15] G. J. Dolan, G. V. Chandrashekhar, T. R. Dinger *et al.*, Phys. Rev. Lett. **62**, 827 (1989).

[16] T. K. Worthington, F. H. Holtzberg, C. A. Feild, Cryogenics **30**, 417 (1990).

[17] M. C. Marchetti and D. R. Nelson, Phys. Rev. B **42**, 9938 (1990).

[18] U. Welp, W. K. Kwok, G. W. Crabtree *et al.*, Appl. Phys. Lett. **57**, 84 (1990).

[19] D. L. Kaiser, F. W. Gayle, L. J. Swartzendruber *et al.*, J. Appl. Phys. **70**, 5739 (1991).

[20] E. M. Gyorgy, R. B. Van Dover, L. F. Schneemeyer *et al.*, Appl. Phys. Lett. **56**, 2465 (1990).

[21] W. K. Kwok, U. Welp, G. W. Crabtree *et al.*, Phys. Rev. Lett. **64**, 966 (1990).

[22] S. Fleshler, W. K. Kwok, U. Welp *et al.*, Phys. Rev. B **47**, 14448 (1993).

[23] I. V. Grigorieva, L. A. Gurevich, L. Ya. Vinnikov, Physica C **195**, 327 (1992).

[24] I. V. Grigorieva, Sup. Sci. Tech. **7**, 161 (1994).

[25] C. A. Durán, P. L.Gammel, R. Wolfe *et al.*, Nature **357**, 474 (1992).

[26] L. A. Dorosinskii, V. I. Nikitenko, A. A. Polyanskii *et al.*, Physica C **219**, 81 (1994).

[27] L. A. Dorosinskii, V. I. Nikitenko, A. A. Polyanskii *et al.*, *Proceedings of 7th Int. Work. on Crit. Currents*, Alpbach, Austria (1994), editor H. W. Weber (World Scientific), p.331.

[28] V. K. Vlasko-Vlasov, L. A. Dorosinskii, A. A. Polyanskii *et al.*, Phys. Rev. Lett. **72**, 3246 (1994).

[29] M. Oussena, P. A. J. de Groot, S. J. Porter *et al.*, Phys. Rev. B **51**, R1389 (1995).

[30] K. Deligiannis, M. Oussena, P. A. J. de Groot *et al.*, Inst. Phys. Conf. Ser. **148**, 559 (1995).

[31] M. Oussena, P. A. J. de Groot, K. Deligiannis *et al.*, Phys. Rev. Lett. **76**, 2559 (1996); Phys. Rev. Lett. **77**, 792 (1996).

[32] R. L. Peterson, J. Appl. Phys. **67**, 6930 (1990).

[33] H. Pastoriza and P. H. Kes, Phys. Rev. Lett. **75**, 3525 (1995).

[34] A. Brass, H. J. Jensen, A. J. Berlinsky, Phys. Rev. B **39**, 102 (1989).

[35] H. J. Jensen, Y. Brechet, A. Brass, J. Low Temp. Phys. **74**, 293 (1989).

[36] A. A. Zhukov, H. Küpfer, H. Clauss *et al.*, Phys. Rev. B **52**, R9871 (1995).

[37] R. J. Wijngaarden, R. Griessen, J. Fendrich *et al.*, Phys. Rev. B **55**, 11832 (1997).

[38] L. Klein, E. R. Yacoby, Y. Yeshurun *et al.*, Phys. Rev. B **49**, 4403 (1994).

[39] T. Hwa, D. R. Nelson, V. M. Vinokur, Phys. Rev. B **48**, 1167 (1993).

[40] S. Senoussi, M. Oussena, G. Collin *et al.*, Phys. Rev. B **37**, 9792 (1988).

[41] J. Groth, C. Reichhard, C. J. Olson *et al.*, Phys. Rev. Lett. **77**, 3625 (1996).

[42] I. B. Khalfin, L. A. Dorosinskii, B. Ya. Shapiro, Phys. Rev. B **51**, 1245 (1995).

[43] U. Welp, T. Gardiner, D. Gunter *et al.*, Physica C **235-240**, 241 (1994).

]44] E. H. Brandt, Phys. Rev. Lett. **69**, 1105 (1992).

[45] L. Balents and M. Kardar, Phys. Rev. B **49**, 13030 (1994).

[46] M. C. Marchetti and V. M. Vinokur, Phys. Rev. Lett. **72**, 3409 (1994).

[47] M. C. Marchetti and V. M. Vinokur, Phys. Rev. B **51**, 16276 (1995).

[48] T. Halpin-Healy and Y.-C. Zhang, Phys. Rep. **254**, 215 (1995).

[49] I. Arsenin, T. Halpin-Healy, J. Krug, Phys. Rev. E **49**, R3561 (1995).

[50] V. M. Vinokur, private communication.

[51] A. A. Zhukov, H. Küpfer, G. Perkins *et al.*, Phys. Rev. B **51**, 12704 (1995).

[52] J. L. Vargas and D. C. Larbalestier, Appl. Phys. Lett. **60**, 1741 (1992).

[53] C. A. Durán, P. L.Gammel, D. J. Bishop *et al.*, Phys. Rev. Lett. **74**, C3712 (1995).

[54] U. Welp, T. Gardiner, D. O. Gunter *et al.*, Phys. Rev. Lett. **74**, R3713 (1995).

[55] G. W. Crabtree, W. K. Kwok, U. Welp *et al.*, *Invited Paper at the Int. Sem. on Sup. in High Mag. Fields*, Tsukuba, Japan (1995).

5. THE $YBA_2CU_3O_{7-\delta}$ PHASE DIAGRAM

5.1 THEORETICAL BACKGROUND

The conventional mean field vortex phase diagram for a pure system consists merely of a Meissner phase for $H_a < H_{c1}$ and a mixed (Shubnikov) phase for $H_{c1} < H_a < H_{c2}$. Above H_{c2} the superconducting-to-normal transition occurs. Continuous second order phase transitions were predicted at H_{c1} and H_{c2} (figure 5.1).

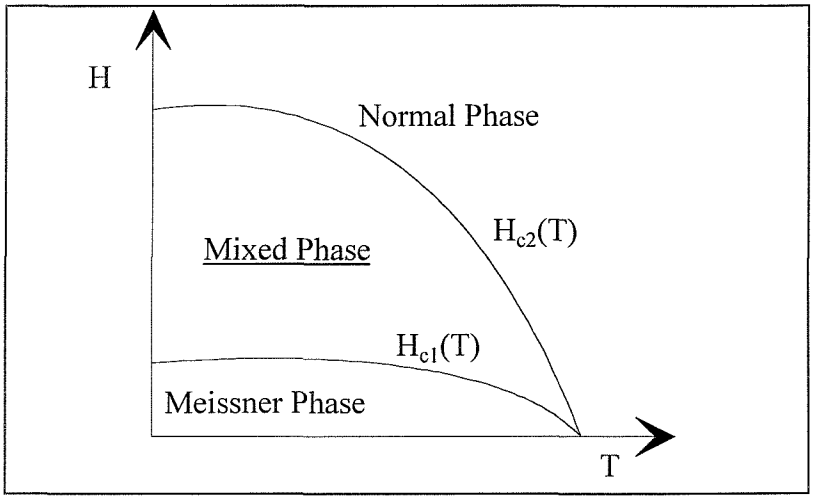

Figure 5.1: *Phase diagram for conventional type II superconductors.*

In this rather simplified picture, thermal fluctuations and their effects on the vortex matter were ignored. Indeed, though it was early conceived that thermal fluctuations can melt the Abrikosov lattice [1], at the time of the low temperature type II superconductors this melting line $H_m(T)$ lied unobservably close to $H_{c2}(T)$ [2,3].

However, in high temperature superconductors, due to the higher anisotropies, the high operating temperatures, the shorter coherence lengths and the nonlocality of the vortex-vortex interactions, the role of thermal energy becomes pivotal and is manifested in an enhanced value of the Ginzburg number Gi. Consequently [2] the destruction of the Abrikosov lattice due to thermal agitation in the H-T phase diagram occurs much

deeper in the Shubnikov phase, being clearly distinguishable and far from the superconducting-to-normal transition. This possibility was first expressed by Brezin *et al.* [4] and by Nelson [5].

Theoretically, the destruction of the Abrikosov lattice via melting has certain characteristics: total loss of translational order and a vanishing shear modulus [2]. However, a complete melting theory is still not available [2,6]. Similarly, the position and the shape of the melting line in the H-T diagram cannot be predicted. It is only the semiquantitative criterion of melting, expressed by Lindemann [7] in 1910 for a crystalline lattice, which covers this theoretical gap of understanding.

According to the Lindemann criterion, a crystalline lattice looses its stability under the influence of thermal fluctuations of its constitutive elements (which can be atoms, vortex lines, etc.) and melts when the mean-squared amplitude of fluctuations $\langle u^2(T)\rangle_{th}$ increases beyond a certain fraction c_L of the lattice constant α_o:

$$\langle u^2(T_m)\rangle_{th} \approx c_L^2 \alpha_o^2 \tag{5.1}$$

The same criterion has been used first by Houghton *et al.* [8] and since then established to estimate the melting temperature of the vortex line lattice. The so called Lindemann number c_L has an approximate value of $c_L \sim 0.1 - 0.2$; this value of c_L should depend only weakly on the specific material of the crystalline lattice [2].

In addition, the Lindemann criterion can be expressed in terms of characteristic energies. The vortex lattice undergoes a melting transition when the thermal agitation energy equals the elastic energy barriers keeping vortices confined in the cage their nearest neighbours produce, at the lattice equilibrium positions (figure 5.2):

$$\kappa_B T_m = E_{el} \tag{5.2}$$

Nevertheless, there are serious questions concerning not only the order of this melting transition but also the vortex phases it separates; recently these problems have been the subject of a hot debate.

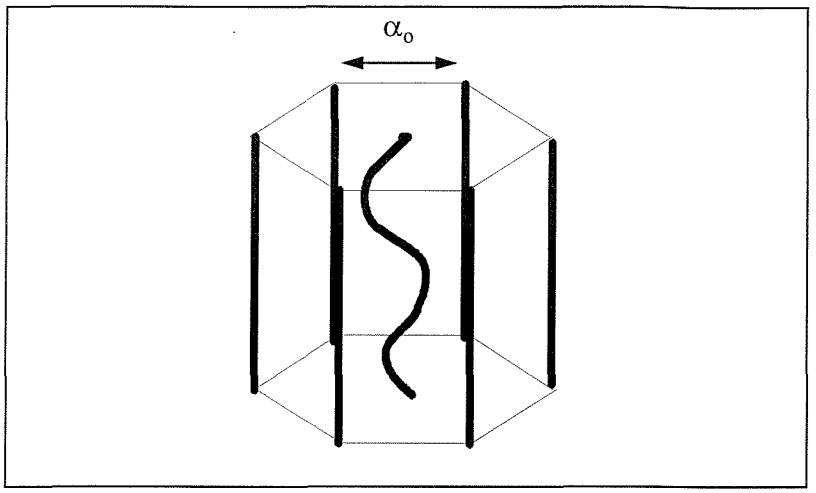

Figure 5.2: *A vortex confined in the cage potential produced by its nearest neighbours: visualisation of the Lindemann criterion.*

In a clean system, above the melting transition there exists a vortex liquid phase, consisting of weakly confined vortex lines and exhibiting linear I-V characteristics. Vortex motion yields the well known flux flow resistivity (eq.(2.2)) which is a field dependent fraction of the normal resistivity and thus the vortex liquid state cannot be characterised as a truly superconducting state. The exact description of vortices in the liquid phase is still an open experimental and theoretical question with possibilities such as entangled or disentangled vortices, pinned or unpinned liquid arising [2].

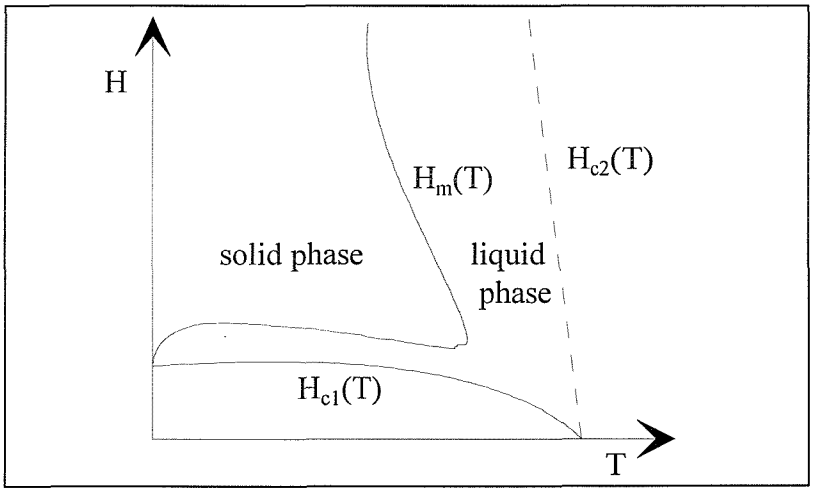

Figure 5.3: *A general form of the H-T diagram in the case of high temperature superconductors.*

Below the melting transition, always considering the clean limit, vortices freeze in the usual hexagonal Abrikosov lattice configuration (see figure 5.3). Brezin *et al.* [4] predicted that a transition of this kind is a first order transition. Strong numerical evidence for a first order melting transition was given by the Monte Carlo simulations of Hetzel *et al.* [9].

Making use of the Lindemann criterion at moderate magnetic fields $H_{c1} << H_a << H_{c2}$, Blatter *et al.* [2,10] estimated the temperature dependence of the melting line, $H_m(T)$. They achieved this by determining the mean-squared amplitude of fluctuations $\langle u^2(T)\rangle_{th}$ using the shear and tilt elastic moduli as given in chapter 2. The estimated temperature dependence of the melting line is then [2]:

$$H_m(T) \approx \beta_m \cdot \frac{c_L^4}{Gi} \cdot H_{c2}(0) \cdot \left(1 - \frac{T}{T_c}\right)^n \qquad (5.3)$$

where $\beta_m \sim 5.6$. Blatter *et al.* [2] derived an exponent $n \sim 2$, i.e. a quadratic dependence of H_m on $T_c - T$, valid as long as the temperature T lies outside the fluctuation regime [2], that is $1 - t \geq Gi$, with $t = T/T_c$. In addition, for $YBa_2Cu_3O_{7-\delta}$ the simple square power-law relation (5.3) holds only several kelvin below T_c, as Blatter and Ivlev [11] have shown, due to the approach at lower temperatures of the melting line close to H_{c2} and the subsequent suppression of the order parameter.

The introduction of disorder in the system complicates the problem. Weak, random, point disorder[1], which is present in all the "real life" high temperature superconductors, should alter the low temperature Abrikosov lattice - but how? The Vortex Glass model, described in chapter 2, was believed to give a satisfying answer to the above question [12-15]. Pinning causes an exponential decay of translational order and destroys the long range periodicity of the lattice, producing a Vortex Glass phase. Simultaneously lattice dislocation defects are favored by disorder [13-15]. However, shear stiffness survives and thus critical currents too. A similar glassy behavior, as we have seen, was predicted by Feigel'man *et al.* [16] in the frame of the collective creep model. Nevertheless, soon a number of contradictions emerged. Noteably, decoration experiments of the vortex lattice revealed large dislocations-free regions [17].

[1] Which will be the case in this chapter.

Simultaneously, new theoretical calculations suggested a slower (logarithmic) growth of disorder induced deformations [18].

Giamarchi and Le Doussal have recently proposed a new possibility for the low temperature solid phase [19,20]. They demonstrated that while disorder induces an algebraic growth of displacements at short length scales, when the lattice's periodicity is correctly taken into account, it takes over at large length scales and leads to a decay of the translational order at most algebraic. Furthermore, the authors [20] demonstrated that for weak disorder in the 3 dimensional case, dislocations are not favorable. The result is a solid phase which is free of dislocations, retains quasi-long range order and which is predicted to exhibit Bragg peaks in neutron scattering experiments. This weak glass state was therefore termed *Bragg Glass* phase. In agreement with the above, a number of other recent theoretical works verify the existence of this "rather ordered quasilattice" at low fields and temperatures, for example the works of Ertas *et al.* [21] and of Vinokur *et al.* [22].

A reference should be made to a few theoretical works which seem opposed to the streamline acceptance of a solid-to-liquid first order transition in the vortex phase diagram. Most notable, Radzihovsky [23,24] shows that the transition at $H_m(T)$ should be continuous. Also Moore [25] suggests that the observed first order transition is in fact a crossover from 3D to 2D behavior once the phase correlation length along the field direction in the liquid[1] state becomes comparable to the sample's dimensions. Finally in a very recent work, Carruzzo *et al.* [26] give an elegant alternative interpretation of this first order transition as a supersoftening transition of the vortex lattice[2].

[1] According to Moore [25] the liquid phase exists over the whole mixed state in the H- T diagram.

[2] According to Carruzzo *et al.* [26] the solid phase exists over the whole mixed state in the H - T diagram.

5.2 EXPERIMENTAL EVIDENCE OF A MELTING TRANSITION

5.2.1 YBCO

The first evidence of a melting transition came from Gammel *et al.* [27], in vibrating reed experiments on $YBa_2Cu_3O_{7-\delta}$ crystals, where they found a sharp peak in the damping of the oscillatory motion, along a field dependent line in the phase diagram, $T_m(H)$. However, it was shown that such results can also be explained naturally, by thermally activated depinning [28]. In this early time of rather dirty samples, transport and ac susceptibility measurements of Worthington *et al.* [29], and low-frequency torsional oscillator data of Farrell *et al.* [30] and Beck *et al.* [31], also gave useful hints about a possible melting transition.

An important step of understanding came with the transport data of Charalambous *et al.* [32], Safar *et al.* [33], and Kwok *et al.* [34], on high quality single crystals. A series of reproducible jumps in the resistive transition at low currents, accompanied by hysteresis in the temperature dependence were the first signs of a first order transition. At these jumps (or kinks) the resistivity sharply drops to zero (upon freezing) within a temperature interval of a width of the order of 100 mK. This transition is shown to be suppressed by extended defects such as the twin planes [34,35].

Safar *et al.* [36], found in high field transport measurements in untwinned samples, a well defined point H_{cp} in the phase diagram, on the $H_m(T)$ line, above which, $H > H_{cp}$, the resistive transition broadens and the melting line becomes voltage criteria dependent. The magnetic field H_{cp} plays the role of a multicritical point where the first order transition terminates, being replaced by a continuous, possibly second order, solid-to-liquid transition [36].

With the same technique, Kwok *et al.* [37] demonstrated an asymmetric hysteresis behavior at H_m which they attributed to the different way the melting and the freezing mechanisms are realised within a pure enough sample. In a following work, Kwok *et al.* [38] detected a precursor to the melting transition peak effect. Upon melting, just below the solid-to-liquid transition, the resistivity decreases before it sharply increases to the

flux flow value ρ_f (see eq.2.2). They interpreted this as a result of shear softening of the solid prior to melting and of the better adjustment of vortices to the pinning sites - a rather classical explanation [39]. Fendrich *et al.* [40], demonstrated how the first order transition can be suppressed by increasing point disorder. In high quality samples with a sharp liquid-to-solid phase transition, controlled point defects were introduced by 1 MeV electron irradiation. The result was a smearing out of the resistive transition and vanishing of the resistive hysteresis.

However, in some nice work by Jiang *et al.* [41], it was shown that since resistivity is not a thermodynamic quantity, it cannot be a safe criterion of a first order transition. They demonstrated that the observed resistive hysteresis can in fact be attributed to a current-induced nonequilibrium effect rather than to a first order transition. Indeed, if the scenario of a first order transition were true convincing thermodynamic evidence like a discontinuity of the entropy S(T,H) and of the magnetisation M(T,H), both first derivatives of the Gibbs free energy G, should be forced out of hiding.

The first unambiguous such evidence came from Liang *et al.* [42] who reported a discontinuity of reversible magnetisation in untwinned $YBa_2Cu_3O_{7-\delta}$ single crystals, by means of SQUID magnetometry. The sample was moved in a minimum length of 1 cm. Liang *et al.* estimated the entropy jumps ΔS_V per vortex per CuO_2 layer in units of κ_B and found good agreement with the numerical results of Hetzel *et al.* [9]. It is:

$$\Delta S_V = -\frac{\Delta M}{H_m} \cdot \frac{d H_m}{d T} \cdot \frac{\Phi_o \cdot d}{\kappa_B} \tag{5.4}$$

where d is the c-axis lattice constant and H_m the melting field. Hetzel *et al.* [9] numerically estimated a value of $\Delta S_V = 0.3\kappa_B$ at $H_m = 10$ T, while Liang and coworkers estimated that at melting fields of 1 and 4 T, ΔS_V is respectively $0.8\kappa_B$ and $0.6\kappa_B$.

Welp *et al.* [43] using SQUID magnetometry showed that the discontinuous jumps of the magnetisation, found in high quality untwinned $YBa_2Cu_3O_{7-\delta}$ single crystals, coincide in the H - T plane with the position of the resistive kinks, convincingly supporting the existence of a melting transition in the vortex phase diagram of $YBa_2Cu_3O_{7-\delta}$. In order to get these results, Welp *et al.* [43] used not only moving but also stationary-sample SQUID magnetometry, by measuring the SQUID voltage as the

temperature of the sample drifts, showing that the observed magnetisation jumps are not a side effect of any field inhomogeneities. Remarkably, Welp and coworkers found that the solid phase becomes denser on melting: this "icelike" melting can be due to the entropy gain of flexible entangled vortices in a denser liquid with long range interactions [44,45]. They estimated a constant with temperature value of $\Delta S_V = 0.65\kappa_B$ below 88 K, which rapidly decreased to zero above this threshold temperature.

The most direct and impressive evidence of a first order transition, however, came by Schilling *et al.* [46], who performed calorimetric measurements in a high purity untwinned $YBa_2Cu_3O_{7-\delta}$ single crystal and observed an entropy discontinuity (latent heat) which appears as a peak in the measured specific heat C. Schilling *et al.* estimated the entropy jumps ΔS_V per vortex per superconducting layer and found close agreement with the values extracted in the same sample by the magnetisation measurements of Welp *et al.* [43] (fig.5.4). An approximately constant value of $\Delta S_V = 0.45\kappa_B$ was found.

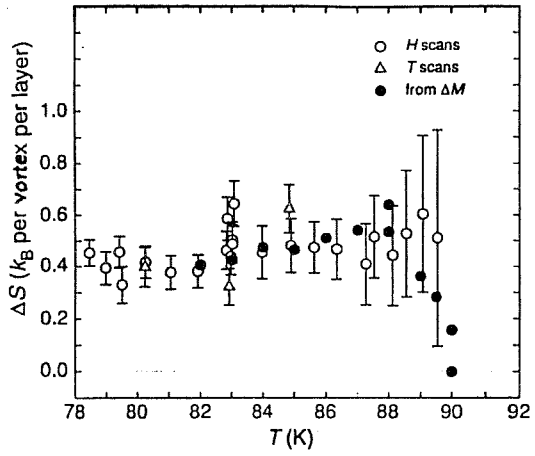

Figure 5.4: *Entropy jump* ΔS *(in text* ΔS_V*) per vortex per superconducting layer as estimated by Schilling et al. [46] for* $YBa_2Cu_3O_{7-\delta}$.

A region of solid and liquid coexistence was found by Fendrich *et al.* [47], who carried out simultaneous magnetisation (stationary-sample SQUID magnetometry) and transport measurements in the same sample. This region is enclosed in the width of the magnetic transition. The magnetic and resistive melting transitions are shown to start, upon freezing, at the same temperature; however the first is completed at a much lower

temperature than the second one. Authors based their interpretation on the influence of the existing chemical inhomogeneities in the sample. They also showed that the melting transition is independent of the motion of the vortex matter.

Finally Wu *et al.* [48], attempted to investigate the c_{66} collapse at the first order transition, by measuring the complex resistivity of the vortex system. Modelling of their results gave a collapse of the shear modulus at H_m by a factor of 400.

5.2.2 BSCCO

Together with $YBa_2Cu_3O_{7-\delta}$, $Bi_2Sr_2CaCu_2O_8$ is the only high temperature superconductor whose the phase diagram has been the focus of so many experimental and theoretical studies. The essential difference in this case is that $Bi_2Sr_2CaCu_2O_8$ has a substantially greater anisotropy γ than $YBa_2Cu_3O_{7-\delta}$. Because of the large anisotropy the various phase transitions in the $Bi_2Sr_2CaCu_2O_8$ phase diagram occur at particularly low fields, compared to $YBa_2Cu_3O_{7-\delta}$, of the order of a few hundred Oe. Furthermore, while for $YBa_2Cu_3O_{7-\delta}$, as we have seen, the first order transition is theoretically and experimentally considered to be a solid-to-liquid melting of vortex lines, in $Bi_2Sr_2CaCu_2O_8$ other possibilities also arise.

Theoretically, Glazman and Koshelev [49] proposed the existence of a temperature independent critical field, B_{2D}. Below B_{2D} pancake vortices in different layers coupled via electromagnetic (EM) and Josephson interactions, are lined up and form vortex lines. Above B_{2D} the energetic cost of in-plane shear deformation is bigger than that of a tilt deformation on the scale of the interlayer distance d [49,50] and the flux lattice decomposes into weakly interacting 2D lattices. Taking the parameter $k_{max} \sim 1/\xi_{ab}$, it is [6,49]:

$$B_{2D} = 2 \cdot \pi \cdot \frac{\Phi_o \cdot \ln(\gamma \cdot k_{max} \cdot d)}{\gamma^2 \cdot d^2} \qquad (5.5)$$

In addition, Glazman and Koshelev [49] predicted that for strongly layered superconductors and $B < B_{2D}$, with increasing temperature first a 3D solid-to-liquid melting transition occurs followed by a decoupling transition from a vortex line liquid

to uncorrelated vortex pancakes. The latter marks the vanishing of the tilt modulus c_{44}. For fields higher than B_{2D} where 2D lattices exist, a melting transition to a hexatic phase is predicted with simultaneous vanishing of c_{44} and c_{66} - this hexatic phase is turned into a liquid at higher temperatures.

Experiments of small-angle neutron diffraction (SANS) by Cubitt *et al.* [51] were the first to show a flux line lattice in $Bi_2Sr_2CaCu_2O_8$ and a rapid drop of the diffraction intensity at $T_m(H)$ with a simultaneous appearance of finite resistance in the mixed state. At the time this result was interpreted as a 3D vortex lattice melting. The diffraction intensity disappeared also at low temperatures with increasing the applied field, due to the flux lattice decomposition above a field B_{2D} as described earlier.

μSR measurements by Lee *et al.* [52] also showed a sharp transition of the flux line lattice, determined from a sudden sign change of the asymmetry of the field distribution, which they associated with flux lattice melting. In addition the low temperature decomposition transition in field was observed.

Magnetic and susceptibility measurements of Pastoriza *et al.* [53] gave the first thermodynamic evidence for the order of the observed transition. An abrupt change in the magnetisation and a frequency and amplitude independent peak of the in-phase component of the ac susceptibility witness a first order transition. The authors found good agreement of their results with the Glazman-Koshelev model [49] and they attributed the first order transition to decoupling. They estimate a $\Delta S_V \sim 0.06\kappa_B$. Similar work by Doyle *et al.* [54] with a miniature mutual inductance technique led to the same conclusion.

In an elegant work, Pastoriza and Kes [55] suggested that in $Bi_2Sr_2CaCu_2O_8$ melting and decoupling can be a simultaneous event. Using a partially masked and irradiated crystal they detected a sharp voltage drop at the freezing temperature T_m due to the appearance of shear vortex-vortex interactions.

An important step was taken by Zeldov *et al.* [56] who used miniature Hall probes to measure the local vortex density. They have shown a discontinuous field and temperature dependent decrease of a thermodynamic quantity, the flux density (dc magnetic induction) which can be directly attributed to a first order transition. Zeldov *et*

al. found an unexplained flattening of the transition line at low temperatures and further down its termination in a critical point. They also observed the freezing expansion of vortex matter and estimated a value of ΔS_V which increased with temperature, figure 5.5. They attributed the transition to *sublimation*, that is simultaneous melting and decoupling of a solid lattice to uncorrelated pancakes.

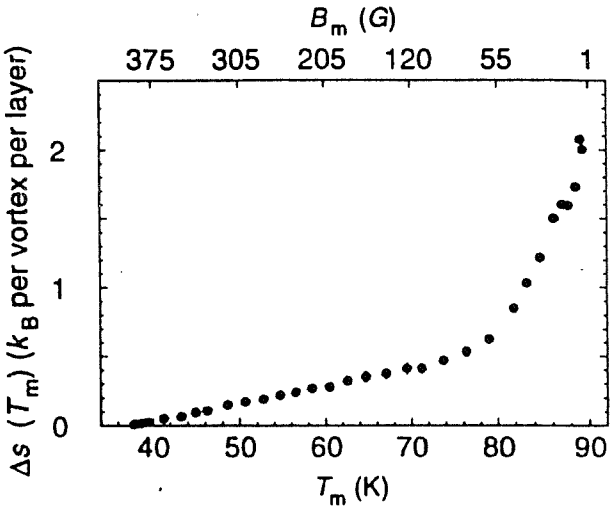

Figure 5.5: *The entropy jump* ΔS *(in text* ΔS_V*) per vortex per superconducting layer as estimated by Zeldov et al. [56] for* $Bi_2Sr_2CaCu_2O_8$.

It is worth mentioning that the thermodynamic origin of the results of Zeldov and his coworkers was challenged by Farrell *et al.* [57], who claimed that the observed jump in local and global magnetisation can be attributed (in the case of $Bi_2Sr_2CaCu_2O_8$ only) to artifacts such as flux inhomogeneities caused by geometrical barriers. Farrell and coworkers demonstrated that the entropy jump is controlled by the magnetic irreversibility, making it difficult to relate it to a true phase transition.

Finally, it was shown by Blatter *et al.* [10] that when one incorporates the EM interactions in the study of the vortex system at high anisotropies, as in the case of $Bi_2Sr_2CaCu_2O_8$, the transition is best described by the power law of eq.(5.3) with n=3/2:

$$H_m(T) \approx \beta_m \cdot \frac{c_L^4}{Gi} \cdot H_{c2}(0) \cdot \left(1 - \frac{T}{T_c}\right)^{3/2} \qquad (5.6)$$

5.3 PEAK EFFECT

Another intriguing feature is the magnetic hysteresis anomaly observed in these high temperature superconducting oxides, namely the increase of the magnetisation with the magnetic field. Contrary to the peak effect in conventional superconductors, observed close to H_{c2}, in the high-T_c oxides the anomaly is evident well below H_{c2}.

In the past, proposed explanations have attributed this peak in the magnetisation to a percolating network of normal zones, like Daeumling *et al.* [58], or reversible zones, like Klein *et al.* [59]. Sample inhomogeneities provide new pinning centers and cause the increase of the critical current with the field. After the peak maximum they turn normal or reversible, the crystal acquires a granular structure and the magnetisation decreases.

A 3D to 2D vortex lattice transition has been also considered, e.g. by Hardy *et al.* in Tl-based single crystals [60]. G. Yang *et al.* [61], working in $Bi_2Sr_2CaCu_2O_8$ suggest a matching effect between the decoupled 2D pancake vortices and dislocations networks present in the crystal, to be the cause of the observed peak effect. Another possible explanation was a crossover between bulk pinning and surface barriers, as Kopylov *et al.* [62] have proposed.

Other possible interpretations of the peak effect are based on the clasical approach of Pippard where the increase of current with magnetic field is due to an improved adjustment of vortices to the pinning potential. This can be a result of elastic softening of the vortex lattice (e.g. work by Zhukov *et al.* [63]).

It was only recently that the peak effect was attributed to a sharp phase transition by Khaykovich *et al.* [64]. As we will analyse in the next session, in their study of the vortex phase diagram in $Bi_2Sr_2CaCu_2O_8$, the authors suggest that the peak effect there is produced by an unprecedented thermodynamic phase transition of the flux line lattice, between two distinct solid phases.

Coming to the specific case of the less anisotropic $YBa_2Cu_3O_{7-\delta}$ the peak in the magnetisation reported until now, commonly called the "fishtail" peak, has two main characteristics: firstly, it is very broad and thus unlikely to result from a relatively sharp

thermodynamic vortex phase transition and secondly, its field position $H_p(T)$ decreases with temperature.

5.4 Results and Discussion

Magnetic measurements were performed in the 12 T VSM in Southampton [65]. Transport measurements were carried out in the cryostat of the VSM [65]. The samples were zero field cooled at the desired temperature and then the magnetic moment was measured as a function of the magnetic field, which was applied at a constant sweep rate.

Transport measurements were performed by S. Pinfold. A conventional four point AC method was used, with an AC current source and a Stanford SR530/830 Lock-in Amplifier to measure the voltage drop. The technique had a resolution of 5 nV and was applied in a field range up to 12 T. Contacts to the samples were made by applying narrow pads of Ag epoxy on the crystal, after its thorough cleaning. The epoxy was Dupont silver conductive composite 7838. For a four point measurement, the current pads covered the two opposite edges of the crystal, so as to provide a uniform current density. The voltage pads were placed on the upper surface of the crystal. Care was taken to avoid any contact between the different pads. The crystal was then placed in the furnace with an oxygen flow. The curing temperature was chosen equal to the annealing temperature, in order to prevent any change of oxygen content. After curing for 1 h the crystal was quenched to room temperature. Gold wires of 50 μm diameter were attached to the pads with Ag epoxy and then dried at 120° C. The resistance of the contacts is typically less than 1 Ω. For the measurements we used a transport current of 0.1 mA. A schematic representation of a crystal with the employed electrical contact configuration can be seen in figure 5.6.

Details of the crystals used can be found in table 5.1, below. DT and TW stands for detwinned and twinned crystals, respectively; α_x is the length, α_y the width and α_z the thickness of the sample. As explained in section 3.5, to produce oxygen concentrations of $7-\delta = 6.90, 6.93, 6.96$ we annealled the samples at 520°, 475° and 450° C respectively, in the presence of oxygen flow.

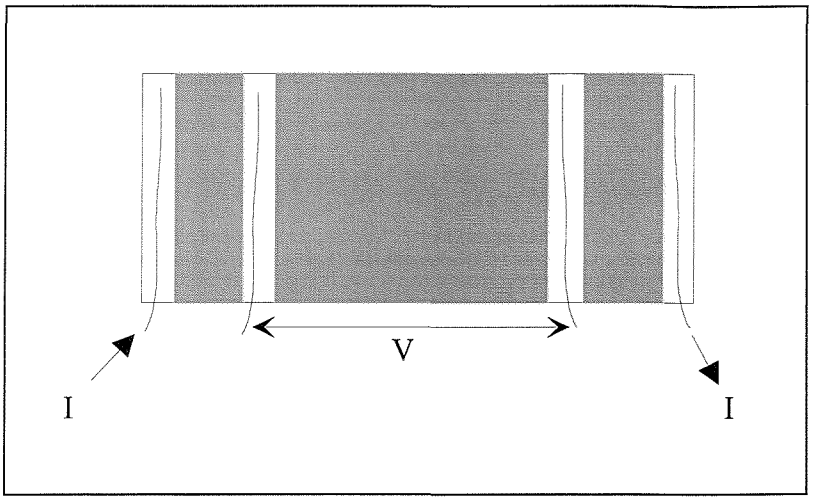

Figure 5.6: *A schematic representation of a sample with the attached electrical contacts for resistive measurements.*

Crystals	α_x (mm)	α_y (mm)	α_z (μm)	m (μg)	7-δ	T_c
DT1A	1.04	0.80	52	293	6.90	92.6
DT1B	//	//	//	//	6.93	93.8
DT1C	//	//	//	//	6.96	93.4
DT2	1.52	0.85	65	495	6.91	93.6
DT3B	0.70	0.70	52	179	6.93	93.8
DT3C	//	//	//	//	6.96	93.4
TW1	2.3	0.80	38	478	6.91	93.6
TW2	1.16	1.00	287	2267	6.91	93.6
TW3	0.58	0.45	180	319	6.91	93.6

Table 5.1: *The studied* $YBa_2Cu_3O_{7-\delta}$ *crystals; DT stands for detwinned, TW for twinned.*

Figure 5.7(a) [65] shows magnetic isotherms for crystal DT1A, from 60 K to 78 K in steps of 2 K and for magnetic field H_a || c-axis, up to 12 T. These data are consistent with all previous reports for the magnetisation peak effect in $YBa_2Cu_3O_{7-\delta}$, e.g. ref.[66-69]. The position of the, broad, main peak in magnetisation goes to lower magnetic field values with increasing temperature.

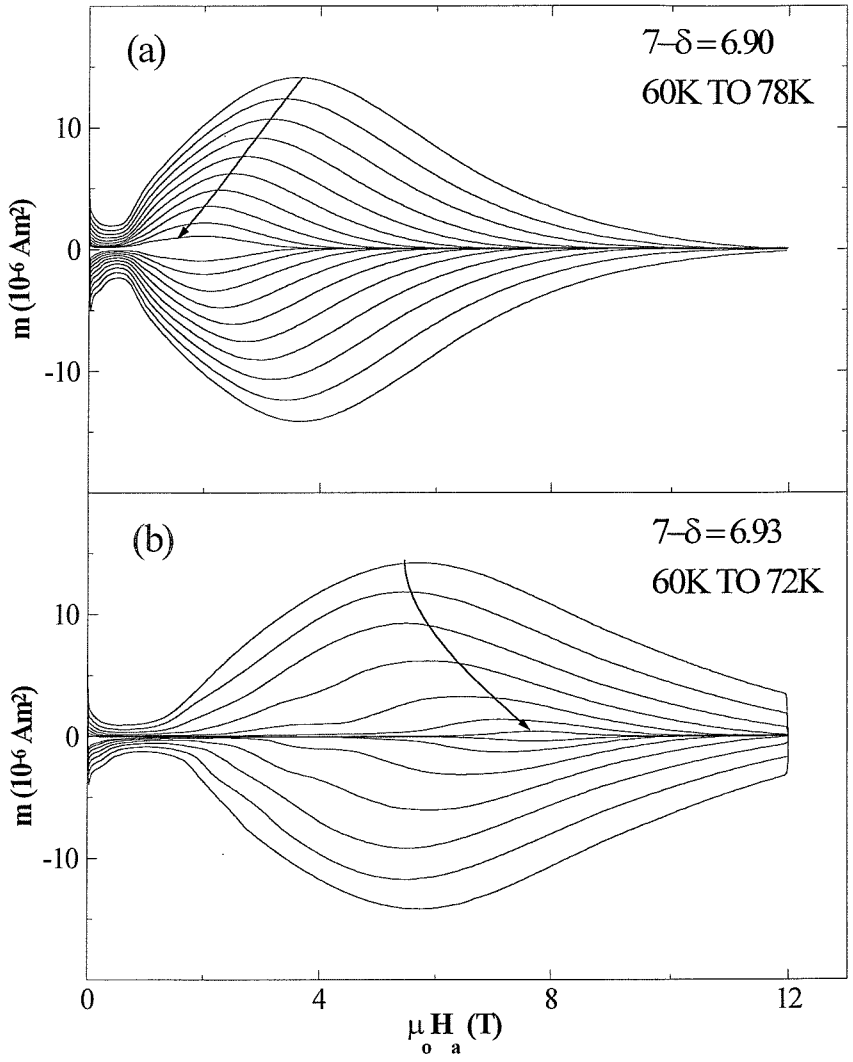

Figure 5.7: *Magnetic isotherms at the indicated temperatures with a step of 2 K for an oxygen content of (a) 6.90 and (b) 6.93. Arrows indicate the temperature dependence of the magnetisation peak field position,* H_p.

Figure 5.7(b) shows similar data for the same crystal but with a higher oxygen concentration (DT1B). The hysteresis loops in this case are taken from 60 K to 72 K, again in 2 K steps. The magnetisation peak position occurs at higher field values as compared to figure 5.7(a). At T = 60 K the peak position is shifted by as much as 2 T; this large variation is a result of only a small change in the oxygen concentration. In addition, at high temperatures and at fields lower than the position of the main peak, H_p, another smallish peak P_l in the magnetisation appears. A "bump" appearing at 66 K marks the "birth" of peak P_l. At a temperature higher by 2 K, the new peak is clearly distinguishable. For detwinned crystals P_l is observed only in a narrow temperature range, approximately 4 K. But what is more surprising in the data of fig.5.7(b), is that the main magnetisation peak (which we call hereafter P_h - high field peak), narrows with increasing temperature and its position shifts to higher magnetic field values.

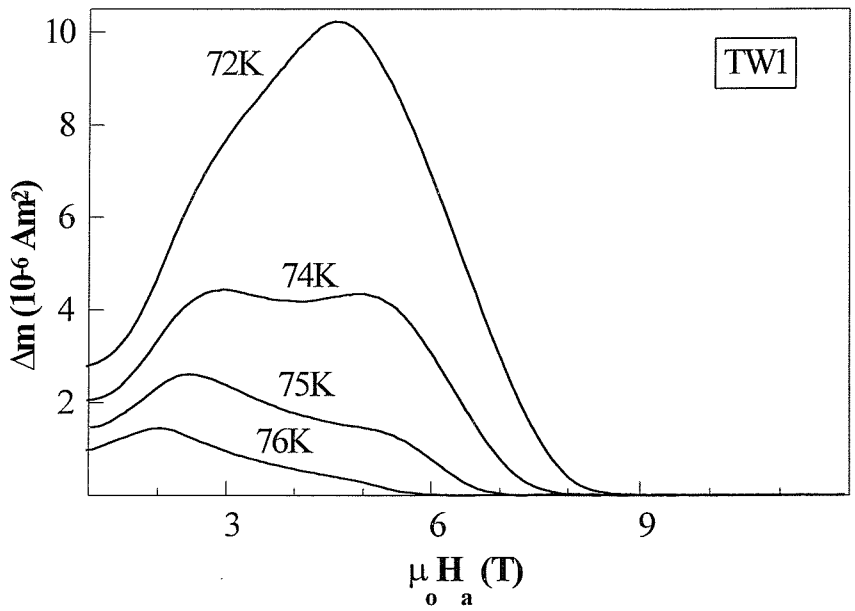

Figure 5.8: *Hysteresis width vs applied field at the indicated temperatures for sample TW1.*

Figure 5.8 demonstrates how the fishtail magnetisation evolves with increasing temperature for the twinned crystal TW1. As depicted, the magnetic field anomaly is a

two step process. We see how the two peaks P_l and P_h evolve with decreasing temperature. Contrary to detwinned crystals, the peak P_l in microtwinned samples is more prominent; it survives and is observed in a broader temperature range, in some cases up to 5 K below T_c.

A closer look at the main magnetisation peak P_h reveals some impressive features. Figure 5.9 [65] illustrates the temperature impact on P_h. It represents the magnetisation peak at T = 72 K and T = 74 K. The peaks are remarkably *sharp* for global magnetisation measurements and the maximum hysteresis width, which is proportional to the critical current density J_c, is strongly temperature dependent:

$$\frac{\Delta M_{max}(72K)}{\Delta M_{max}(74K)} \approx 4 \tag{5.7}$$

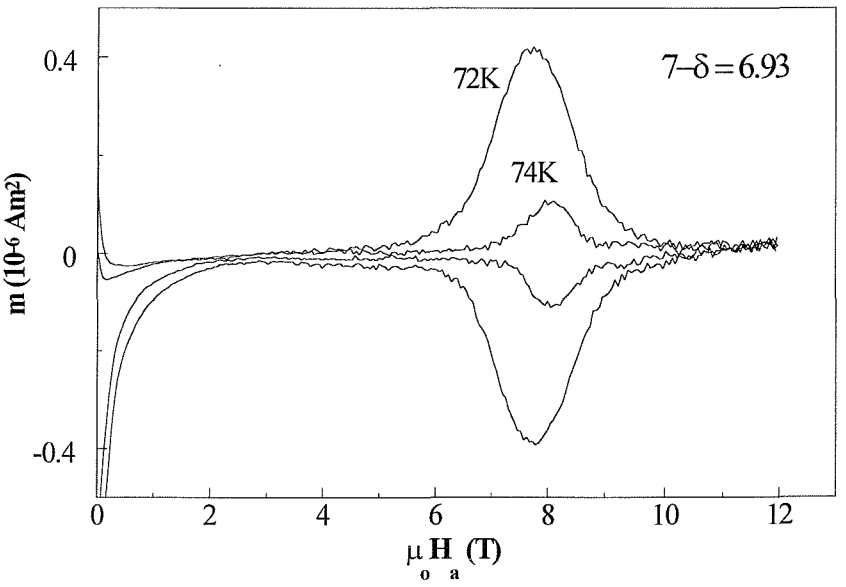

Figure 5.9: *Hysteresis loops for DT1B at 72, 74 K. The globally measured magnetisation peak appears only after 6 T and is sharper than anything shown before for* $YBa_2Cu_3O_{7-\delta}$.

Figure 5.10 [65] depicts the width of the magnetic moment, Δm, for three hysteresis loops of crystal DT2, at a temperature of 74 K and 76 K. These loops were performed

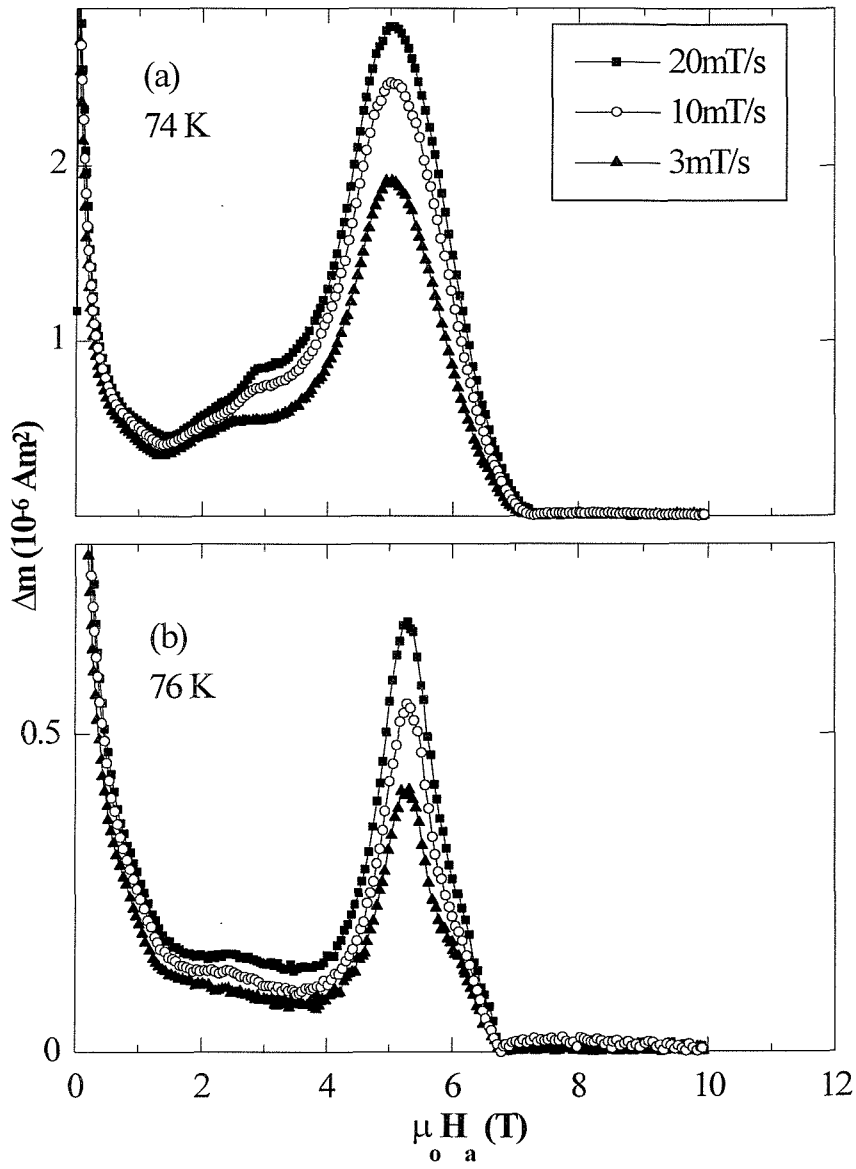

Figure 5.10: *Hysteresis width vs applied field for three different magnetic field sweep rates (voltage criteria) at (a) 74 K and (b) 76 K, for crystal DT2.*

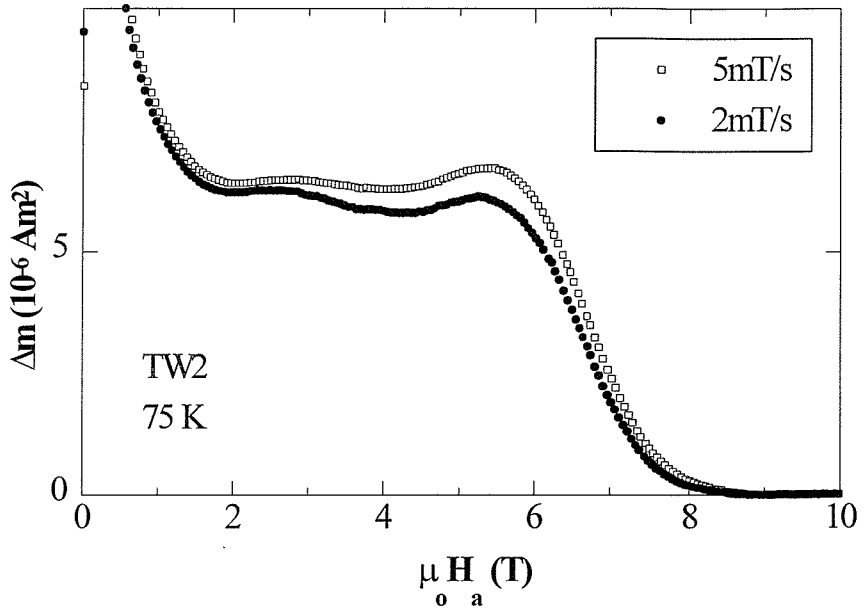

Figure 5.11: *Hysteresis width for two different sweep rates, for crystal TW2.*

with different sweep rates: 3, 10 and 20 mT/s. Due to the equivalence of applied field sweep rate and electric field, $dH_a/dt \propto E$, these three loops correspond to different voltage criteria. As is clearly seen, the peak P_l separates two different relaxation regimes. However the position of the remarkably sharp high field peak P_h is voltage criteria independent. Furthermore, the maximum magnetic moment producing the peak P_h is not only temperature dependent, as we have shown in fig.5.9, but also bears a strong time dependence. Figure 5.11 exhibits an identical response of the two peaks, but for a twinned crystal. In our measurements we have varied the field sweep rate in the maximum available window, 3 to 20 mT/s, obtaining always the same result: the lower field peak P_l marks the onset of an increased relaxation rate, while the position of the high field peak P_h is independent of the voltage criteria.

In contrast to our studies, previous studies on $YBa_2Cu_3O_{7-\delta}$ reported either resistivity measurements where a sudden resistivity drop at T_m was found due to vortex solidification, or magnetic measurements which showed a "fishtail" peak in the

magnetisation. It is one of the key features of the present work that for the first time both techniques have been combined to study the *same* crystals.

Shown in figure 5.12 are the magnetisation peak positions of detwinned and microtwinned crystals with the *same oxygen concentration*, namely 7-δ = 6.91. In agreement with the discussion in chapter 4 concerning the suppression of the magnetisation peak due to vortex channelling, in order to get the magnetic peak positions of microtwinned crystals at low temperatures, T < 65 K, hysteresis loops have been carried out with a magnetic field tilted away from the twin planes by an angle of 10°. As we have shown, this angle is enough at this temperature range for vortices to break loose from twin planes and interact with them at points. At high temperatures the positions of both peaks P_l and P_h are represented.

Also shown in figure 5.12 is the melting line of crystal DT2 deduced from magnetotransport measurements, as done by Safar *et al.* [33]: a rapid drop of resistance observed at a well defined point (H_m, T_m) in the H - T plane for $H_a < H_{cp}$ was assigned to a first order transition. We also find a critical point H_{cp} where the first order transition terminates, being replaced by a continuous, probably second order, solid-to-liquid transition [22,33,70]. For applied fields larger than H_{cp}, similarly to Safar and coworkers [70] we observe a broadening of the resistive transition, and the melting line becomes voltage criteria dependent. Furthermore, the expression (5.3) gives an excellent fit to the experimental melting line, for a fitting exponent n = 1.45:

$$H_m(T) \approx 132 \cdot \left(1 - \frac{T}{T_c}\right)^{1.45} \qquad (5.8)$$

This exponent is in the range estimated in previous published works: with an upper limit of n = 2 [30] from Farrell's torque data, a fit to Safar's transport data [33,34] gives n = 1.39 and similarly to Kwok's transport data [34] n = 1.41. From magnetisation measurements, Liang *et al.* [42] find a melting exponent n = 1.34 while Welp *et al.* [43] estimate n =1.36.

As illustrated in fig.5.12, for crystal DT2 the broadening of the resistive transition takes place at fields above $\mu_0 H_{cp}$ = 4.5 T. We observe that this value is about the same as the magnetic field position of the peak P_h close to the melting line. This is a result

which has not been previously reported for $YBa_2Cu_3O_{7-\delta}$. Measurements on twinned crystals, but with H_a tilted away from twin boundaries by an angle of 7.5° for the reasons explained above, lead to similar results.

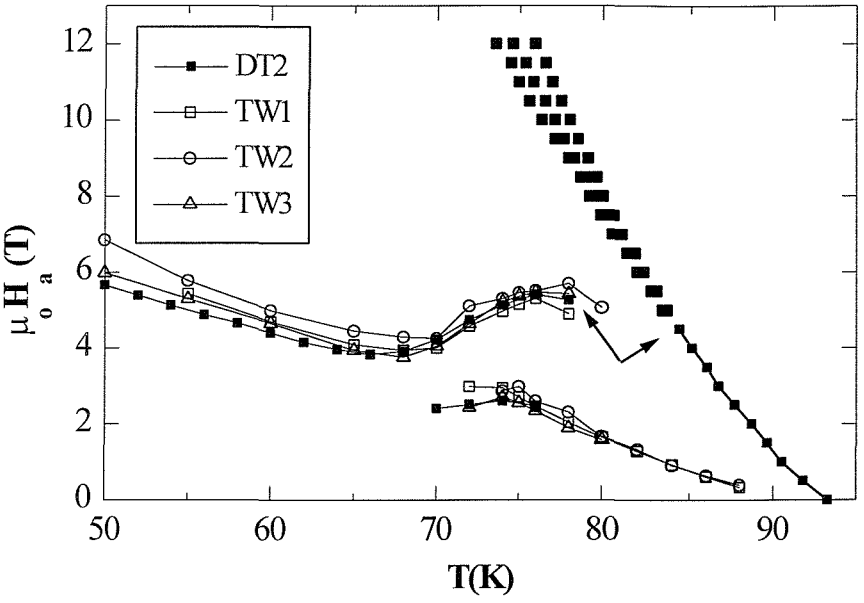

Figure 5.12: $H_m(T)$ *line for DT2, defined with different voltage criteria (0.05, 0.15, 0.3 μV) and the magnetisation peak line for TW and DT crystals of the same oxygen content, 7-δ = 6.91. Arrows indicate the critical point* H_{cp} *above which* $H_m(T)$ *becomes voltage criteria dependent and the last data point of* $H_p(T)$ *for DT2.*

Recently it was shown experimentally that the peak effect in $YBa_2Cu_3O_{7-\delta}$ is due to an elastic to plastic creep crossover [71], marking the activation of topological defects in the vortex system. These authors considered dislocation mediated plastic creep of vortices, similar to the diffusion of dislocations in atomic solids [72]. In this frame, the plastic deformations of the flux line lattice are due to the motion of dislocations over the Peierls barriers associated with the periodic structure of the lattice [72]. This is *not* expected to be a thermodynamic transition [73]. Our results clarify even further the situation. As shown in figure 5.13(a), we obtained a perfect fit for the position of the

peak P_l in the phase diagram, with the theoretical temperature dependence of the peak position resulting from this dislocations mediated plastic creep model [71], with $\alpha = 2$:

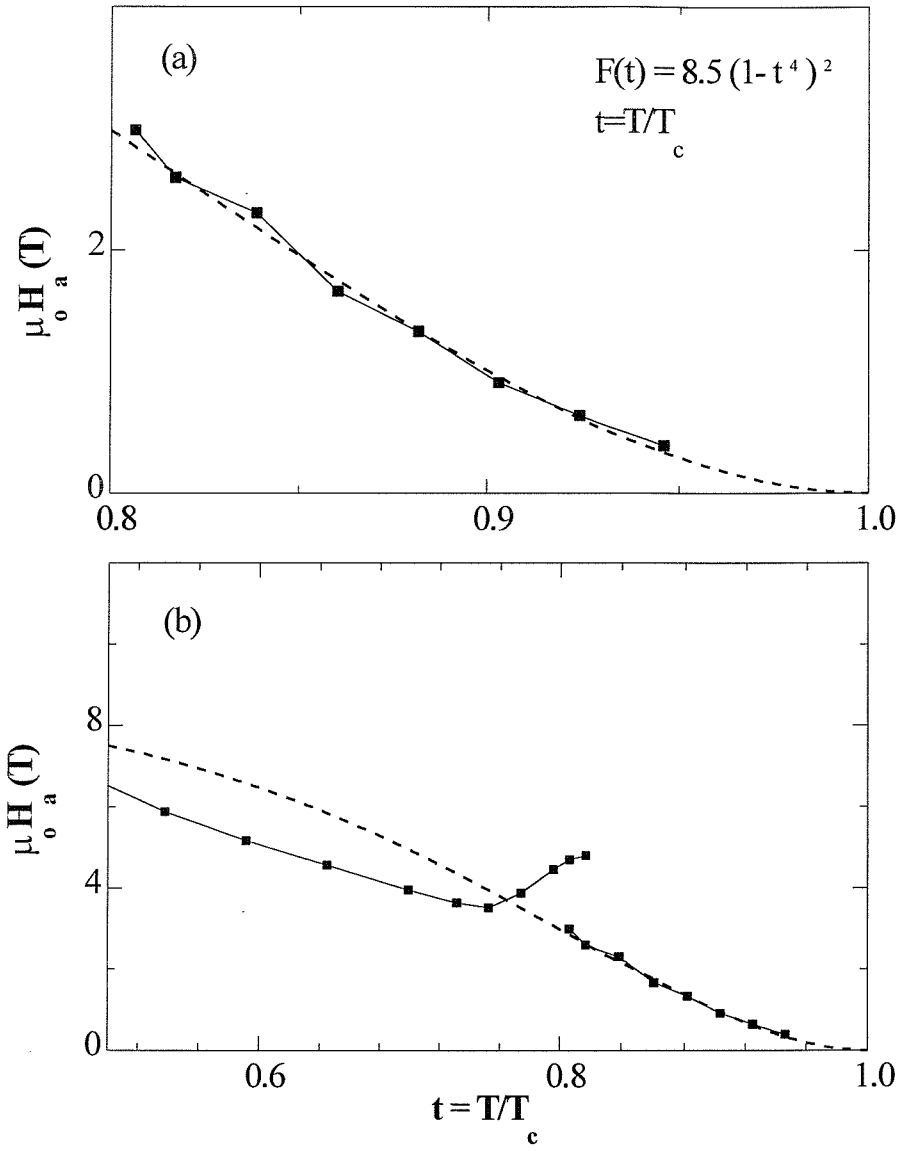

Figure 5.13: *Fitting of data for crystal TW2 with the dislocations mediated plastic creep model, eq.(5.9). The fit shown by the dashed line, (a) is nearly perfect for the peak* P_l *(b) but it is totally unsuccessful with the main magnetisation peak,* P_h.

$$H_p(T) \propto \left[1-\left(\frac{T}{T_c}\right)^4\right]^{\alpha} \qquad (5.9)$$

However, the fit is unsuccessful at lower temperatures, before the splitting of the fishtail peak (fig.5.13(b)). Indeed, Abulafia *et al.* [71], who used weakly twinned crystals [73], considered the model in the temperature regime that only the peak P_l appears, that is above 80 K, as our data in twinned crystals show.

Thus, it becomes clear that the aforementioned model cannot account for the appearance of the peak at lower temperatures, before its splitting, and P_h. This resulting crossover line in the vortex phase diagram, $H_p(T)$, exhibits on its own a surprising similarity with the equivalent peak effect line in $Bi_2Sr_2CaCu_2O_8$. Lately it has been proposed [19-22] that the Bragg Glass can be "melted" not only by thermal fluctuations, but also by quenched disorder. In this picture, $H_p(T)$ separates two distinct solid phases: a weakly disordered quasilattice associated with the Bragg Glass phase [19,20] and a highly disordered solid at higher fields [21,22]. These two phases, together with the liquid phase connect to a multicritical point (H_{cp},T_{cp}) [21,22]. In $Bi_2Sr_2CaCu_2O_8$, due to the sharpness of this vertical transition it was suggested that it represents a second order thermodynamic transition [64]. As further evidence, it was also shown by Khaykovich *et al.* [64] that the magnetisation peak correlates to the multicritical point. The same impressive results in $Bi_2Sr_2CaCu_2O_8$ were produced by Tanegai *et al.* 74] and Ooi *et al.* [75], with local magnetisation measurements. Coming back to our particular case, the additional observation of a voltage criteria *independent* peak, which also correlates to the multicritical point, seems to reinforce this scenario.

In the comparison with $Bi_2Sr_2CaCu_2O_8$ one should also take into account the striking similarity in the temperature behaviour of $H_p(T)$ in the phase diagram (fig.5.13). As in $Bi_2Sr_2CaCu_2O_8$ [64] the same non-monotonic temperature dependence is observed. The astonishing similarity of the temperature dependence between the peak effect in $YBa_2Cu_3O_{7-\delta}$ and in $Bi_2Sr_2CaCu_2O_8$ is more apparent when one compares with the results in the latter compound presented in refs.[74,75].

To test this observed identical behaviour of $H_p(T)$ in YBCO and in Bi:2212, we went further and studied its response to different oxygen stoichiometry. Oxygen doping

decreases the out-of-plane anisotropy γ, leading to more isotropic samples. It has been also shown that it can affect the microscopic pinning, by reducing the number of oxygen vacancies [63,76]. In $Bi_2Sr_2CaCu_2O_8$ it was demonstrated by Khaykovich *et al.* [64] that oxygen doping shifts both the first order transition line and $H_p(T)$ to higher fields in the phase diagram. Numerous other reports have since then confirmed this result for $Bi_2Sr_2CaCu_2O_8$ [74,75,77,78].

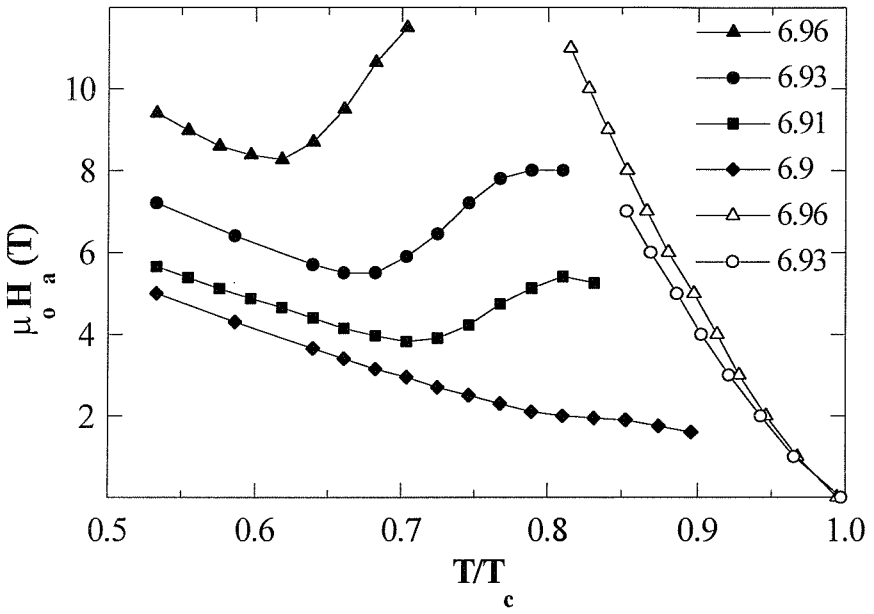

Figure 5.14: *Position in the H-T plane of the magnetisation peak line,* $H_p(T)$*, and the melting line terminated at the multicritical point, for crystals with different oxygen concentration.*

Figure 5.14 [65] illustrates the magnetic peak positions in the phase diagram for different oxygen concentrations. Data are from (two) crystals DT1A, DT1B, DT1C and DT2. As depicted, $H_p(T)$ shifts systematically and reversibly up and down in magnetic field, with the oxygen concentration increasing and decreasing respectively. As for $Bi_2Sr_2CaCu_2O_8$, the non-monotonic temperature dependence of $H_p(T)$ *strengthens* with oxygen doping. Also in fig. 5.14 is the melting line for two different oxygen concentrations of crystal DT3: DT3B and DT3C. At an oxygen content of 6.93 the multicritical point is found at 7 T, in agreement with $H_p(T)$. By doping the melting line

is pushed upwards. We varied the field up to 11T; however, no sign of broadening of the resistive drop at the first order transition was observed. Identically with $Bi_2Sr_2CaCu_2O_8$, $H_p(T)$ is pushed by oxygen doping upwards in the vortex phase diagram *coherently* with the multicritical point. This response provides impressive evidence for the universality of the phase diagram in the high-T_c superconducting oxides with weak random point disorder.

Theoretically, the field-driven transition of the vortex lattice between a quasi-ordered and a highly disordered solid phase is still not fully understood [21,22,79,80]. At some characteristic field the pinning energy becomes equal to the elastic energy barriers of the vortex lattice:

$$E_{pin} = E_{el} \tag{5.10}$$

At this point the destruction of the quasilattice occurs. At the present [20,21] suggestions are that it involves disorder induced relative displacements (transverse wanderings) of the order of α_0, the vortex lattice spacing, and finally permutation of neighbouring vortices. The resulting frozen configuration of twisted vortices can be characterised as an entangled solid, see fig.5.15 [21,22]. Loss of translational and topological order of the vortex matter leads to the domination of dislocations. On the contrary, the existing Bragg Glass phase below the transition retains translational order at long distances and perfect topological order [19,20,79,80]. Using the relation (5.10), Vinokur and coworkers [22] have shown explicitly that for $YBa_2Cu_3O_{7-\delta}$ the magnetic field values at which this transition is expected to occur vary proportionally to $(\gamma\ \Delta)^{-2}$, where γ is the anisotropy and Δ is the strength of the point disorder, in agreement with the obtained experimental results [65].

Very recently it was pointed out that for the destruction of the Bragg Glass not only the appearance of dislocations is important, but also the length scales at which these dislocations appear relatively to α_0 [81]; in this frame, a scenario was proposed for $YBa_2Cu_3O_{7-\delta}$ which explains the peak effect at fields lower than the multicritical point. Our measurements strongly suggest that exactly as predicted by Giamarchi *et al.* [81], at high temperatures, thermally induced unbound dislocations can invade[1] the vortex

[1] If the translational order is sufficiently weak.

system first at large length scales compared to α_o, affecting the critical current and producing a peak effect (P_l). However, the first order transition and the field-driven transition to the entangled state remain unaffected, since the relevant and important length scale for these transitions is α_o. In any case, at higher fields, massive large scale plasticity due to multiple creation of topological defects at the disorder induced field-driven transition occurs, with destruction of the quasi-ordered lattice at all length scales, down to α_o. The main magnetisation peak (P_l) marks the transition to the highly disordered vortex state. The picture of this field-driven transition is similar to the one given by numerical simulations results of Ryu *et al.* [82], who found a highly disordered solid phase above a threshold field, with an "explosive invasion of infinite defect loops meandering across the layers and colliding with each other" [82].

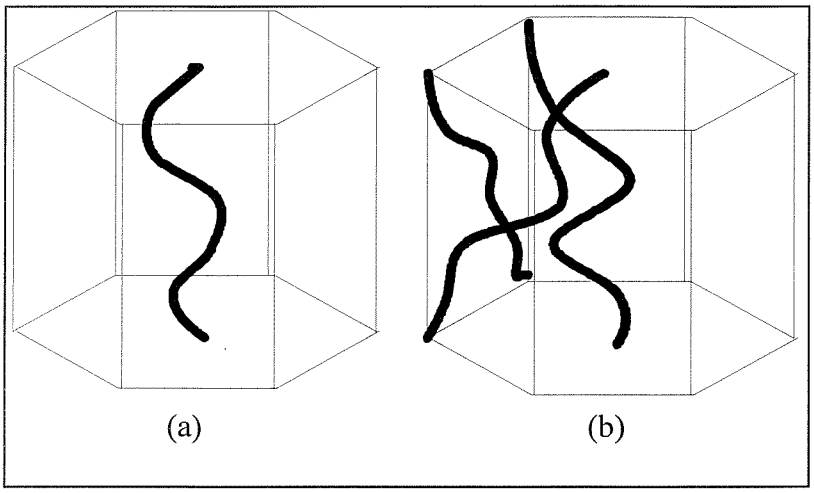

Figure 5.15: *The mechanical entanglement transition: increasing the external field the initially confined in its cage potential vortex (a), switches positions and twists with its neighbours (b), ending up in a configuration of entangled flux lines.*

Since the necessary condition for both the first order and the field-driven transition is the existence of the basic hexagonal vortex lattice cell, extended defects such as the twin planes should not affect the position in the H - T plane of $H_p(T)$. Indeed, this is evident in figure 5.12, where we observe $H_p(T)$ to be the same for detwinned and twinned crystals, with the same oxygen content. For the transition to the "frozen liquid" (i.e. entangled solid) to occur, the relative displacements of the nearest neighbors in the cage

potential have to be of the order of α_0 [22,81]. Twin planes pin a certain number of vortices and enhance the critical current; however their pinning range is quite limited, 10-50 Å, see for example ref.[83]. Unlike point defects such as oxygen vacancies which are randomly distributed, a relatively low density of twins cannot affect the decisive local ordering and therefore twins can leave the field-driven transition unaffected [84]. As mentioned in section 4.3, the distance between the twin planes d_{TP} varies in our samples between 0.5 and 5 μm. Thus, for example, at a field of H_a = 4 T, the vortex lattice constant is $\alpha_0 \sim 22.7$ nm. Considering an average value of $d_{TP} \sim 2$ μm, means that the untwinned region between two adjacent twin boundaries can accomodate across its width around 90 delocalised vortices, which are positioned in a proper hexagonal lattice formation and undergo the transitions. On the other hand, the presence of extended defect structures (e.g. twins) is predicted to weaken the translational order [84,85] making the quasi-ordered Bragg Glass more unstable to dislocations. This explains what we observe as an enhancement of P_l in the twinned samples.

In agreement to the above, the non-monotonic temperature dependence of $H_p(T)$ can be naturally understood by considering the combined effect of disorder induced wandering and thermal fluctuations displacements on vortices [21,22]: the decrease of the pinning energy E_{pin} with temperature, due to the softening of the pinning potential in the presence of thermal fluctuations, leads to an increase of the solid-to-solid transition fields [21,22]. This increase occurs above a certain temperature T^* which is equal to the depinning temperature [21]. Our results (fig.5.13) show a $T^* \sim 70$ K, in good agreement with the theoretical estimations for the depinning temperature in $YBa_2Cu_3O_{7-\delta}$ (for example Blatter *et al.* [2]), see figure 5.16.

Our phase diagram depicted in fig.5.16(b) is in accordance with the recent theoretical suggestions [20-22,79-82]. Two solid phases, a quasi-ordered Bragg Glass phase and a highly disordered entangled solid phase, are separated by an entanglement transition, see figure 5.16(a). Liquidification occurs via two different transitions: a first order transition for the Bragg Glass and a second order transition for the entangled solid. All phases, solid and liquid, meet in a critical point.

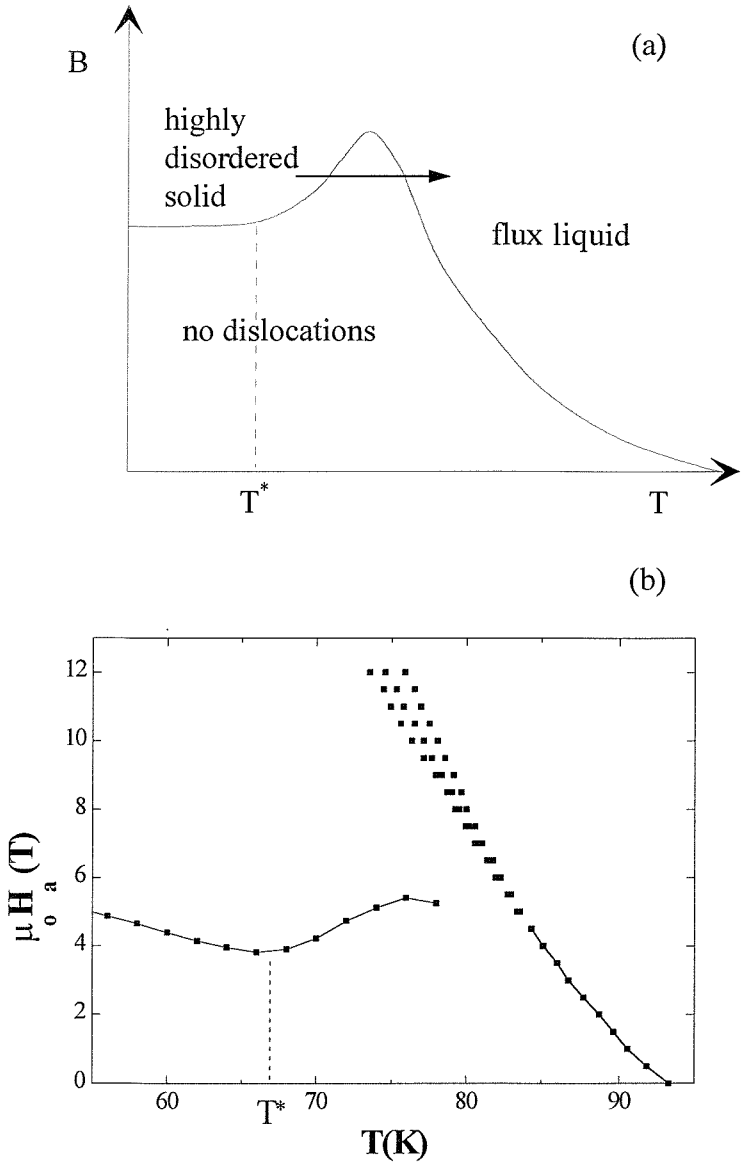

Figure 5.16: *(a) Schematic phase diagram after Ertas and Nelson, ref.[21] (b) Phase diagram for DT2 as derived by our combined magnetic and transport measurements.*

5.5 CONCLUSIONS

In conclusion, our results in high purity single crystals of $YBa_2Cu_3O_{7-\delta}$ reveal the existence of a sharp, voltage criteria independent magnetisation peak. The magnetisation width at the peak is observed to be strongly dependent on temperature and sweep rate. Combining transport and magnetic data we have shown that the resulting magnetisation peak line $H_p(T)$ in the vortex phase diagram of $YBa_2Cu_3O_{7-\delta}$ represents a well defined crossover which shifts to higher fields with increasing oxygen doping and temperature, always correlating with the multicritical point.

We have shown that our results can naturally be fitted in the recently suggested picture of the existence of two distinct solid phases, a quasi-ordered lattice at low fields and a highly disordered solid at higher fields. By its turn, this picture suggests the existence of a generic phase diagram for all the high temperature superconductors. Moving in this direction, our results show an apparent and remarkable similarity with results obtained for the highly anisotropic $Bi_2Sr_2CaCu_2O_8$.

Finally, our results demonstrate that low densities of extended defects, in this case twin boundaries, cannot affect the position of the field-driven transition in the vortex phase diagram, or suppress it. This transition is based on the existence of a quasi-ordered vortex lattice in the presence of random, weak, point defects such as oxygen vacancies. Given the limited pinning range of twin planes, these conditions are still met in the untwinned regions, that is the regions enclosed between a pair of planar defects. Consequently, the resulting magnetisation peak line $H_p(T)$ in the phase diagram remains for detwinned and twinned crystals of equal oxygen content, virtually the same.

REFERENCES

[1] G. Eilenberger, Phys. Rev. Lett. **164**, 928 (1967).

[2] G. Blatter, M. V. Feigel'man, V. B. Geshkenbein *et al.*, Rev. of Mod. Phys. **66**, 1125 (1994).

[3] G. Blatter, Physica C **282-287**, 19 (1997).

[4] E. Brezin, D. R. Nelson, A. Thiaville, Phys. Rev. B **31**, 7124 (1985).

[5] D. R. Nelson, Phys. Rev. Lett. **60**, 1973 (1988).

[6] E. H. Brandt, Rep. Prog. Phys. **58**, 1465 (1995).

[7] F. Lindemann, Phys. Z. (Leipzig) **11**, 69 (1910).

[8] A. Houghton, R. A. Pelcovits, A. Subdø, Phys. Rev. B **40**, 6763 (1989).

[9] R. E. Hetzel, A. Subdø, D. A. Huse, Phys. Rev. Lett. **69**, 518 (1992).

[10] G. Blatter, V. Geshkenbein, A. Larkin *et al.*, Phys. Rev. B **54**, 72 (1996).

[11] G. Blatter and B. I. Ivlev, Phys. Rev. B **50**, 10272 (1994).

[12] D. Feinberg, J. Phys. III **4**, 169 (1994).

[13] M. P. A. Fisher, Phys. Rev. Lett. **62**, 1415 (1989).

[14] D. S. Fisher, M. P. A. Fisher, D. A. Huse, Phys. Rev. B **43**, 130 (1991).

[15] D. A. Huse, M. P. A. Fisher, D. S. Fisher, Nature **358**, 553 (1992).

[16] M. V. Feigel'man, V. B. Geshkenbein, A. I. Larkin *et al.*, Phys. Rev. Lett. **63**, 2303 (1989).

[17] D. Grier *et al.*, Phys. Rev. Lett. **66**, 2270 (1991).

[18] T. Nattermann, Phys. Rev. Lett. **64**, 2454 (1990).

[19] T. Giamarchi and P. Le Doussal, Phys. Rev. Lett. **72**, 1530 (1994).

[20] T. Giamarchi and P. Le Doussal, Phys. Rev. B **52**, 1242 (1995).

[21] D. Ertas and D. R. Nelson, Physica C **272**, 79 (1996).

[22] V. Vinokur, B. Khaykovich, E. Zeldov, unpublished.

[23] L. Radzihovsky, Phys. Rev. Lett. **74**, 4722 (1995).

[24] D. E. Farrell, private communication.

[25] M. A. Moore, Phys. Rev. B **55**, 14136 (1997).

[26] H. M. Carruzzo and C. C. Yu, preprint.

[27] P. L. Gammel, L. F. Schneemeyer, J. V. Waszczak *et al.*, Phys. Rev. Lett. **61**, 1666 (1988).

[28] E. H. Brandt, P. Esquinazi, G. Weiss, Phys. Rev. Lett. **62**, C2330 (1989).

[29] T. K. Worthington, F. H. Holtzberg, C. A. Feild, Cryogenics **30**, 417 (1990).

[30] D. E. Farrell, J. P. Rice, D. M. Ginsberg, Phys. Rev. Lett. **67**, 1165 (1991).

[31] R. G. Beck, D. E. Farrell, J. P. Rice *et al.*, Phys. Rev. Lett. **68**, 1594 (1992).

[32] M. Charalambous, J. Chaussy, P. Lejay, Phys. Rev. B **45**, 5091 (1992).

[33] H. Safar, P. L. Gammel, D. A. Huse *et al.*, Phys. Rev. Lett. **69**, 824 (1992).

[34] W. K. Kwok, S. Fleshler, U. Welp *et al.*, Phys. Rev. Lett. **69**, 3370 (1992).

[35] S. Fleshler, W. K. Kwok, U. Welp *et al.*, Phys. Rev. B **47**, 14448 (1993).

[36] H. Safar, P. L. Gammel, D. A. Huse *et al.*, Phys. Rev. Lett. **70**, 3800 (1995).

[37] W. K. Kwok, J. Fendrich, S. Fleshler *et al.*, Phys. Rev. Lett. **72**, 1092 (1994).

[38] W. K. Kwok, J. Fendrich, C. J. Van der Beek *et al.*, Phys. Rev. Lett. **73**, 2614 (1994).

[39] A. B. Pippard, Philos. Mag. **19**, 217 (1969).

[40] J. A. Fendrich, W. K. Kwok, J. Giapintzakis *et al.*, Phys. Rev. Lett. **74**, 1210 (1995).

[41] W. Jiang, N.-C. Yeh, D. S. Reed *et al.*, Phys. Rev. Lett. **74**, 1438 (1995).

[42] R. Liang, D. A. Bonn, W. N. Hardy, Phys. Rev. Lett. **76**, 835 (1996).

[43] U. Welp, J. A. Fendrich, W. K. Kwok *et al.*, Phys. Rev. Lett. **76**, 4809 (1996).

[44] D. R. Nelson, Nature **375**, 356 (1995).

[45] G. W. Crabtree and D. R. Nelson, Phys. Today **50**, 38 (1997).

[46] A. Schilling, R. A. Fisher, N. E. Phillips *et al.*, Nature **382**, 791 (1996).

[47] J. A. Fendrich, U. Welp, W. K. Kwok *et al.*, Phys. Rev. Lett. **77**, 2073 (1996).

[48] H. Wu, N. P. Ong, R. Gagnon *et al.*, Phys. Rev. Lett. **78**, 334 (1997).

[49] L. I. Glazman and A. E. Koshelev, Phys. Rev. B **43**, 2835 (1991).

[50] C. M. Aegerter, S. L. Lee, H. Keller *et al.*, Phys. Rev. B **54**, R15661 (1996).

[51] R. Cubitt, E. M. Forgan, G. Yang *et al.*, Nature **365**, 407 (1993).

[52] S. L. Lee, P. Zimmermann, H. Keller *et al.*, Phys. Rev. Lett. **71**, 3862 (1993).

[53] H. Pastoriza, M. F. Coffman, A. Arribére *et al.*, Phys. Rev. Lett. **72**, 2951 (1994).

[54] R. A. Doyle, D. Liney, W. S. Seow *et al.*, Phys. Rev. Lett. **75**, 4520 (1995).

[55] H. Pastoriza and P. H. Kes, Phys. Rev. Lett. **75**, 3525 (1995).

[56] E. Zeldov, D. Majer, M. Konczykowski *et al.*, Nature **375**, 373 (1995).

[57] D. E. Farrell, E. Johnston-Halperin, L. Klein *et al.*, Phys. Rev. B **53**, 11807 (1996).

[58] M. Daeumling, J. M. Seutjens, D. C. Larbalestier, Nature **346**, 332 (1990).

[59] L. Klein, E. R. Yacoby, Y. Yeshurun *et al.*, Phys. Rev. B **49**, 4403 (1994).

[60] V. Hardy, A. Wahl, A. Ruyter *et al.*, Physica C **232**, 347 (1994).

[61] G. Yang, P. Shang, S. D. Sutton *et al.*, Phys. Rev. B **48**, 4054 (1993).

[62] V. N. Kopylov, A. E. Koshelev, I. F. Schegolev *et al.*, Phys. Rev. Lett. **69**, 1263 (1992).

[63] A. A. Zhukov, H. Küpfer, G. Perkins *et al.*, Phys. Rev. B **51**, 12704 (1995).

[64] B. Khaykovich, E. Zeldov, D. Majer *et al.*, Phys. Rev. Lett. **76**, 2555 (1996).

[65] K. Deligiannis, P. A. J. de Groot, M. Oussena *et al.*, Phys. Rev. Lett. **79**, 2121 (1997).

[66] L. Krusin-Elbaum, L. Civale, V. M. Vinokur *et al.*, Phys. Rev. Lett. **69**, 2280 (1992).

[67] P. D. Panetta, J. E. Ostenson, D. K. Finnemore *et al.*, Phys. Rev. B **52**, 15570 (1995).

[68] N. Kobayashi, K. Hirano, T. Nishizaki *et al.*, Physica C **251**, 255 (1995).

[69] O. B. Hyun, M. Yoshida, T. Kitamura *et al.*, Physica C **258**, 365 (1996).

[70] H. Safar, P. L. Gammel, D. A. Huse *et al.*, Phys. Rev. Lett. **70**, 3800 (1993).

[71] Y. Abulafia, A. Shaulov, Y. Wolfus *et al.*, Phys. Rev. Lett. **77**, 1596 (1996).

[72] V. Geshkenbein, A. Larkin, M. Feigel'man *et al.*, Physica C **162-164**, 239 (1989).

[73] E. Zeldov, private communication.

[74] T. Tamegai, R. Yamada, S. Ooi *et al.*, Physica C **282-287**, 2029 (1997).

[75] S. Ooi, T. Tanegai, T. Shibauchi, J. Low Temp. Phys. **105**, 1011 (1996).

[76] J. L. Vargas and D. C. Larbalestier, Appl. Phys. Lett. **60**, 1741 (1992).

[77] Y. Ando, S. Komiya, Y. Kotaka *et al.*, Phys. Rev. B **52**, 3765 (1995).

[78] T. Hanaguri, T. Tsuboi, A. Maeda *et al.*, Physica C **256**, 111 (1996).

[79] T. Giamarchi and P. Le Doussal, Physica C **282-287**, 363 (1997).

[80] T. Giamarchi and P. Le Doussal, to be published in *Spin Glasses and Random Fields*, Editor A. P. Young (World Scientific).

[81] T. Giamarchi and P. Le Doussal, Phys. Rev. B **55**, 6577 (1997).

[82] S. Ryu, A. Kapitulnik, S. Doniach, Phys. Rev. Lett. **77**, 2300 (1996).

[83] G. W. Crabtree, W. K. Kwok, U. Welp *et al.*, *Invited Paper at the Int. Sem. On Sup. In High Mag. Fields*, Tsukuba, Japan (1995).

[84] T. Giamarchi, private communication.

[85] G. P. van der Meij, PhD thesis, University of Leiden (1984).

6. LOCK-IN OSCILLATIONS

6.1 VORTEX STRUCTURE PARALLEL TO THE LAYERS

In a layered structure of Josephson coupled superconducting planes, the interlayer distance d is by far the most important length scale when considering the vortex structure. As predicted back in the seventies [1,2], when ξ_c is smaller than the interlayer distance d (more precisely when $\xi_c(T) < d/\sqrt{2}$) the assumption of a smooth variance of the order parameter Ψ from layer to layer is not valid and new effects are expected. The temperature at which this dimensional crossover occurs is denoted as T^*; in $YBa_2Cu_3O_{7-\delta}$ the condition $\xi_c(T) < d/\sqrt{2}$ is valid for temperatures up to 80K [3]. As a result, the 3D anisotropic Ginzburg-Landau and London models become inapplicable, since they describe anisotropic but uniform superconductors, ignoring any effects of discreteness. Thus the need for a new model emerges, a model that will implement the discrete nature of the order parameter.

A simple model of this type is the Lawrence-Doniach (LD) model, which describes a stack of superconducting layers weakly connected via Josephson coupling [1]. Containing the 3D anisotropic models as a limiting case for $\xi_c > d/\sqrt{2}$, the LD model assumes a 2D order parameter $\Psi_n(x,y)$ which does not vary smoothly from one layer to the other but on the contrary vanishes in the region between the layers [4]. In this approach, the layered structure can be visualised as a stack of alternating superconducting and insulating planes (SIS structure) [3,5]. Thus, in the free energy functional, the LD model replaces the gradient of the order parameter along the z axis by a finite difference. The LD model introduces a new length scale, which depends on the anisotropy γ, the *Josephson length* $\lambda_j = \gamma d$. The Josephson length is a measure of the "shear stiffness" of the order parameter, Ψ_n: large differences of the order parameter between two adjacent layers, Ψ_{n+1}-Ψ_n are allowed only within a range equal to λ_j.

The free energy functional in the anisotropic Ginzburg-Landau case reads [3,6]:

$$F = \int d^3r \left[\begin{array}{l} a(T)|\Psi|^2 + \frac{1}{2}\beta(T)|\Psi|^4 + \frac{\hbar^2}{4m_{ab}}\left|\left(i\nabla_{//} + \frac{2e}{\hbar}\vec{A}_{//}\right)\Psi\right|^2 \\ + \frac{\hbar^2}{4m_c}\left|\left(i\nabla_z + \frac{2e}{\hbar}A_z\right)\Psi\right|^2 \end{array} \right] + \int d^3r \frac{B^2}{2\mu_o} \tag{6.1}$$

where a(T) and β(T) are two temperature dependent coefficients, $\vec{A}$ the vector potential, $\vec{A}_{//} = (A_x, A_y, 0)$ and $\vec{B} = \text{curl}\vec{A}$. Instead, within the LD frame, taking into account the Josephson coupling of the layers f_j, the proposed phenomenological functional now becomes:

$$F = d\int d^3r \left[\begin{array}{l} a(T)|\Psi_n|^2 + \frac{1}{2}\beta(T)|\Psi_n|^4 + \frac{\hbar^2}{4m_{ab}}\left|\left(i\nabla_{//} + \frac{2e}{\hbar}\vec{A}_{//}\right)\Psi_n\right|^2 \\ + f_j\left|\Psi_{n+1} - \Psi_n \exp\left(\frac{2ie}{\hbar}\int_{nd}^{(n+1)d} A_z dz\right)\right|^2 \end{array} \right] + \int d^3r \frac{B^2}{2\mu_o} \tag{6.2}$$

leading to some important conclusions. First and foremost, it was realised that the modulation of the order parameter along the c-axis gives to the layers the features of a periodic pinning structure of extended defects [7]. Thus, secondly, the direction of the applied field H_a with respect to the layers is crucial for the structure and the characteristics of vortices.

Indeed, for fields applied at an angle θ with the ab plane below a critical angle θ^*, vortices lock-in between the layers, running parallel to them [3]. Lock-in is accompanied by a "transverse Meissner effect": contrary to the predictions of the 3D anisotropic models, the component of $\vec{B}$ perpendicular to the planes is zero [3], resulting in a complete screening of the perpendicular component of the applied field. In this locked-in situation, the strength of the interlayer superconducting coupling, as characterised by ξ_c, affects crucially the structure of the vortex core. The resulting vortices are called *Josephson vortices* or *Josephson strings* [4]. Compared to Abrikosov vortices, Josephson strings are similar but with a different core size and structure. The

vortex core prefers to run parallel and in-between the layers, having a width parallel and perpendicular to the planes equal respectively to λ_j and d [8], figure 6.1. This confinement in between two adjacent superconducting layers, grants to the string a 2D morphology. The usual Ginsburg-Landau (normal) core is absent and the amplitude of the order parameter in the adjacent layers is either not at all suppressed or merely weakly suppressed but not zero, depending on temperature [3,8,9]. These new cores are called Josephson cores or nuclei or phase cores since they sustain large layer-to-layer phase differences. Surrounding the core, similarly to Abrikosov vortices, there is a region of exponentially decaying screening currents flowing around the axis of the string at lengths λ_{ab} and λ_c, perpendicular and parallel to the ab plane, respectively.

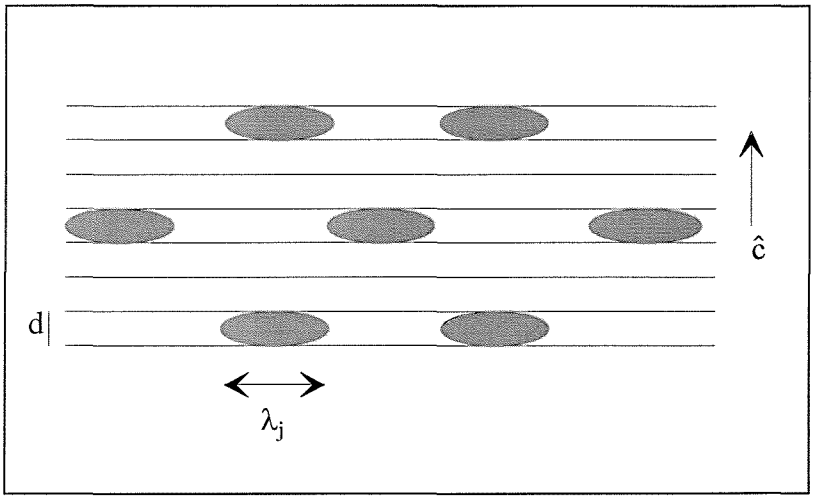

Figure 6.1: *Structure of the Josephson vortex lattice - the case of a parallel to the layers applied field. Dark areas represent the section of the Josephson nuclei.*

In the case of a magnetic field applied at angles larger than θ^*, a staircase structure succeeds the locked-in state. Vortices consist of 2D pancake vortices on each layer, with the usual normal core, connected via portions of Josephson-like cores with width parallel to the planes equal to λ_j [8]. With the direction of the applied field approaching even closer to the c-axis, the staircase structure gives in to a tilted vortex lattice [3,8,9].

Above T^* one enters the *quasi-3D* regime. The coherence length perpendicular to the layers is large enough ($\xi_c > d/\sqrt{2}$) for the discreteness of the layered structure to weaken but not completely disappear and an effective anisotropic 3D description to be

applicable again. As in the quasi-2D case, the centre of the vortex core prefers to be positioned between the layers. The essential difference is that the core now consists of two components: a normal core of section $\xi_{ab}\xi_c$ including in its centre a Josephson nucleus of cross section $\lambda_J d$ [3]. The amplitude of the order parameter is now readily suppressed in the layers, within the complex core section of $\xi_{ab}\xi_c$ [3], figure 6.2.

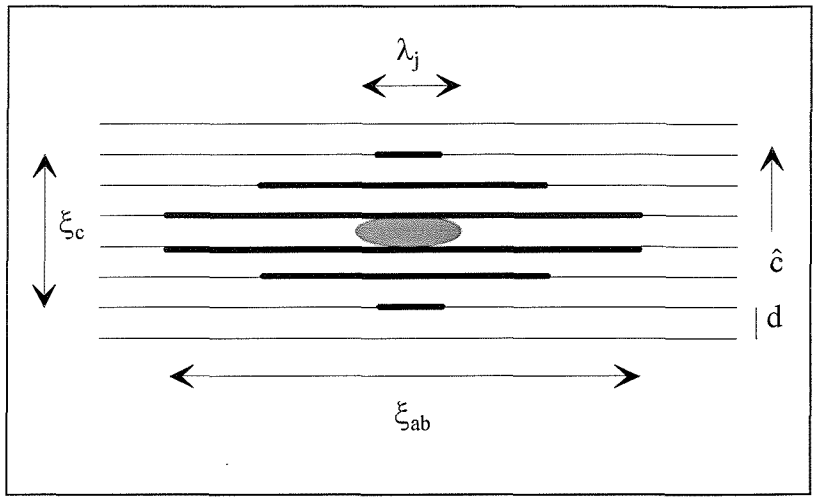

Figure 6.2: *Vortex core structure for a parallel to the layers external field, in the case of elevated temperatures,* $T > T^*$ *(stable configuration). Bold lines show the reduced order parameter on the layers; the dark area is the Josephson nucleus.*

6.2 Experimental Evidence of Lock-In

In this frame new, exotic vortex structures and lattices have been predicted, leading to a very rich phenomenology. The existence of vortex chains, for example, has been theoretically discussed [10,11] and experimentally observed [12,13] for magnetic fields close to H_{c1}, applied at an angle to the c-axis. Predictions of a decomposed or a combined lattice [14-16] have also been experimentally verified [13,17].

A great deal of experimental interest has been directed at detecting the locked-in vortex state with the theoretically predicted, accompanying, intrinsic pinning. An anomaly in torque measurements, observed on an untwinned $YBa_2Cu_3O_{7-\delta}$ single crystal by Farrell *et al.* [18], was attributed to a transition to the locked-in state [19]. More

precisely, as the applied field H_a rotates towards the ab plane, at θ^* due to the lock-in of the vortices their angle with H_a increases, resulting in a torque larger than the conventional anisotropic London model predicts [8]. A similar anomaly was observed in single crystals of $Bi_2Sr_2CaCu_2O_8$ by Steinmeyer *et al.* [20] and of $Tl_2Ba_2CaCu_2O_8$ by Chung *et al.* [21]. Transport measurements in $YBa_2Cu_3O_{7-\delta}$ on the other hand, exhibit an abrupt, impressive drop of resistivity for fields applied in the ab plane and flux motion geometry vertical to the layers [22,23], due to intrinsic pinning. In detecting the lock-in transition, vector magnetisation measurements [24,25] can be also useful, by monitoring the accompanying transverse Meissner effect.

The aforementioned techniques have certain limitations. Torque measurements are unable to give any essential information on the dynamics that govern the behavior of locked-in vortices. Even their apparent use in finding out the angular boundaries of the locked-in state can be restricted due to thermal fluctuations and extrinsic pinning effects which can mask or extinguish the transition [26,27]. Coming to magnetotransport studies, their confinement to high temperatures, above 80 K, makes the study of the quasi-2D regime and consequently the detection of the 2D to 3D transition temperature T^* impossible. Furthermore, in interpreting a transverse Meissner effect one has to be aware of possible electrodynamic and not thermodynamic (vortex lock-in) origins [25]. In any case, these techniques, for different reasons, were not in a position to enlighten us about the behavior of the 2D Josephson strings system or verify the existing theories for the vortex lattice structure and behavior in the quasi-2D regime.

6.3 Results and Discussion

We investigated high purity untwinned $YBa_2Cu_3O_{7-\delta}$ single crystals with an oxygen content $7-\delta = 6.91$. Magnetic hysteresis measurements were carried out on the 12 T Vibrating Sample Magnetometer in Southampton, in collaboration with Dr. M. Oussena. Samples were first zero field cooled at the desired temperature and then subjected to a magnetic field H_a. Unless specified, in our measurements the direction of H_a is in the plane defined by either the a-axis or the b-axis and the normal to the ab plane. The angle

that H_a makes with the basal plane is measured with the accuracy of our setup, $\theta < 1°$. Measurements were performed with a constant sweep rate of 5 mT/sec.

Table 6.1 shows the relevant details of the studied $YBa_2Cu_3O_{7-\delta}$ samples.

Crystals	α_x (mm)	α_y (mm)	α_z (μm)	m (μg)	7-δ	T_c(K)
DT0	1.45	1.2	125	1479	6.91	93.6
DT3	1.69	1.08	91	1129	6.91	93.6

Table 6.1: *Details of the two crystals used in our experimental studies with α_x, α_y and α_z being the length, width and thickness, respectively.*

In the locked-in state the known shape of the magnetic hysteresis changes fundamentally, as first observed by Oussena *et al.* [28]. Shown in figure 6.3 are the magnetisation curves at different temperatures, up to 60 K, for crystal DT0, in an increasing applied field up to H_a = 12 T. The applied field is parallel to one of the principal axis of the ab plane (each separate case is indicated on fig.6.3); in order to see the effects clearly we shifted the curves along the vertical axis, a procedure that does not qualitatively affect the signal. As it is clear, the magnetic isotherms exhibit a strong oscillatory behavior, with oscillations whose periodicity increases with field. As demonstrated in fig.6.3, and below we will show in much more detail, the maxima of these oscillations are temperature independent. The observed oscillations are a direct consequence of the interaction of the locked-in Josephson vortex lattice with the periodic pinning structure that the layers represent and hence we will refer to them as lock-in oscillations. The observation of lock-in oscillations allows us to probe the nature of the lattice and the mechanism of vortex motion at the low temperature quasi-2D regime.

Here we give a full account of the mechanism, pictured in fig.6.4, comparing the theoretical predictions to the experimental results as mapped in figure 6.3 [29]. The anisotropic London model predicts for nearly parallel fields a hexagonal vortex lattice

compressed along the c-axis and expanded in the plane direction of the crystal [3,30], with a field independent ratio $a/l = 2\gamma/\sqrt{3}$, see also fig.6.1. Here a and l stand for the average vortex distance parallel and perpendicular to the ab plane, respectively, see

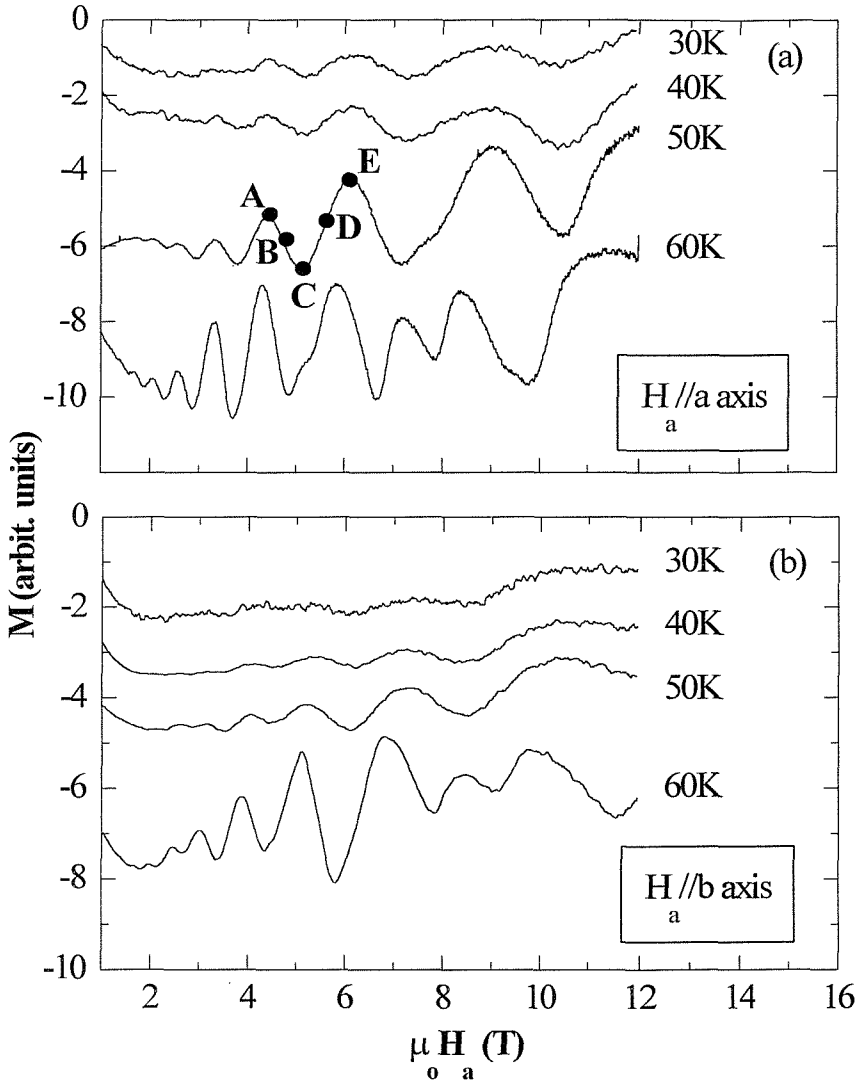

Figure 6.3: *Magnetisation results for an increasing up to 12 T applied field in the* ab *plane, at the indicated temperatures, for crystal DT0.*

fig.6.4(a). The vortex lattice with the a/l ratio predicted by the anisotropic London model is a state of minimum vortex-vortex interaction energy. This state in the layered cuprate superconductors will be commensurate with the order parameter modulation

along the c-axis, for certain only values of the applied field, H_n. For $H_a = H_n$, $l = nd$, where n = 1, 2, 3... and the cores of the strings, members of the compressed hexagonal lattice, lie in between the layers. This is the case in the dips of the magnetic hysteresis (e.g. points A and E in figure 6.3).

Increasing H_a but staying near H_n, any changes in the vortex density can be accommodated with motion of the cores parallel to the layers (fig.6.4(b)). There are only two factors opposing such a guided motion: firstly the repulsive vortex-vortex interaction, which initially, for the commensurate values of a, is expected to be minimum and secondly the pinning of Josephson vortices by extrinsic defects. Taking into account the absence of a normal core, one expects Josephson strings to be much less effectively pinned by extrinsic defects; this was explicitly shown by Blatter *et al.* [6], who demonstrated the reduction of the elementary pinning force acting on a Josephson vortex, compared with the force acting on an Abrikosov one, by a factor of approximately $(\xi_{ab}/\lambda_j)^3$, both for δT_c and δl pinning. We should also remember that as analysed in section 2.2 (eq.2.16) for the case of vortices laying parallel to the layers there is a dramatic softening of the component of the shear modulus parallel to the basal plane, $c_{66}^{\parallel}$. Due to the aforementioned reasons, the motion of the strings is facilitated for directions parallel to the layers. This explains the extremely weak irreversibility measured for the field lying in the ab plane: the scaled to size width of the hysteresis for transverse geometry (H_a // c-axis) increases up to around 30 times. Thus, returning to our description, any increase of H_a will lead to a decrease of the vortex spacing a and an accompanying enhancement of the mutual repulsion of the strings (points of upward curvature like B in figure 6.3).

Nevertheless, in order to proceed from one commensurate state, H_{n+1} with $l = (n+1)d$, to the next, H_n with $l = nd$, changes in l have to occur for field values in the intermediate region of H_{n+1} and H_n. This is illustrated in figure 6.4(c) and has been a theoretical suggestion long before the observation of lock-in oscillations [3,31]. The increase of H_a leads to a point where the parallel motion of the cores is prohibited due to strong repulsion applied by the other cores in the same "channel"; now it is favorable for the nuclei to actually *cross* the CuO_2 layers by the creation and motion of pairs of kinks and antikinks. A fast reorganisation of vortices from the n+1 to the n

commensurate state begins. In the quasi-2D regime, which is the case for the temperature regime discussed here, the kink - antikink pair is a 2D Abrikosov vortex - antivortex pair in the ab plane [3]. In this incommensurate state, the pair has to face the enhanced pinning interactions present in the CuO_2 plane. Thus, one expects the effective pinning force to maximise resulting to a peak in the magnetic hysteresis. This is the case in our lock-in oscillations for points as C in figure 6.3.

As it is obvious from the geometry of the problem [3], the kink-antikink pair faces a force parallel to the ab plane and once it is nucleated, it also moves in the direction parallel to the layers (points of downward curvature like D in fig.6.3). In this way, the whole vortex line is "transported" to the neighbouring interlayer spacing. Finally the vortex system arrives at the new commensurate state and the circle is then repeated (fig.6.4(d)).

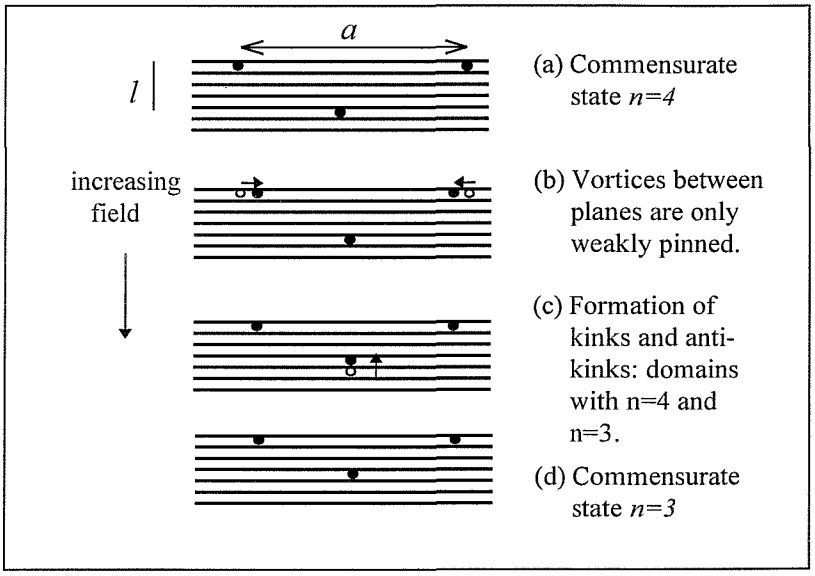

Figure 6.4: *A schematic representation of the transition between two successive commensurate states, producing the observed lock-in oscillations.*

Interestingly, the above description is valid up to magnetic fields of the order of $H_0 = \Phi_0/\gamma d^2 \sim 200$ T, in $YBa_2Cu_3O_{7-\delta}$. Above H_0, all the interlayer spaces are occupied and any further increase of H_a results to a mere further stacking of nuclei in each of the interlayer spaces [3,15].

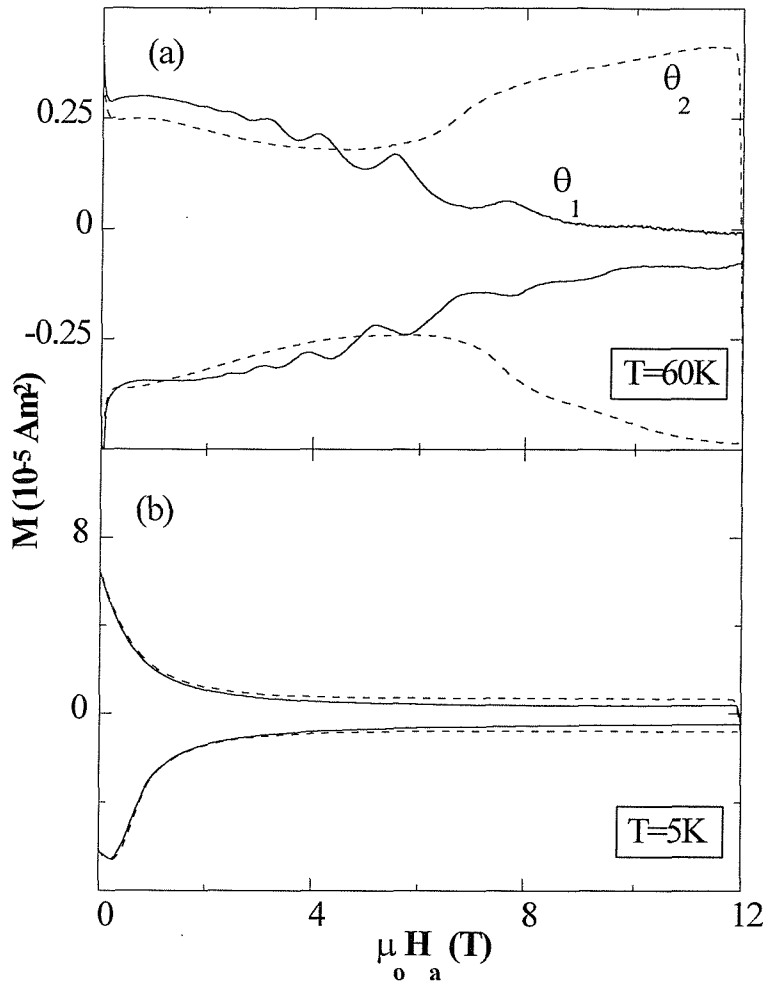

Figure 6.5: *Magnetic hysteresis loops for* H_a // b-axis *and two orientations* θ_1, θ_2 *(see text) for (a)* T = *60 K and (b)* T = *5 K.*

Figure 6.5 [29] illustrates the competitive nature of point disorder and layered structure, critical for the appearance of the lock-in transition. Pictured are the magnetic hysteresis loops for crystal DT0, for two different temperatures, 5 K and 60 K. H_a is parallel to the b-axis. In one case the misalignment from the ab plane is $\theta_1 < 1°$ while in the other we intentionally created a misalignment of $\theta_2 \approx 2°$. For θ_1 lock-in oscillations appear at 60 K, indicating that we are below the critical angle for lock-in, θ^*. On the other hand, for $\theta = \theta_2$ at 60 K the absence of oscillations in the magnetic hysteresis verifies that this second angle is above the critical one. As Blatter *et al.* [6] have shown,

θ^* can be considered either temperature independent, or even weakly increasing with decreasing temperature. Therefore, we expect to observe lock-in oscillations also at 5 K, for $\theta = \theta_1$. However, as fig.6.5(b) shows, no oscillations appear at this temperature and the magnetic hysteresis is essentially the same as for the second, misaligned, orientation. At these very low temperatures, even for our high purity samples, the pinning energy of the random point disorder background is quite large and, as Tachiki [32] predicted, kinks can be nucleated at the defects. The creation of such kinks destroys the alignment of vortices [32] and spoils the lock-in transition between the layers [3] and hence the absence of oscillations. The purity of the samples is therefore an important factor in the determination of the lock-in transition and the observation of lock-in oscillations.

One has to note that the theoretical prediction of jumps in the magnetisation existed long before their observation in our group. They were one of the possible consequences considered of commensurability effects between the interlayer distance and the vortex lattice spacing along the c-axis [3,31,33] . Bulaevskii and Clem [31] estimated, using the anisotropic London model, the field dependence of l to be:

$$l = (\Phi_0\sqrt{3}/2\gamma)^{1/2} B_a^{-1/2} \tag{6.3}$$

with $B_a = \mu_0 H_a$. Considering, next, the existence of the layered structure and incorporating their results in the LD model, they predicted that the transition from one commensurate to another commensurate state by jumps in l (and consequently[1] in a), is accompanied by jumps in the measured magnetisation. In addition, lock-in oscillations allow us to monitor the position of the Josephson strings along the c-axis in the sample in a very accurate way. From eq.(6.3) it is straightforward to show that:

$$\left(\frac{\sqrt{3}\,H_o}{2H_n}\right)^{1/2} = n \tag{6.4}$$

Taking, for example, the data for crystal DT0 (pictured in figure 6.3), we find one of the commensurate states at T = 50 K, for H_a parallel to the a-axis, at H_n = 3.45 T. For this value equation (6.4) gives n = 7.94 that is, by taking the integer part of the result, n = 8. This means that the Josephson vortex lattice has a spacing perpendicular to the ab

[1] The unit cell of the Josephson vortex lattice is given by $al = \Phi_0/H_a$ [31].

plane of l = 8d; in other words a buffer zone of 7 empty interlayer spaces separates every occupied one.

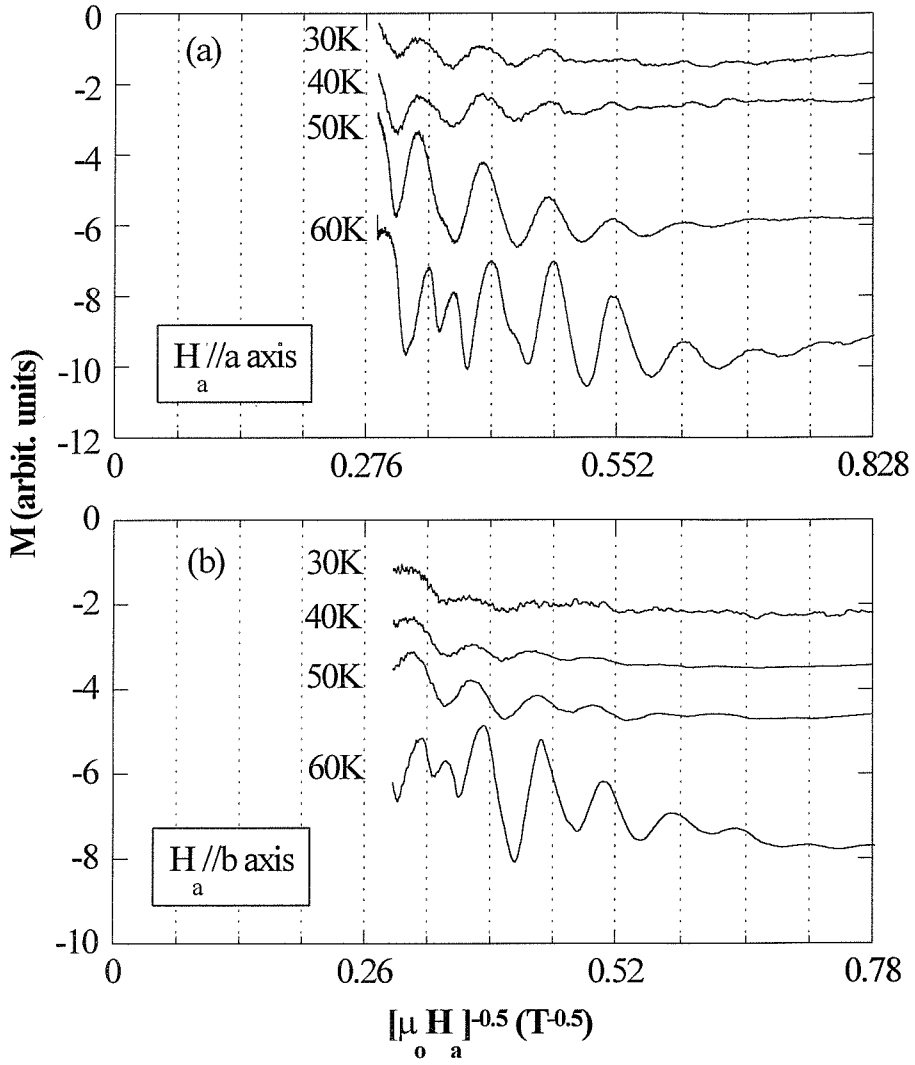

Figure 6.6: *Lock-in oscillations for DT0, for* H_a *along the* a-axis *(a) and along the* b-axis *(b).*

The periodicity that characterises the layered structure and the succession of the commensurate states, together with the field dependence of l as given by eq.(6.3), are the reasons for the periodicity of the magnetisation in the $H_a^{-1/2}$ space, as depicted in figure 6.6. Data are for DT0, at temperatures of 30, 40, 50 and 60 K with H_a applied

parallel to a-axis and b-axis and increasing (data corresponds to these of figure 6.3). Again the curves have been moved vertically for clarity. We observe a remarkable periodicity of the lock-in oscillations with their period being the same for all temperatures. The temperature independence of the periodicity of the lock-in oscillations is in agreement with the case of pinning caused by matching of the perpendicular vortex lattice spacing *l* with the layered structure.

We should mention that the magnetic loops for $T \geq 60$ K display some additional characteristics, namely a slight shift of lock-in oscillations towards lower fields, which we discuss below, and the appearance of additional peaks at high fields (e.g. between 0.345 and 0.414 $T^{-1/2}$ for H_a // a-axis). The existence of these additional peaks has not yet been elucidated. They are observed for any orientation of the applied field within the ab plane. They are also observed at field values comparable to the VSM's accessible range, around 10 T (fig.6.3), which makes their study problematic. Though one could speculate that at this point other regular vortex structures which do not have minimal free energy (with *a/l* ratio other than $2\gamma/\sqrt{3}$) become energetically favorable, in the field range we can access these extra peaks appear only when increasing the magnetic field.

Importantly, lock-in oscillations can be used as an accurate tool for measuring essential physical parameters of $YBa_2Cu_3O_{7-\delta}$ as is the out-of plane and in-plane anisotropy. From eq.(6.3) and the periodicity of the lock-in oscillations in the $H_a^{-1/2}$ space, it is straightforward to extract γ as:

$$\gamma = \frac{\sqrt{3}}{2}\Phi_o\left(\frac{\Delta\left[B_a^{-1/2}\right]}{d}\right)^2 \qquad (6.5)$$

In eq.(6.5), we took into account that in each period of the magnetisation oscillations $\Delta[B_a^{-1/2}]$, *l* is changing by d. Using the reported value at T = 120 K of $d = 1.164 \times 10^{-9}$ m [34], $\Phi_o = 2.067 \times 10^{-15}$ Vs and that for crystal DT0 $\Delta[B_a^{-1/2}]$ is equal to 0.069 and 0.065 $T^{-1/2}$ for the direction of the applied field parallel to the a-axis and b-axis, respectively, we end up with:

$$\gamma_{cb} = \sqrt{\frac{m_c}{m_b}} = 6.3 \pm 0. \qquad H_a \text{ // a-axis} \qquad (6.6)$$

$$\gamma_{ca} = \sqrt{\frac{m_c}{m_a}} = 5.6 \pm 0.1 \qquad H_a \text{ // b-axis} \qquad (6.7)$$

The difference of the anisotropy factors γ_{cb} and γ_{ca}, expected from the observed difference of the periodicity of the lock-in oscillations for H_a // a and H_a // b-axis (fig.6.6), verifies previous measurements of in-plane anisotropy in $YBa_2Cu_3O_{7-\delta}$ [12], where by a Bitter decoration technique a factor γ_{ab} ranging from 1.11 to 1.15 was obtained. In our case γ_{ab} is estimated as the ratio of γ_{cb}/γ_{ca} and is equal to 1.13 ± 0.04.

The values of the out-of-plane anisotropy parameter reported in the literature until now for $YBa_2Cu_3O_{7-\delta}$ by means of various techniques, are scattered between 3-10 [35-39]. One of the techniques for extracting γ, suffering by fewer ambiguities, has proved to be measurements of torque magnetisation [40]. Based on torque measurements, reports in the literature give for $YBa_2Cu_3O_{7-\delta}$ single crystals of similar critical temperature with the ones presented here ($T_c > 90$ K, near the optimum doped regime) values of γ between 4-10 [39,40].

While our out-of-plane and in-plane γ values, extracted from lock-in oscillations, are in good agreement with all the aforementioned cases, we went further and performed another check: we carried out measurements of torque magnetometry on one of the crystals which exhibited lock-in oscillations, namely crystal DT3. For this reason, we collaborated with Dr. Luc Früchter, in the Université Paris-Sud in Orsay, who has a long standing expertise in torque measurements in $YBa_2Cu_3O_{7-\delta}$ and other layered high temperature superconductors [41,42].

As Kogan [43] pointed out, the fact that in high-T_c oxides the screening current loops have the tendency to flow preferentially close to the ab plane has an important consequence: the magnetisation has a normal to the applied field component. The result is the existence of an anisotropy torque τ given by:

$$\frac{\vec{\tau}(\phi)}{V} = \left|\vec{M} \times \vec{H}_a\right| \qquad (6.8)$$

V is the volume of the sample and ϕ is the angle between the external field H_a and the c-axis. For temperatures close to T_c, by an anisotropic London treatment, equation (6.8) can be translated to a more practical relation, yielding the angular dependence of the

reversible torque [43]:

$$\frac{\tau(\phi)}{V} = \frac{\Phi_o \cdot H_a \cdot \sin(2\phi) \cdot (\gamma^2 - 1)}{64 \cdot \pi^2 \cdot \lambda_{ab}^2(T) \cdot \varepsilon(\phi) \cdot \gamma} \cdot \ln\left(\frac{\beta \cdot H_{c2}^{\perp}(T) \cdot \gamma}{H_a \cdot \varepsilon(\phi)}\right) \qquad (6.9)$$

where β is a constant of the order unity, $H_{c2}^{\perp}(T)$ the upper critical field measured along the c-axis, perpendicularly to the layers, and $\varepsilon(\phi) = \sqrt{\sin^2\phi + \gamma^2 \cdot \cos^2\phi}$. As Farrell has demonstrated [18] in $YBa_2Cu_3O_{7-\delta}$ the above equation is valid for temperatures $T \geq 80$ K; there is also a field requirement [43], namely $H_a >> H_{c1}$. In our measurements we worked in temperatures $T > 87$ K with an applied field $H_a = 1$ T, satisfying both conditions.

Figure 6.7 [29] shows torque data for sample DT3. In the case of fig.6.7(a) H_a was rotated from the c to the a-axis, while in fig.6.7(b) to the b-axis. For each orientation $\tau(\phi)$ was measured at a number of different temperatures, in the [0°,90°] interval. The measurement regime is completely reversible. To eliminate the contribution of the normal state, arising from the normal susceptibility of the sample and the sampleholder, we used the usual procedure: we subtracted from the raw signal the measured torque in the same applied field, but at a temperature T = 99 K.

To deduce the anisotropy, we fitted each of the experimental curves of fig.6.7 with eq.(6.9), using as fitting parameters γ, $\lambda_{ab}(0)$ and $\beta H_{c2}^{\perp}(T)$. As clearly seen, eq.(6.9) provides an excellent fit. The resulting values for γ, for both orientations, are shown in figure 6.8. For rotation of H_a in the ca plane, we find [43] an average anisotropy factor $\gamma_{cb} = 7.56 \pm 0.14$ while for rotation in the cb plane the average out-of-plane anisotropy is $\gamma_{ca} = 6.51 \pm 0.22$. This leads to an in-plane anisotropy $\gamma_{ab} = 1.16 \pm 0.05$. On the other hand, for the same crystal, we find the periodicity of the lock-in oscillations to be 0.071 and 0.063 $T^{-1/2}$ for H_a // a and H_a // b-axis, respectively (see also fig.6.9). From eq.(6.4) we estimate the anisotropy factors to be, correspondingly, $\gamma_{cb} = 6.57 \pm 0.20$ and $\gamma_{ca} = 5.24 \pm 0.20$, i.e. an in-plane anisotropy of $\gamma_{ab} = 1.22 \pm 0.06$. The results are in reasonable agreement with those obtained by torque with the maximum deviation from them being ~ 14% in the case of γ_{ca}. It is interesting to note that this small deviation may point towards a possible temperature dependence of γ. The slightly increased γ values come from torque, which was employed in the temperature regime around 90 K,

whereas we extract γ from lock-in oscillations at much lower temperatures. A similar temperature dependence of γ for $YBa_2Cu_3O_{7-\delta}$ single crystals with $T_c = 91$ K was found by Pugnat *et al.* [44], from magnetisation vector measurements. However, further systematic studies are needed to examine this possibility.

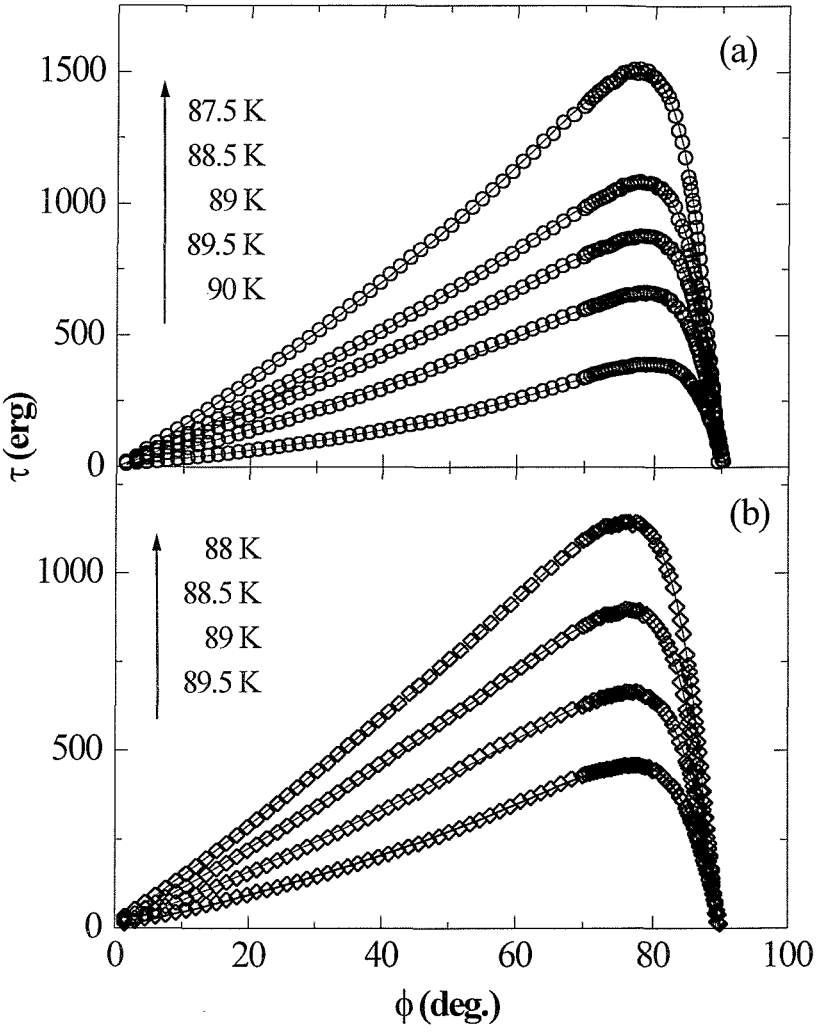

Figure 6.7: *The measured torque for the indicated temperatures and* H_a *rotated in (a) the* ca *plane and (b) the* cb *plane. Angles are measured from the* c-axis. *Symbols are the experimental data and lines represent the theoretical fits, using eq.(6.9).*

Thus, lock-in oscillations provide an alternative reliable way of estimating the in-plane and out-of-plane anisotropy factors for $YBa_2Cu_3O_{7-\delta}$. Due to the great impact of the anisotropy parameters on vortex dynamics (e.g. elastic moduli), it is obvious that the lock-in oscillations can be extremely useful in extracting valuable information on a variety of other research problems (e.g. the phase diagram of Abrikosov vortices); this is especially true in $YBa_2Cu_3O_{7-\delta}$, where the additional complication of in-plane anisotropy can introduce new effects.

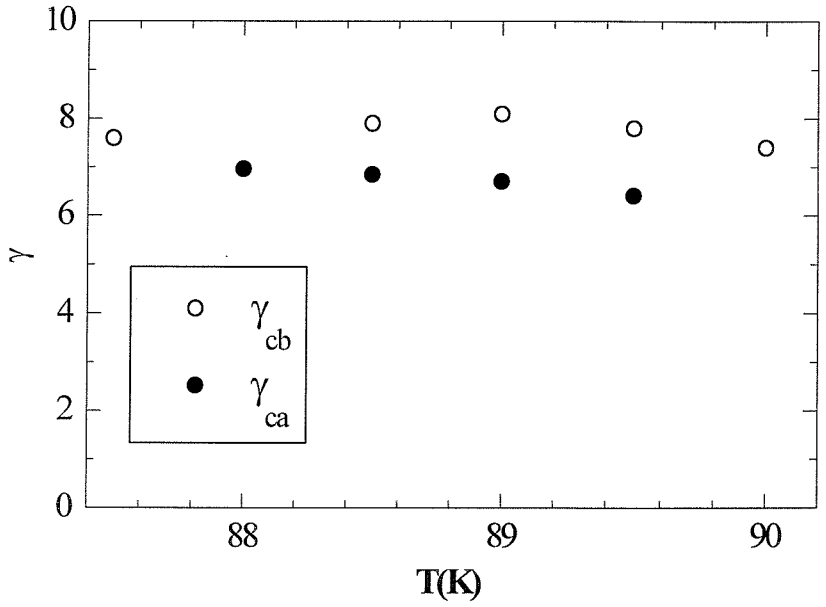

Figure 6.8: *The anisotropy values extracted from fitting the experimental data of fig.6.7 with eq.(6.9).*

Figure 6.9 displays lock-in oscillations for DT3, at 60 K and H_a // ab plane, at 3 different orientations: for the applied field along the two principal axes (a and b) of the basal plane and at an angle of 41° ± 2° with the b-axis [29]. For the last orientation of the applied field, tilted at an angle ϑ (in our case ϑ = 41°) from the b-axis within the ab plane, and the geometry of the flowing supercurrents the relevant effective mass will be an average of m_a and m_b [43]:

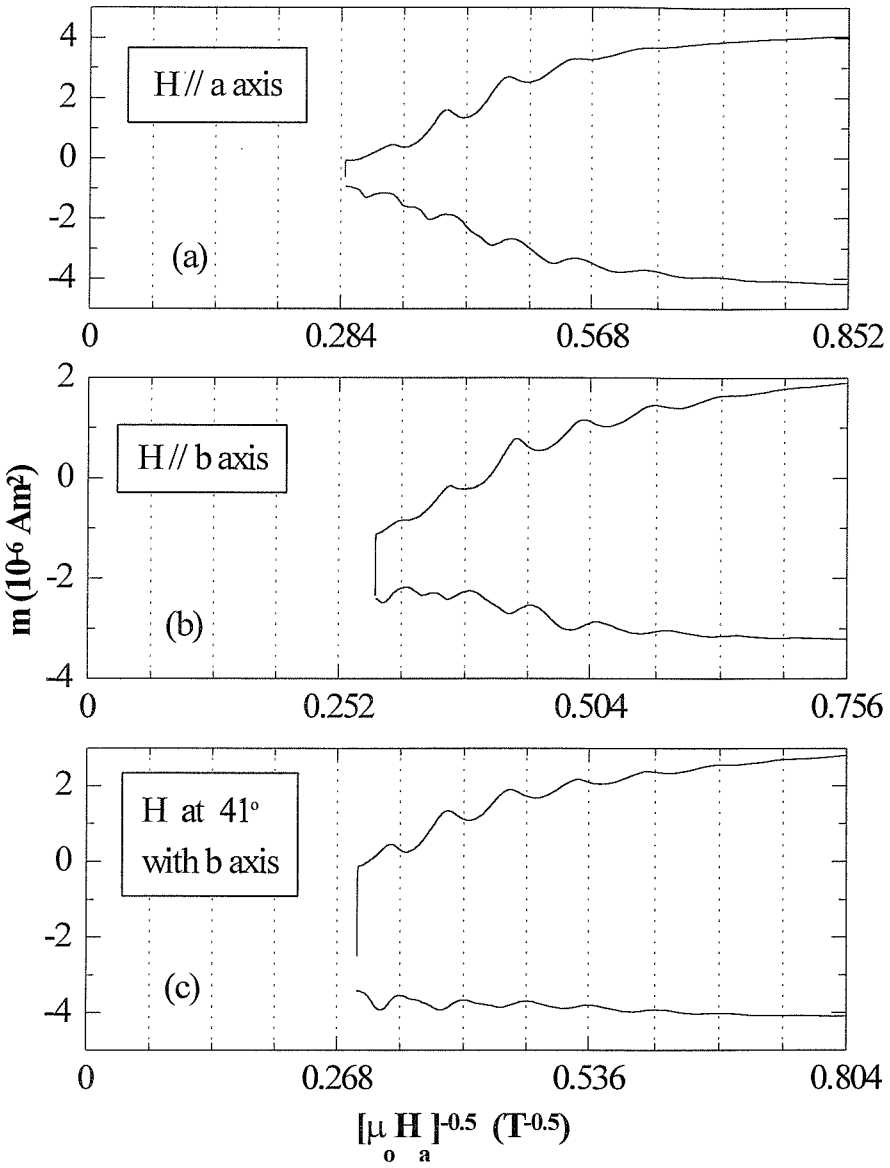

Figure 6.9: *Lock-in oscillations for DT3, with* H_a *in the* ab *plane and (a) parallel to the* a-axis *(b) parallel to the* b-axis *and (c) in an angle* $\vartheta \sim 41°$ *with the* b-axis.

$$m(\vartheta) = m_a \cdot \cos^2\vartheta + m_b \cdot \sin^2\vartheta \tag{6.10}$$

This leads to:

$$\gamma_{41} \cong \sqrt{\frac{m_c}{m(41°)}} = \sqrt{\frac{\gamma_{ca}^2 \cdot \gamma_{cb}^2}{\gamma_{cb}^2 \cdot \cos^2 41 + \gamma_{ca}^2 \cdot \sin^2 41}} \tag{6.11}$$

Taking into account that, as mentioned before, the values of the anisotropy parameters extracted from the oscillations are $\gamma_{cb} = 6.57 \pm 0.20$ and $\gamma_{ca} = 5.24 \pm 0.20$, from eq.(6.11), one expects γ_{41} to be approximately equal to 5.71 ± 0.15. From lock-in oscillations now, we find the periodicity for (H_a, b-axis) = $41° \pm 2°$ to be $0.067\ T^{-1/2}$, i.e. using eq.(6.5) $\gamma_{41} = 5.95 \pm 0.20$, in good agreement with the expected result.

Since, according to the above, the periodicity of the lock-in oscillations depends only on the characteristics of the layered structure, it should be unaffected by the angle of the applied field with the ab plane, as long as this remains below the critical angle θ^*. Figure 6.10 illustrates magnetic hysteresis loops at 60 K, for crystal DT0, with H_a parallel to the b-axis and at three different angles with the ab plane. Angles θ_1 and θ_2 are all less than 1°. In all these measurements lock-in oscillations are present. We also created a misalignment between the sample and the layered structure of $\theta_3 = 2° \pm 0.5°$; as seen in figure 6.10, for this angle the oscillations disappear. Thus, our results indicate the existence of a critical angle of the order of 1°. Furthermore, figure 6.10 verifies the independence of the position of the maxima and minima of the oscillations from the orientation of H_a, in the locked-in state.

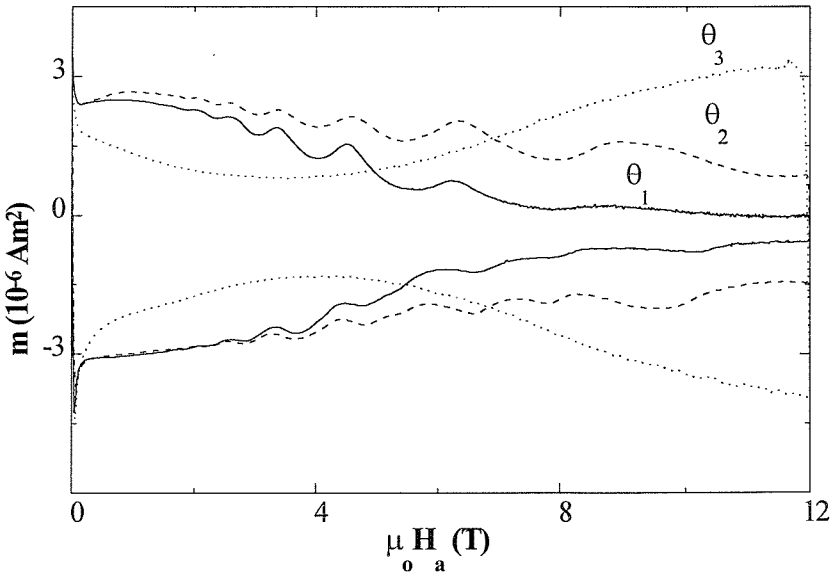

Figure 6.10: *Lock-in oscillations for different angles (see text), at 60K, for DT0 and* H_a *//* b-axis.

In figure 6.11 we present for the first time [29] the temperature development of the magnetisation lock-in oscillations for crystal DT3, with H_a along the a-axis, at an angle θ smaller than 1° from the ab plane. Measurements for temperatures up to 80 K are pictured.

Between 30 K and 40 K the width of the hysteresis Δm is decreasing with temperature; the oscillations are weak. They appear, with a small amplitude, at high magnetic fields larger than approximately 6 T. As demonstrated before, at lower temperatures the pinning energies of the random point disorder prevent vortices from being locked between the CuO_2 planes; kinks consisting of 2D vortex pancakes with normal cores are created in the ab planes and pinned by point defects [32]. As a result, the oscillations are expected in this case to be either absent or weak.

In the temperature interval 42-52 K two are the major findings. First, we observe an enhancement in the amplitude of the oscillations. This is expected: having moved away from low temperatures, in this temperature regime, the creation of kinks at the point defects is less favorable due to the depression of the elementary pinning energies. Therefore, an increased number of vortices becomes now locked-in. This increased number of locked-in vortices can account for the increase in the amplitude of the oscillations.

However, we also find that the total width Δm of the hysteresis unexpectedly increases with temperature. Indeed, figure 6.12 depicts the temperature dependence of the width of the magnetic hysteresis Δm (proportional to the critical current) for two constant applied fields of 3.3 T and 8.4 T. We verified this result for all crystals that give lock-in oscillations and for both orientations of the applied field within the ab plane, i.e. parallel to both principal axes, a and b. For the increase of the total width of the hysteresis, one has to consider another possible effect. For a parallel to the layers applied field H_a, due to the easy entrance of vortex cores between the layers, the irreversibility measured by magnetisation is weak and reflects the extrinsic pinning, i.e. pinning of the Josephson cores from the extrinsic defects [3]. As we mentioned before, this pinning for Josephson vortices is, in the absence of a normal core, also weak. Feinberg theoretically predicts that raising the temperature this source of pinning can actually *strengthen*, due to the increased suppression of the order parameter in the phase

core, leading to an increase of the measured magnetic hysteresis width. Indeed, Blatter *et al.* [6], have calculated that the suppression of the order parameter in the centre of a Josephson nucleus increases with temperature proportionally to ξ_{ab}^2. Thus, we consider our results to be the first experimental evidence in single crystals, of the J_c anomaly predicted by Feinberg [3]. In addition, one can take into account that the layered structure offers now to an increased number of locked-in strings an enhanced screening of thermal fluctuations and effectively makes these fluctuations 2D (vortex waving between two adjacent layers), restricting dissipation.

Increasing the temperature further, Δm is reduced. At these elevated temperatures, the energy to create kinks is reduced [3,6]. Thermal energy is now sufficiently strong to spontaneously activate vortex kinks-antikinks pairs, introducing another important mechanism of dissipation [3,8]. Experimentally, the oscillations are no longer observed above 80 K. Taking this temperature as the temperature T^* at which vortices enter the quasi-3D regime and the lock-in transition is not any more realisable due to the increase of ξ_c above the $d/\sqrt{2}$ limit [18,25], one can extract $\xi_c(T=0)$ from the temperature dependence of the transverse coherence length [3,6,8]:

$$\xi_c(T) = \xi_c(0) \cdot \left(1 - \frac{T}{T_c}\right)^{-1/2} \tag{6.12}$$

For $T = T^*$ we have $\xi_c(T^*) = d/\sqrt{2}$. In $YBa_2Cu_3O_{7-\delta}$, with the spacing between the superconducting layers being equal to $d = 11.64$ Å [33], we estimate from eq.(6.12) that $\xi_c(0) = 3.14$ Å. The result agrees with estimations of $\xi_c(0)$ by other methods. For example, estimating $\xi_c(0)$ from the thermodynamic critical field H_c derived from specific heat measurements, results in a value of $\xi_c(0) = 3.2$ Å [45]. Welp *et al.* [46] using dc magnetisation measurements have found $\xi_c(0) = 3$ Å.

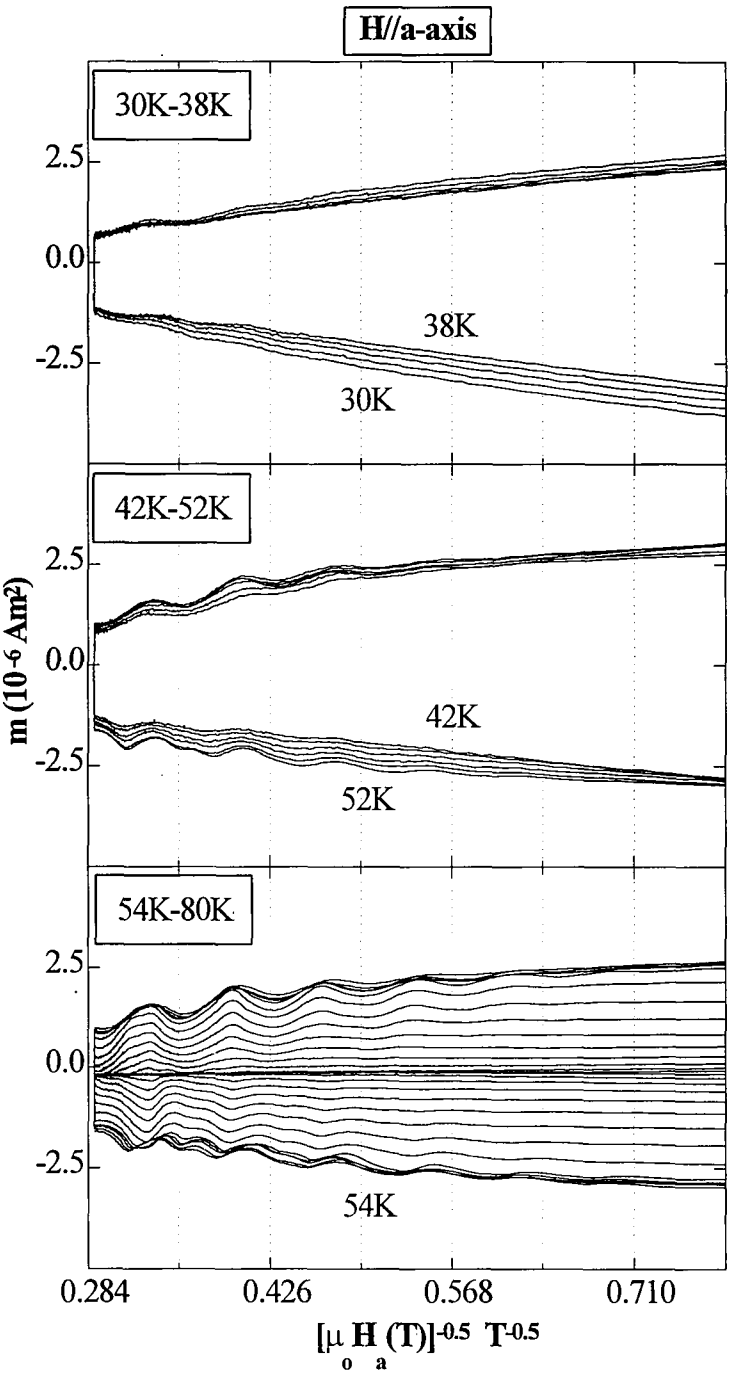

Figure 6.11: *Temperature development of the lock-in oscillations in the range 30-80 K, for crystal DT3,* H_a // a-axis.

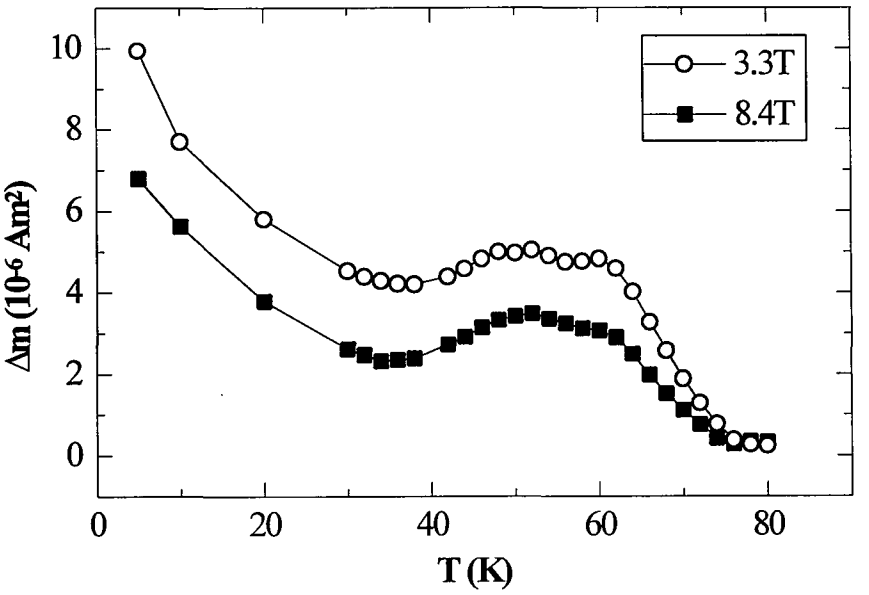

Figure 6.12: *Temperature dependence of the width of the magnetisation at two different applied fields, 3.3 and 8.4 T, as derived for the data depicted in fig. 6.11.*

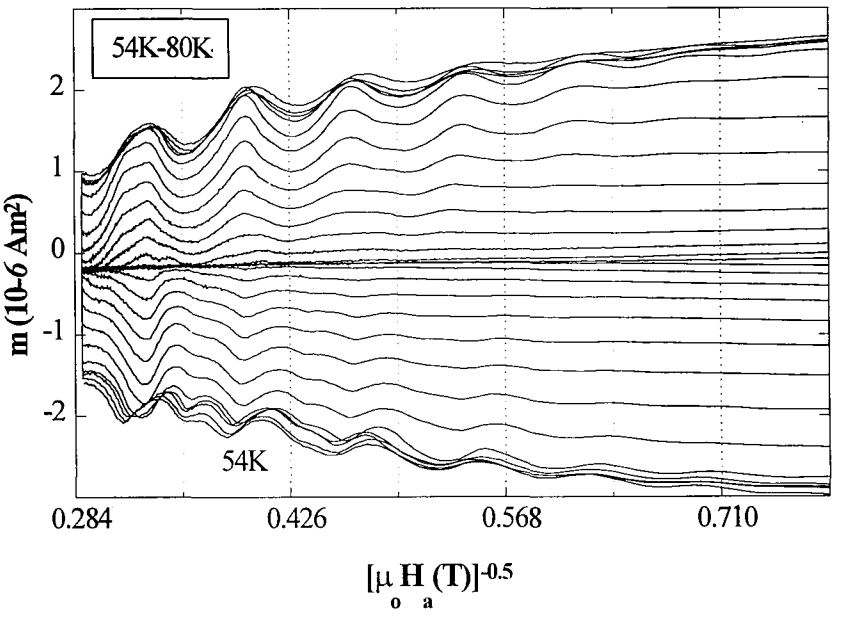

Figure 6.13: *A slight shift of the period of the lock-in oscillations at elevated temperatures. Data are for DT3, with* H_a // a-axis.

Finally, figure 6.13 [29] offers a closer look at the data presented in fig.6.11 for crystal DT3 and H_a // a-axis, at elevated temperatures. As mentioned before the magnetisation isotherms at higher temperatures, T > 50 K, display a slight shift of the lock-in oscillations at lower fields. This is because at elevated temperatures and as the temperature rises, the periodic pinning potential of the layered structure weakens [3,33] and the nucleation of pairs of kinks, necessary condition for the crossing of the layers, is now favorable for the Josephson cores at slightly lower fields. Note that in a recent numerical study of the lock-in oscillations, Ichioka [47] verified this slight lowering of the critical fields H_n with the increase of temperature.

6.4 CONCLUSIONS

To conclude, we have presented a magnetic study for a large range of magnetic fields and temperatures, using longitudinal geometry, i.e. with the external field in the basal plane of the samples. We have demonstrated that, for fields applied parallel to the layers, the observation of lock-in oscillations in the magnetic hysteresis loops of $YBa_2Cu_3O_{7-\delta}$ can be a powerful tool for the study of the low temperature quasi-2D regime.

The method offers considerable advantages over other techniques, especially since it covers an extended temperature regime. We can accurately map the position of Josephson vortices - their spacing along the c-axis - in the sample and the structure of the Josephson strings lattice. We can reliably extract essential parameters, such as the out-of-plane and in-plane anisotropy, $\xi_c(0)$ and the temperature T^* the dimensional crossover from the quasi-2D to the quasi-3D region occurs.

We have also illustrated the competing nature of point disorder and layered structure. The first tends to destroy the lock-in transition and quench lock-in oscillations, by offering to vortices favorable locations for the creation of kinks and spoiling their perfect alignment between the layers, even for an external field applied at an angle below the lock-in critical angle. Thus, the need for high purity samples is essential in order to observe the magnetisation oscillations.

Finally, we have presented the temperature dependence of lock-in oscillations up to a temperature of 80 K. Our results show a surprising non-monotonic temperature dependence of the width of the magnetisation curve and consequently of the measured critical current: these two - proportional - quantities increase with temperature, at intermediate temperatures. Our results can be explained by considering the interaction of Josephson vortices with extrinsic pinning centres, as random point defects, together with the reduced thermal dimensionality of the locked-in vortices.

REFERENCES

[1] W. E. Lawrence and S. Doniach, *Proc. 12th Int. Conf. on Low Temp. Physics*, Kyoto (1971), ed. E. Kanda (Keigaku, Tokyo 1971), p.361.

[2] L. N. Bulaevskii, Zh. Eksp. Teor. Fiz. **64**, 2241 (1973) [Sov. Phys. JETP **37**, 1133 (1973)]; Int. J. Mod. Phys. B **4**, 1849 (1990).

[3] D. Feinberg, J. Phys. III **4**, 169 (1994) and references therein.

[4] E. H. Brandt, Rep. Prog. Phys. **58**, 1465 (1995).

[5] A. M. Ettouhami, PhD thesis, University of Grenoble (1994).

[6] G. Blatter, M. V. Feigel'man, V. B. Geshkenbein *et al.*, Rev. of Mod. Phys. **66**, 1125 (1994).

[7] M. Tachiki and S. Takahashi, Solid. St. Comm. **70**, 291 (1989).

[8] D. Feinberg and A. M. Ettouhami, Int. J. Mod. Phys. B **7**, 2085 (1993).

[9] D. Feinberg and A. M. Ettouhami, Physica Scripta **T49**, 159 (1993).

[10] A. M. Grishin, A. Yu. Martynovich, S. V. Yampolskii, Sov. Phys. JETP **70**, 1089 (1990).

[11] B. I. Ivlev and N. B. Kopnin, Phys. Rev. B **44**, 2747 (1991).

[12] G. J. Dolan, F. Holtzberg, C. Feild *et al.*, Phys. Rev. Lett. **62**, 2184 (1989).

[13] C. A. Bolle, P. L. Gammell, D. G. Grier *et al.*, Phys. Rev. Lett. **66**, 112 (1991).

[14] D. Feinberg, Physica C **194**, 126 (1992).

[15] L. N. Bulaevskii, M. Ledvij, V. G. Kogan, Phys. Rev. B **46**, 366 (1992).

[16] S. Theodorakis, Phys. Rev. B **42**, 10172 (1990).

[17] D. A. Huse, Phys. Rev. B **46**, 8621 (1992).

[18] D. E. Farrell, J. P. Rice, D. M. Ginsberg *et al.*, Phys. Rev. Lett. **64**, 1573 (1990).

[19] L. N. Bulaevskii, Phys. Rev. B **44**, 910 (1991).

[20] F. Steinmeyer, R. Kleiner, R. Müller *et al.*, Europhysics Letters **25**, 459 (1994).

[21] D. H. Chung, M. Chaparale, M. J. Naughton, *Proc. VIth NYSIS Conf. On Superconductivity*, Buffalo, USA (1992), AIP (New York, 1993).

[22] W. K. Kwok, U. Welp, V. M. Vinokur *et al.*, Phys. Rev. Lett. **67**, 390 (1991).

[23] J. N. Li, A. A. Menovsky, J. J. M. Franse, Phys. Rev. B **48**, 6612 (1993).

[24] S. Kolesnik, T. Skoskiewicz, J. Igalson *et al.*, Phys. Rev. B **54**, 13319 (1996).

[25] Yu. V. Bugoslavsky, A. A. Zhukov, G. K. Perkins *et al.*, preprint.

[26] M. Tinkham, *Introduction to Superconductivity*, Mc Graw-Hill, Singapore (1996).

[27] J. C. Martinez, S. H. Brongersma, A. Koshelev *et al.*, Phys. Rev. Lett. **69**, 2276 (1992).

[28] M. Oussena, P. A. J. de Groot, R. Gagnon *et al.*, Phys. Rev. Lett. **72**, 3606 (1994).

[29] K. Deligiannis, P. A. J. de Groot, L. Früchter *et al.*, in preparation.

[30] V. G. Kogan, Phys. Lett. **85A**, 298 (1981).

[31] L. N. Bulaevskii and J. R. Clem, Phys. Rev. B **44**, 10234 (1991).

[32] M. Tachiki and S. Takahashi, Solid. St. Comm. **72**, 1083 (1989).

[33] S. E. Burkov, Phys. Rev. B **44**, R2850 (1991).

[34] R. M. Hazen, *Physical Properties of High Temperature Sup. II*, editor D. M. Ginsberg (World Scientific, Singapore 1990), p.121.

[35] T. K. Worthington, W. J. Gallagher, T. R. Dinger, Phys. Rev. Lett. **59**, 1160 (1987).

[36] A. Umezawa, G. W. Crabtree, J. Z. Liu *et al.*, Phys. Rev. B **38**, 2808 (1988).

[37] T. K. Worthington, D. L. Kaiser, F. H. Holtzberg *et al.*, Physica **153-155**, 32 (1988).

[38] L. Krusin-Elbaum, A. P. Malozemoff, Y. Yeshurun, *et al.*, Phys. Rev. B **39**, 2936 (1989).

[39] T. R. Chien, W. R. Datars, B. W. Veal *et al.*, Physica C **229**, 273 (1994).

[40] D. E. Farrell, C. M. Williams, S. A. Wolf *et al.*, Phys. Rev. Lett. **61**, 2805 (1988).

[41] L. Früchter and I. A. Campbell, Phys. Rev. B **40**, 5158 (1989).

[42] A. Hamzic, L. Früchter, I. A. Campbell, Nature **345**, 515 (1990).

[43] V. G. Kogan, Phys. Rev. B **38**, 7049 (1988).

[44] P. Pugnat, G. Fillion, H. Noel *et al.*, Europhys. Lett. **35**, 49 (1996).

[45] N. E. Hussey, J. R. Cooper, R. A. Doyle *et al.*, Phys. Rev. B **53**, 1 (1996).

[46] U. Welp, W. K. Kwok, G. W. Crabtree *et al.*, Phys. Rev. Lett. **62**, 1908 (1989).

[47] M. Ichioka, Phys. Rev. B **51**, R9423 (1995).

7. SUMMARY

The measurements described in this thesis represent an investigation into the magnetic phase diagram and pinning properties of high purity $YBa_2Cu_3O_{7-\delta}$ single crystals, in the vortex phase. The use of a high field Vibrating Sample Magnetometer (VSM) allowed the study of this compound in applied fields up to 12 T and in a large temperature regime. A 6 T SQUID magnetometer was also employed, while torque data was obtained for one of the samples. This chapter reiterates and collects together the main conclusions of our research in a brief summary.

7.1 VORTEX CHANNELING

By measuring the dc magnetisation of $YBa_2Cu_3O_{7-\delta}$ single crystals in a broad temperature and magnetic field regime, we demonstrate that, contrary to previous reports, twin planes can actually *decrease* the magnetic hysteresis width and the critical current density, by providing easy paths for vortex motion. Our measurements show that of major importance is the existence of intersections of different colonies of twin planes in the samples, which provide strong columnar-like defects and prevent vortex channeling.

We illustrate that channeling of vortices along the twin planes occurs only when the pinning force in the untwinned regions is stronger than the pinning force in the twin planes. When this condition is not met, twin planes enhance the critical current by acting as strong pinning centres.

By measuring the magnetisation for different angles θ of the applied field with the twin planes, we experimentally demonstrate, for the first time, the existence of *two* critical angles, a lock-in angle θ_L and a trapping angle θ_K. For $\theta < \theta_L$ vortices are locked-in the twin planes. For $\theta_L < \theta < \theta_K$ vortices form a kinked structure with parts lying in the untwinned regions and parts locked in the twin planes; in this phase the

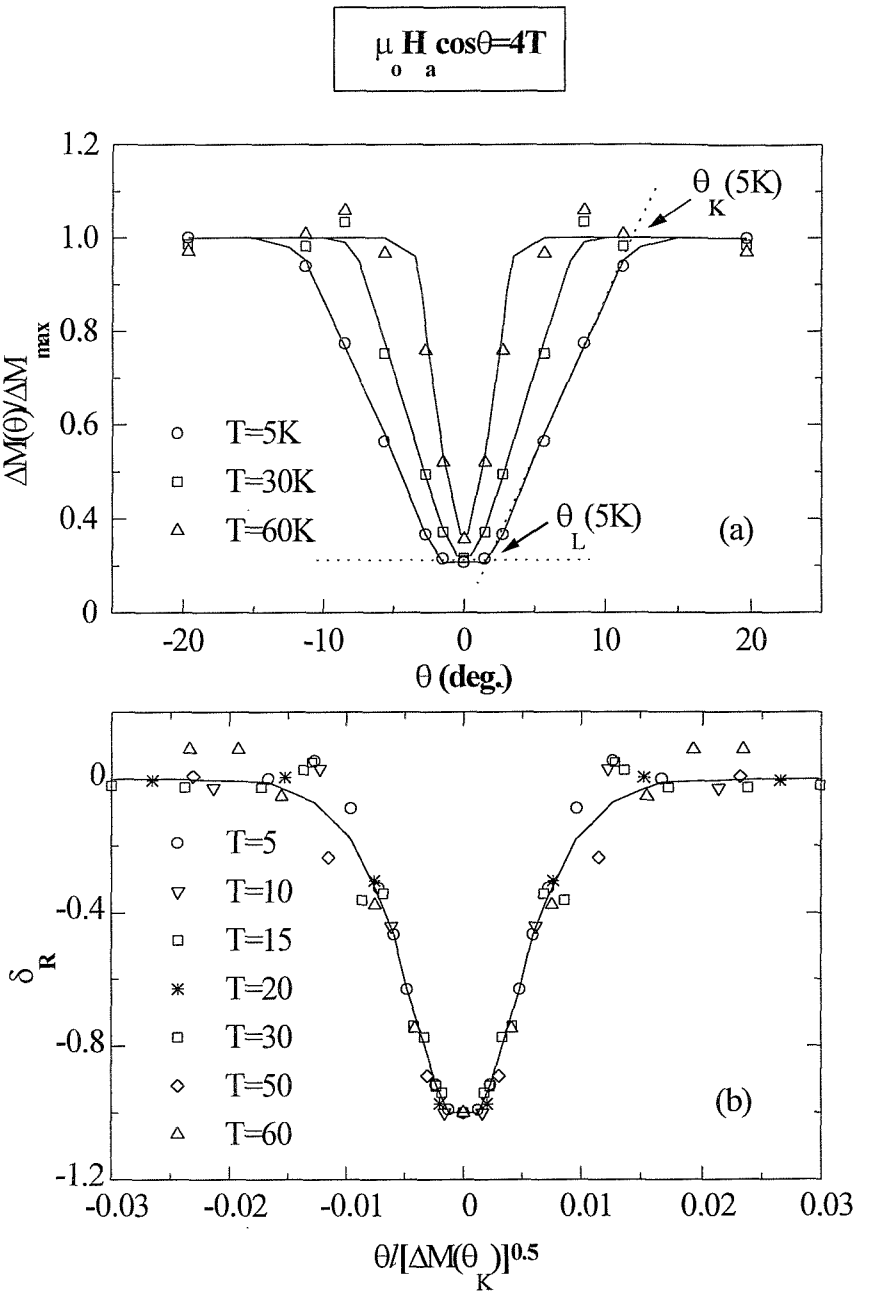

Figure 7.1: *(a) Angular dependence of the normalised* ΔM *to its maximum value, at the indicated temperatures and at a fixed applied field of* $\mu_o H_a \cos\theta = 4$ *T along the* c-axis. *Note the existence of two characteristic angles* θ_L *and* θ_K. *(b) Scaling of the curves illustrated in (a), with* δ_R *being the relative decrease of* ΔM. *The lines are a guide to the eye.*

width of the magnetisation grows linearly with θ. Finally, for $\theta > \theta_K$ vortices intersect twin planes at points and the influence of twin boundaries is negligible.

Furthermore, our results show that both these two angles, θ_L and θ_K, have the same temperature and field dependence and evidently they are controlled by the disorder in the untwinned regions. We show that the two critical angles surprisingly scale with the hysteresis width obtained for $\theta > \theta_K$ (fig.7.1). Our results verify the theoretical predictions for the existence, in the case of vortices trapped in the twin planes, of a localisation width larger than the width of the twin boundaries.

7.2 THE $YBa_2Cu_3O_{7-\delta}$ VORTEX PHASE DIAGRAM

Our results demonstrate the existence of a remarkably sharp, voltage criteria independent magnetisation peak in $YBa_2Cu_3O_{7-\delta}$. We show that the magnetic field values this peak occurs when mapped onto the vortex phase diagram result to a well defined crossover line, $H_p(T)$. This line exhibits a surprising non-monotonic temperature dependence, shifting to higher fields at elevated temperatures.

By using magnetotransport measurements, we also detect the solid-to-liquid first order transition in the phase diagram, which terminates in a critical point. Combining resistivity and magnetisation data, we demonstrate that $H_p(T)$ correlates to this critical point. By oxygen doping we observe both the magnetisation peak line in the phase diagram $H_p(T)$ and the critical point to shift upwards *maintaining* their correlation.

We show that our data verify and can naturally fit in the newly proposed frame of the coexistence of two distinct solid phases: a well ordered solid phase at lower fields, associated with the Bragg Glass phase, and a highly disordered solid phase at higher fields, associated with a mechanically entangled vortex phase. Theoretical reasoning suggests that these two phases together with a liquid phase connect, in the vortex phase diagram, at the critical point, in agreement with our results (fig.7.2).

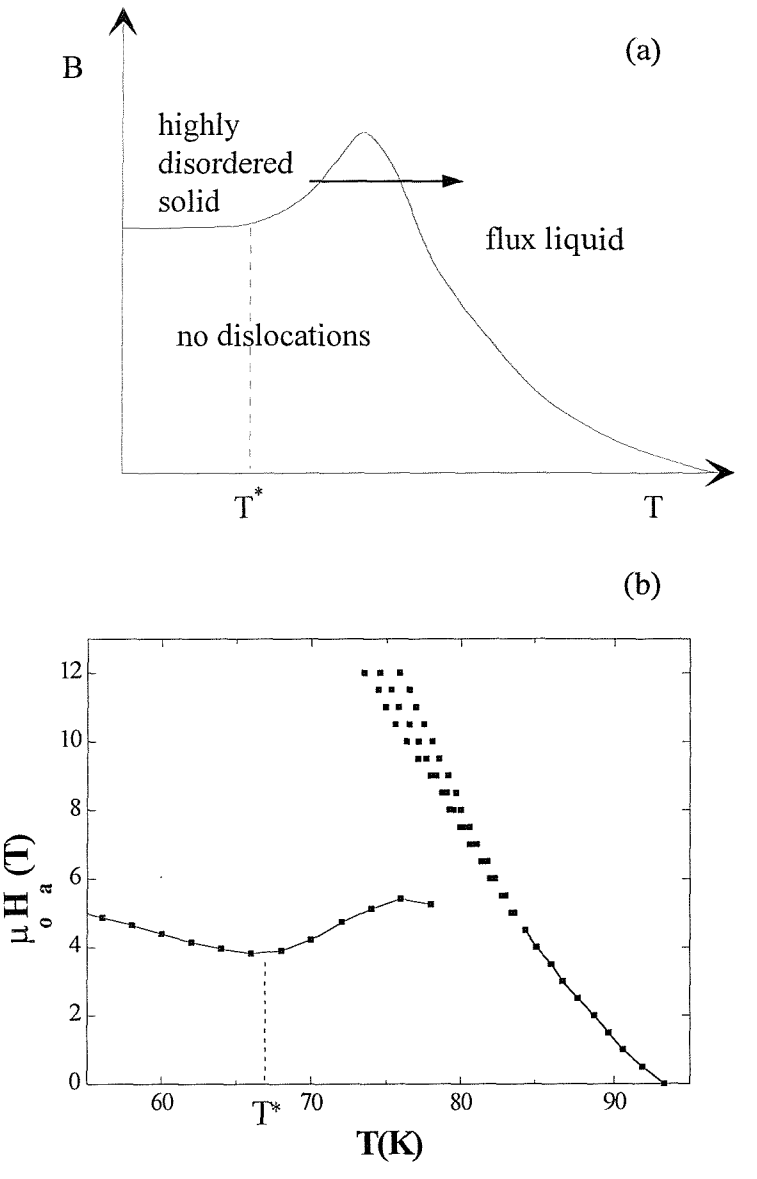

Figure 7.2: *(a) Theoretical vortex phase diagram for high temperature superconductors, after Ertas and Nelson. (b) Phase diagram for* $YBa_2Cu_3O_{7-\delta}$ *as derived by our combined magnetic and transport measurements.*

This picture suggests the existence of a generic vortex phase diagram for all the high temperature superconductors. Unification of the phase diagrams of all layered superconductors in a single picture has been a major challenge for vortex physics, for years now. Our results, moving in this direction, provide strong evidence on the existence of such a phase diagram. Indeed, our data in the moderately anisotropic

$YBa_2Cu_3O_{7-\delta}$ exhibit a surprising qualitative similarity and agreement with recent results for the very anisotropic $Bi_2Sr_2CaCu_2O_8$ compound.

Finally, since the existence of a well ordered hexagonal lattice in the presence of random point disorder is the reason of the observed field-driven transition, extended defects at low densities should not suppress this vertical crossover. Our results demonstrate that in the presence of twin planes the position of $H_p(T)$ in the phase diagram remains virtually the same.

7.3 LOCK-IN OSCILLATIONS

For an applied field H_a parallel to the CuO_2 layers, oscillations are observed in the measured magnetisation. We show that these oscillations are temperature and orientation independent and that they are induced by a succession of transitions between states for which the vortex lattice is commensurate with the layered structure of $YBa_2Cu_3O_{7-\delta}$. Due to the restriction of the quasi-2D regime at low temperatures, the observation of lock-in oscillations in the magnetisation is a valuable tool for the study of Josephson vortices.

Indeed, our measurements verify the existence of a compressed Josephson vortex lattice, with the predicted by the the anisotropic London model vortex lattice spacings parallel and perpendicular to the c-axis. Furthermore, for every value of the magnetic field we can map the position of the 2D Josephson vortices along the c-axis.

Even more important is the fact that using the theoretically expected and experimentally exhibited periodicity of lock-in oscillations in $H_a^{-1/2}$ we can estimate essential physical parameters. We demonstrate that lock-in oscillations are a reliable tool for the calculation of both the out-of-plane and in-plane anisotropy factors. In addition, lock-in oscillations indicate the temperature at which the dimensional crossover from the quasi-2D to the quasi-3D regime occurs. This allows us an accurate estimation of the zero temperature transverse coherence length, $\xi_c(0)$.

Our data illustrates the competing nature of point defects and layered structure in the lock-in transition. The first destroy the vortex alignment between the layers and

consequently the lock-in state, by offering favorable sites for the creation of kinks. Therefore, purity is a basic condition for the experimental observation of lock-in oscillations.

Finally, we present a systematic study of the temperature dependence of the magnetisation in the longitudinal geometry, in a large temperature regime. Our results show a surprising J_c anomaly at intermediate temperatures: the critical current *increases* with temperature. We explain our results considering the interaction of the Josephson cores (appropriate in the case of parallel fields) with the extrinsic (point) defects and the reduced thermal dimensionality of the locked-in vortices.